



---

# Forces in needle interventions

## Measuring tip forces

---

Master Thesis by  
**Mart Gähler**

Supervisors:  
**Kirsten Henken**  
**John van den Dobbelsteen**

August 24, 2012



---

# Forces in needle interventions

## Measuring tip forces

Master of Science Thesis

For obtaining the degree of Master of Science in  
BioMedical Engineering At Delft University of Technology

M.C. Gähler  
Delft University of Technology  
*Department of BioMechanical Engineering*







---

## Preface

This Master Thesis concludes my research on forces during percutaneous needle interventions. The research was performed at the BioMechanical Engineering department of the faculty of Mechanical, Maritime and Materials Engineering (3ME) at Delft University of Technology. Within the field of percutaneous needle interventions, I investigated the application of a force sensor in the shaft of a trocar needle. With the higher goal to increase the accuracy of insertion and which may help to improve the effectiveness of the therapy or diagnosis.

## Acknowledgement

This thesis could not have been completed without the support of others, for which I am very grateful. First of all, I would like to thank my supervisors, Dr. John J. van den Dobbelsteen and Ir. Kirsten R. Henken, for their guidance and motivation during my graduation. Their support was without a doubt crucial in the completion of this written work. I would like to thank Prof. dr. Jenny Dankelman for her time and support during the regular MISIT meetings. I would like to thank graduation committee member Dr. Ir. Marijke Melles for her time evaluating my work.

I would like to thank Mario van der Wel and Geert Springeling who build the prototype presented in this thesis. I would like to thank Harry Jansen and Patrick van Holst for their support with the calibration of the prototype and the deflection measurements of the shape sensing prototype. I would like to thank Dr. Mark Vogt and Ir. Wouter Boessenkool allowing me to be present at their cadaver experiments and allowing me to perform a pilot test in situ on a fresh piglet cadaver. I would like to thank Ir. Joost van Zwieten helping me with some Matlab and Latex problems. Many thanks to all the people in the MISIT Lab and other graduation students for a pleasant and supportive working environment.

Last but not least, I would very much like to thank my parents and Eva. For always being there and showing their love, support and encouragement.

Mart Gähler, August 2012





---

## Abstract

Accurate positioning of the needle tip during insertion is essential to ensure a maximum effect of the treatment. Target error is a problem and a lot research fields aim to improve needle insertions. The possibility to measure cutting force and stiffness force separately from friction forces supports the development of new types of needles, needle insertion simulators and needle insertion robots for use in a clinical environment. The goal of this work is to create a needle that can measure these forces. The design is used in an insertion experiment, to determine if this force information can be used to determine tissue properties and differentiate between tissue layers.

A new trocar needle design is presented for measuring forces in the tip of the cutting stylet, only measuring the cutting forces and stiffness forces and excluding the friction forces on the shaft. Through the centre of the stylet of a 20 cm 18 G trocar needle runs an optic fibre with a fibre Bragg grating close to the tip, that will function as an optical strain sensor. The interrogator measures the Bragg wavelength shift caused by a change in strain. The grating is embedded in a PVC jacket to increase the strain in the grating. Calibration was performed in a universal test machine to determine the force - wavelength relationship in a range of 0 - 10 N at different constant temperatures.

The calibrated prototype was used in insertion experiments in a phantom model and in an ex vivo tissue model. The total axial force is compared to the prototype output. The calibration revealed a linear force - wavelength relationship where the slope coefficient increases with increasing temperature. The calibration showed an average error of 0.1069 N. In the insertion experiment the output of the prototype has a good correlation with the total axial force. Puncture events are clearly identified in both samples. In the phantom tissue it is seen that the different layers can be differentiated by the gradual change in the output profile. The force from the prototype was overestimated, because insertion experiments were performed outside the calibrated temperature range. To conclude force measurement at the tip of needles is feasible, but has to be further investigated. As a first step this design can be improved by the addition of a method for temperature compensation and the improvement of the measurement accuracy.



---

## Nomenclature

### Abbreviations

CCD	Coupled Charge Device
DOF	Degrees of freedom
FBG	Fiber Bragg Grating
MRI	Magnetic Resonance Imaging
RMS	Root mean square
WDM	Wavelength Division Multiplexing

### Notations

$A$	Area of cross section needle
$D$	Diameter of cross section needle
$E$	Young's modulus
$F$	Force in Newton
$I$	Second moment area of inertia
$L$	Length needle shaft
$R$	Curvature radius
$T$	Temperature
$r$	Radius of cross section needle
$\Delta D$	Pixel coordinate change from FBG interrogator
$f_{total\ axial}$	Total axial force at the hub of the needle
$f_{cutting}$	Cutting force
$f_{stiffness}$	Stiffness force
$f_{friction}$	Friction force
$\alpha$	Slope coefficient
$\sigma$	Normal stress
$\varepsilon$	Strain
$\rho$	Resistivity
$\lambda_b$	Bragg wavelength
$\Lambda$	Grating period
$n_{eff}$	Effective refractive index
$\delta$	displacement



## CONTENTS

<b>Preface</b>	<b>i</b>
<b>Abstract</b>	<b>iii</b>
<b>Nomenclature</b>	<b>v</b>
<b>Concept Paper</b>	<b>ix</b>
<b>Report</b>	<b>1</b>
1 Introduction . . . . .	3
1.1 Background . . . . .	3
1.2 Goal . . . . .	4
1.3 Layout . . . . .	4
2 Conceptual Design . . . . .	5
2.1 Requirements . . . . .	5
2.2 Concept . . . . .	8
2.3 Design . . . . .	14
3 Calibration . . . . .	21
3.1 Calibration Set-up . . . . .	21
3.2 Calibration Protocol . . . . .	23
3.3 Calibration Results . . . . .	24
3.4 Conclusion calibration . . . . .	28
4 Insertion experiment . . . . .	29
4.1 Experimental Set-up . . . . .	29
4.2 Experimental Protocol . . . . .	29
4.3 Experimental samples . . . . .	31
4.4 Insertion Results . . . . .	33
4.5 Conclusion insertion . . . . .	36
5 Discussion . . . . .	37
5.1 Design . . . . .	37
5.2 Calibration . . . . .	38
5.3 Insertion experiment . . . . .	40
6 Conclusion . . . . .	43
7 Future work . . . . .	45
7.1 Temperature compensation . . . . .	45
7.2 Calibration improvements . . . . .	45
7.3 Incorporating deflection measurement . . . . .	45



---

<b>Appendices</b>	<b>51</b>
A Pilot needle insertion in pig liver . . . . .	51
A.1 Discussion . . . . .	51
B Polynomial curve fit . . . . .	53
C Deflection experiment . . . . .	55
C.1 Introduction . . . . .	55
C.2 Results . . . . .	58
C.3 Discussion . . . . .	64
D Assembly . . . . .	65
E Calibration Protocol . . . . .	69
F Drawings . . . . .	70

# Concept Paper



# Forces in needle interventions. 'Measuring tip forces'

Mart Gähler, Kirsten Henken, Jenny Dankelman, John van den Dobbelsteen

**Abstract**—Accurate positioning of the needle tip during insertion is essential to ensure a maximum effect of the treatment. Target error is a problem and a lot of research fields aim to improve needle insertions. The possibility to measure cutting force and stiffness force separately from friction forces supports the development of new types of needles, needle insertion simulators and needle insertion robots for use in a clinical environment. The goal of this work is to create a needle that can measure these forces. The design is used in an insertion experiment, to determine if this force information can be used to determine tissue properties and differentiate between tissue layers.

A new trocar needle design is presented for measuring forces in the tip of the cutting stylet, only measuring the cutting forces and stiffness forces and excluding the friction forces on the shaft. Through the centre of the stylet of a 20 cm 18 G trocar needle runs an optic fibre with a fibre Bragg grating close to the tip, that will function as an optical strain sensor. The interrogator measures the Bragg wavelength shift caused by a change in strain. The grating is embedded in a PVC jacket to increase the strain in the grating. Calibration was performed in a universal test machine to determine the force - wavelength relationship in a range of 0 - 10 N at different constant temperatures.

The calibrated prototype was used in insertion experiments in a phantom model and in an ex vivo tissue model. The total axial force is compared to the prototype output. The calibration revealed a linear force - wavelength relationship where the slope coefficient increases with increasing temperature. The calibration showed an average error of 0.1069 N. In the insertion experiment the output of the prototype has a good correlation with the total axial force. Puncture events are clearly identified in both samples. In the phantom tissue it is seen that the different layers can be differentiated by the gradual change in the output profile. The force from the prototype was overestimated, because insertion experiments were performed outside the calibrated temperature range. To conclude force measurement at the tip of needles is feasible, but has to be further investigated. As a first step this design can be improved by the addition of a method for temperature compensation and the improvement of the measurement accuracy.

**Index Terms**—Needle insertion, haptic feedback, force feedback, tip sensor, fibre Bragg grating.



## 1 INTRODUCTION

NEEDLE-based interventions are among the most common procedures in medicine. For the procedures into solid organs in deep seated parts of the body small diameter needles are used to create a passage through multiple soft tissue layers to reach a target area. Examples are liver, prostate and breast. When the needle tip has reached the target area different procedures are possible which can be either diagnostic or therapeutic. For diagnostic purposes needles are used to take biopsies; through a hollow needle tissue or fluid samples are extracted. For therapeutic interventions drug delivery, seed placement, thermal ablation and drainage are some of the possibilities.

Accurate positioning of the needle is essential to ensure maximum effect of the treatment. Accurate positioning of these long slender needles in deep seated parts of the body is very difficult with the limited amount of feedback that is available. Inaccuracy of needle placement leads to target error; clinical studies have revealed that target error is due to imaging limitations, image

misalignments, target uncertainty, human errors, target movement due to tissue deformation and needle deflection [2]. As an example of target error, post seed implantation measurements showed an average misplacement of 6.5 mm on prostate gland volume in the range of 25-55 cubic centimetres [3].

### 1.1 Background

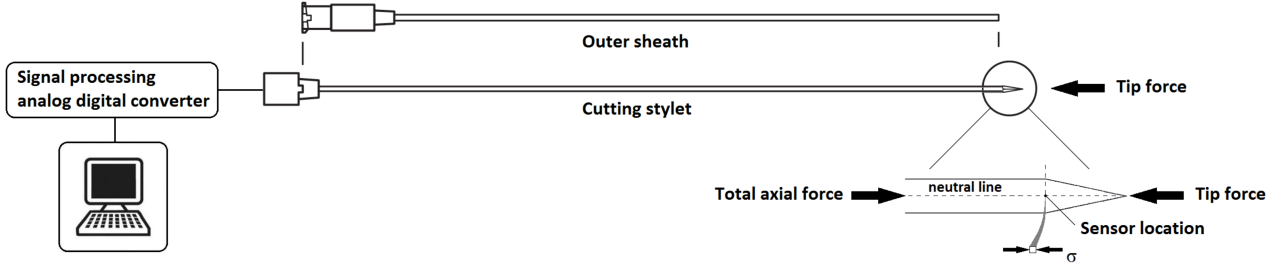
A lot of research is performed in the field of percutaneous needle procedures with the aim to improve insertion accuracy. Research fields include the mathematical modelling and insertion robotics. In the survey by Abolhassani et al. [2] an overview is given of research in needle insertions into soft tissue. Needle modelling and tissue modelling are covered as well as the application of these models for automated needle insertion.

Targeting accuracy in percutaneous needle insertion procedures can be improved by using a robot to insert needles [4]. The work by Cowan et al. [5] describes the advances made in needle design, modelling, planning and image guidance for the steering of flexible needles. Robotic insertion systems are used in combination with track and target planning to actively steer the needle tip through different tissue layers to the desired goal.

For all these research fields the use of accurate force data is important. Accurate real time force measurement

• Department of BioMedical Engineering, Faculty of 3mE, Delft University of Technology.  
E-mail: j.j.vandendobbelsteendelft.nl

August 24, 2012



**Fig. 1:** Schematic representation of the general concept. Trocar needle consisting of outer sheath and cutting stylet. The stylet contains the sensing element in the tip. The signal is converted to a digital signal so data analysis can be performed on a computer. Force acting on the stylet causing stress in the material. See the stress  $\sigma$  at a element, this is the ideal sensor location. In the neutral line there is no stress caused by bending of the needle [1].

is a valuable tool for needle interventions [6]. In the survey by Van Gerwen et al. [7] experimental needle-tissue interaction force data were collected available in literature. The amount of useful data is small, and many research questions about forces in needle interventions remain open for investigation. The method for measuring forces in most researches is the same and measures the external total axial force at the hub of the needle, and models are used to reconstruct the different components in the load distribution. The challenge is to directly measure these force components. Literature shows the developments in force sensors for needle interventions, such as multiple degree of freedom sensors at the hub where the main focus lies on MRI compatibility [8]. In the work by Kataoka et al. [9] a seven-axis load cell at the hub of the needle was designed to independently measure the tip and friction forces. The current work is the first step in gathering force information directly at the tip of the needle using a sensing element inside the shaft of the needle.

## 1.2 Goal

The goal of this current study is to directly measure the forces acting at the tip of the needle and to design a needle which can directly measure these forces with a sensor at the tip and to prove the feasibility of such a design. This design can be used to improve force information needed to increase the accuracy of needle interventions and to investigate if this force information can be used to determine tissue properties and differentiate between tissue layers.

## 2 MATERIAL & METHODS

### 2.1 Conceptual Design

The design created in this research starts with a list of requirements. These are divided in functional and geometrical requirements. The needle must be able to measure the axial forces directly at the tip of the needle. The total axial force (at the hub of the needle) during needle insertion is a combination of normal and shear loads distributed along the surface of the needle. The

total axial force can be modelled as a summation of three components [10].

$$f_{total\ axial}(z) = f_{stiffness}(z) + f_{cutting}(z) + f_{friction}(z) \quad (1)$$

The stiffness force and cutting force act at the tip, the design must measure these tip forces in a range of 0 - 15N [7], excluding the friction force acting on the shaft. The accuracy of the needle must be lower than 0.01 N [11], and with a minimum sampling frequency of 100 Hz. A 20 cm 18 G trocar needle with a tri-facet diamond tip (Trocar needle G02901 DTN-18-20.0-u, Cook Medical Inc., USA) is selected as the basis for the geometrical requirements, which is a typical size used in procedures in solid soft tissues such as liver, prostate, kidney and breast [12].

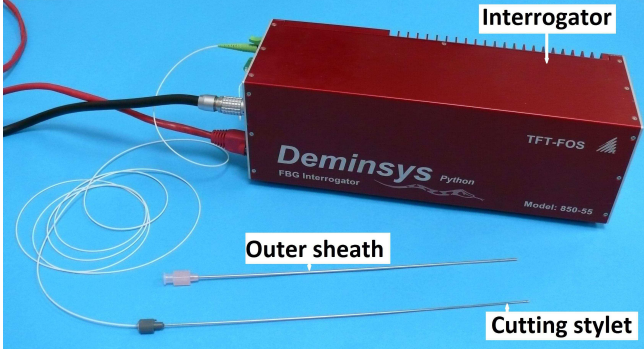
The general concept is a trocar needle consisting of an outer sheath and a cutting stylet with the geometry taken from an existing 18 G trocar needle. The cutting stylet contains the sensor for the force measurement, and is based on a strain measurement. The ideal position for the sensor is in the neutral line of the stylet as close to the tip as possible, in order to exclude friction forces and stress components caused by bending. To measure this strain an optic fibre containing an fibre Bragg grating (FBG) is used. An FBG is a periodical change in the refractive index written in the core of an optical fibre. This acts as a wavelength specific (Bragg wavelength) dielectric mirror in the core. The Bragg wavelength shifts due to index or grating period changes according to.

$$\lambda_b = 2n_{eff}\Lambda \quad (2)$$

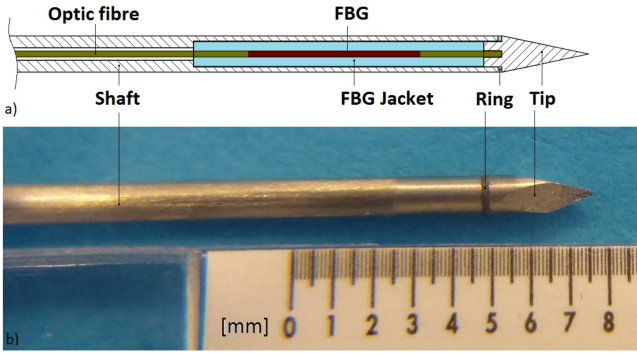
Where  $n_{eff}$  is the effective refractive index and  $\Lambda$  the grating period. These are affected by strain and temperature. The FBG is interrogated with the Deminsys system (Deminsys Python 850-55, Technobis Mechatronics BV, Uitgeest), the wavelength shift is measured and expressed in a pixel coordinate.

If the FBG is directly bonded in the ideal sensor position to a metal stylet shaft, the strain over the measurement range would be very low ( $97.4\mu\epsilon$ ). To increase the strain over the range the FBG is embedded in a jacket

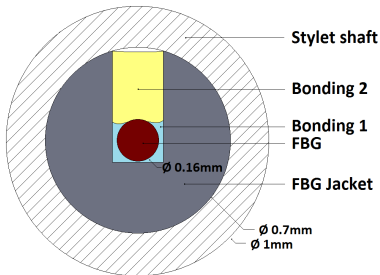
made from PVC. The tip compresses the FBG jacket directly, to allow for a more compliant movement the tip is attached to the shaft with a PVC ring (see Figure 3). The optic fibre runs through the centre of the shaft and through the centre of the hub. The assembled prototype can be seen in Figure 2.



**Fig. 2:** Prototype needle with sensing element in the cutting stylet. Outer sheath taken from Cook 18 G trocar needle (Cook Medical Trocar needle G02901 DTN-18-20.0-u, Cook Medical Inc., USA).



**Fig. 3:** (a) Cross section of the needle tip of the concept design. The tip creates the passage through the tissue and compresses the FBG jacket. The ring forms the connection between the tip and the shaft. The FBG jacket surrounds the FBG which measures the strain. (b) Photograph of prototype needle tip.



**Fig. 4:** Cross-section of the stylet prototype at the sensor, the FBG lies in a PVC jacket. The FBG is bonded in the FBG jacket with an acrylate bonding (bonding 1). The jacket is filled with a bonding (bonding 2) to form a circular section.

## 2.2 Calibration

A calibration procedure is necessary to calculate the force-wavelength relation between the interrogator output and tip force. The calibration is performed in a universal testing machine (Zwick Roell Allround-line Z005, Zwick Roell GmbH Co. KG). The calibration is performed inside a temperature chamber. In Figure 10a the setup can be seen. The prototype is axially loaded onto the loadcell in a range from 0-10 N. The needle is calibrated at different temperatures because the FBG has a cross-sensitivity to temperature. The temperature range is taken from 26-40 °C with 2 °C increments, at each temperature 5 calibration cycles are executed. The force, position and temperature from the testing machine are sampled at 10 Hz, the output for the interrogator is down-sampled to 100 Hz. A calibration cycle profile consists out of a zero measurement (30 s), loading with constant speed until 10 N, constant force at 10 N (60 s) and unloading with constant speed. Data analysis is performed in Matlab R2011b (Matlab R2011b, The Mathworks Inc.). The output of the prototype is filtered using a 5<sup>th</sup> order low pass Butterworth filter with a cut off frequency at 10 Hz. The output of the prototype is matched to the force data from the universal testing machine with a least squares error approach. To determine the force-wavelength relationship the loading step the data is approached with a best fit straight line. The slope coefficients are determined for Equation 3, and the error for this fit is determined.

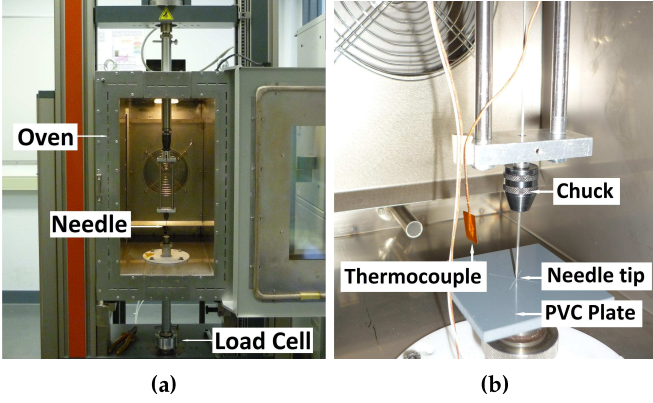
$$\Delta F[N] = \alpha \Delta D[\text{Pixel}] \quad (3)$$

In this equation  $\Delta D$  is the wavelength shift given in pixel coordinate,  $\Delta F$  is the tip force change in Newton and  $\alpha$  is the slope coefficient. The difference between the filtered data and the fit is the linearity error which is a measure for the accuracy of the prototype.

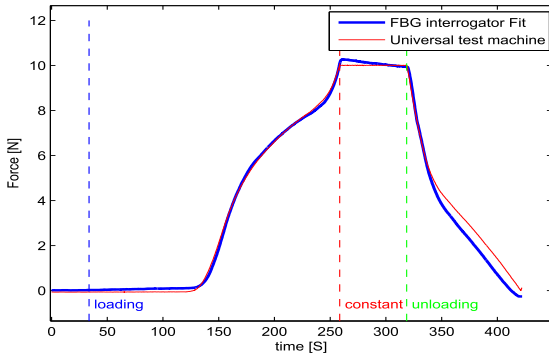
## 3 RESULTS

Figure 6 shows the force profile from the universal testing machine together with the filtered output of the interrogator converted to force (see Equation 3). The root mean square error between the raw data and the filtered signal of the prototype is 0.0015 [Pixel]. In Figure 7 the force is plotted against wavelength, it can be seen that there is a linear relation. The slope coefficients  $\alpha$  for the different temperature sets are determined (see Figure 8), with an increasing temperature the slope coefficient also increases. The standard deviations of the coefficients are low.

The errors are determined using the medians for the slope coefficients for the temperature sets (see Figure 9). The mean error for all calibration cycles is 0.1069 N. This error is biggest in the lower region of the measurement range. The results show that the force-wavelength relationship is linear, but the accuracy does not meet the demands that were stated in the requirements.



**Fig. 5:** Calibration set-up. (a) Calibration set-up on the universal testing machine, set-up is within a temperature chamber. The needle is placed in a vise attached to the translation stage. The needle is mounted perpendicular to the load cell. The load cell is placed at the bottom outside the oven. (b) Calibration set-up at needle tip. The needle is held by a self centre chuck to prevent needle buckling. The tip presses on a PVC plate to protect the tip. The PVC plate is rigidly attached to the load cell. The thermocouple measures the temperature near the needle tip.



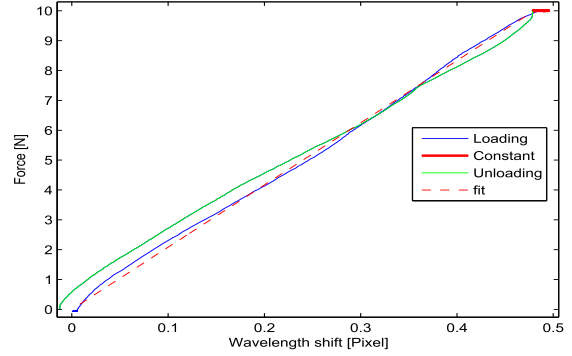
**Fig. 6:** Force profile from the calibration set-up is given in red. The needle is loaded with a constant speed of  $17 \mu\text{m/s}$  (blue vertical line) then the force is constant and there is no travel for a period of 60 seconds (red vertical line) before unloading the needle with the same constant speed (green vertical line). With a linear increase in position there is a nonlinear increase in force. The output from the interrogator is fitted and shown with the blue line.

## 4 MATERIALS & METHODS

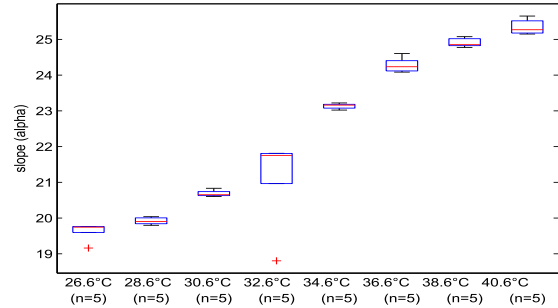
### 4.1 Insertion Experiment

The prototype is meant to be used in a clinical environment. The force information can be used to improve insertion procedures. One of the uses for the force information is the identification of different tissue layers along the path of insertion. An insertion experiment is performed to validate if the prototype can detect differences between different tissue layers. The total axial force is compared to the output of the prototype.

The set-up for the experiments uses a linear stage (Aerotech PRO 115, Aerotech Inc.) to control the inser-



**Fig. 7:** Force versus the FBG output of 1 cycle, the blue line indicates loading, the red line indicates a constant force and the green line indicates unloading. The dotted line is the linear regression fit for the loading cycle between 0-10 N.



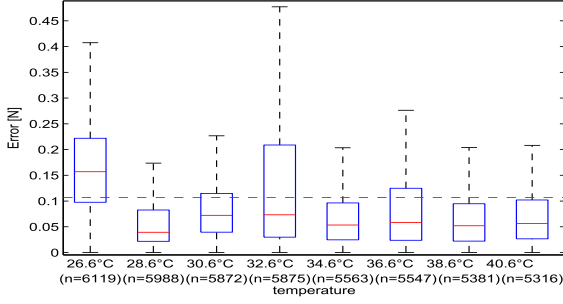
**Fig. 8:** Boxplot of slope parameter  $\alpha$  for all temperature sets see Equation 3. The markers in the set of  $26.6^\circ\text{C}$  and  $32.6^\circ\text{C}$  indicates an outlier.

tion. The prototype is mounted at the hub on a load cell (RDP SLC31, RDP Electronics Ltd.) to measure the total axial force. At constant speed the needle is inserted into the sample container and stops at a predetermined end point. The total axial force and position are sampled at 1kHz, the FBG output is down sampled to 100Hz. A thermocouple is inserted in the sample container to measure the sample temperature. The sample temperature is used to interpolate the coefficient  $\alpha$ , with Equation 3 the output is converted to force. Analysis is performed in Matlab. The output of the prototype and experimental set-up are filtered with a  $5^{\text{th}}$  order low pass Butterworth filter with a cut off frequency at 25 Hz.

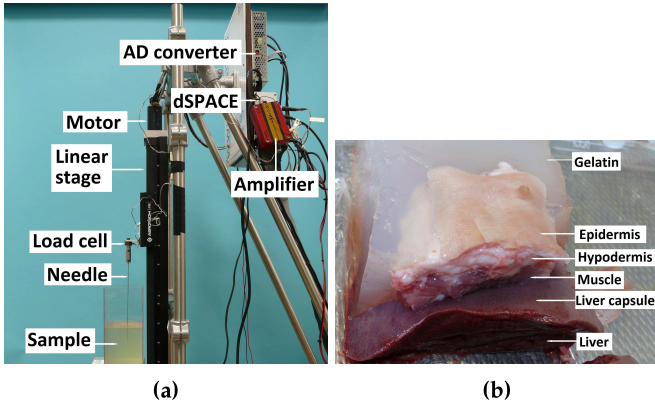
### 4.2 Experimental samples

Two types of samples are used for the experiment. The first sample is a phantom tissue consisting out of gelatin layers with different gelatin concentrations. The different layers are used to mimic different soft tissue layers encountered during needle insertion (see Table 1). A cellophane membrane is used to mimic the thin peritoneum. The stiffness of the gel sample is measured but depends on temperature. In the tissue phantom 25 insertions are made with different constant speeds (5, 10,





**Fig. 9:** Boxplot of linearity error for a calibration range of 0-10 N for all data points per temperature set. The coefficients used for the fit are the medians of the slope coefficient in a temperature set (see Figure 8). The red line indicates the mean of the error (0.1069 N) for all data samples from all temperature sets.



**Fig. 10:** (a) Experimental set-up with the phantom tissue. The sample is the phantom tissue. (b) Cross section of the ex vivo porcine tissue sample consisting out of epidermis, hypodermis, muscle and liver embedded in gelatin.

15, 20 and 25 mm/s).

The second sample is an ex vivo sample taken from porcine cadaver. The tissue layers are epidermis, hypodermis, muscle and liver embedded in a gelatin gel. The epidermis is incised to prevent needle buckling, this layer is too tough to insert without needle guidance. In the ex vivo sample 35 insertions are made at different constant speeds (5, 10 and 15 mm/s).

**TABLE 1:** Phantom tissue layers. Gelatine layers and their concentration, Young's modulus measured with compressive test at 16 °C

Sample type	Gelatin concentration [%]	Layer thickness	measured Young's Modulus[kPa]
Dermis	17.8	12 mm	80
Hypodermis	26.3	6 mm	130
Muscle	13.0	21 mm	52
Peritoneum	- (cellophane)	0.0125 mm	$3 \cdot 10^6$
Liver	6.8	50 mm	15

## 5 RESULTS

Figure 11 shows the total axial force and the output of the prototype for an insertion in the phantom tissue. The prototype output is converted to force using extrapolated calibration results. For all the insertions at the same speed similar force profiles are recorded. A clear puncture peak is visible for the membrane. The transitions between the other layers are not indicated by a puncture peak but a gradient change is visible. The corresponding output for the prototype shows a good correlation with the total axial force. It also shows a clear puncture peak for the membrane and the gradient changes for the different layers. Overall it is seen that the force range is very low, and these forces decreased with increasing temperature of the phantom tissue. This is the reason why the experiments were executed with a temperature below the calibration range, and the coefficient for Equation 3 had to be extrapolated.

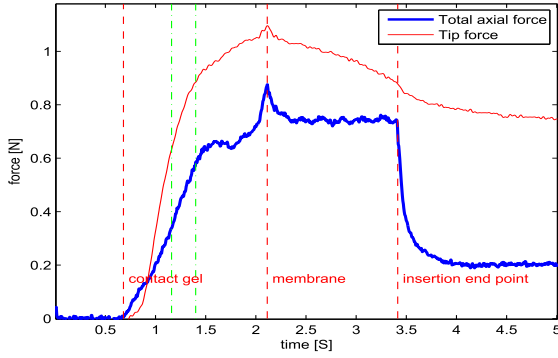
Figure 12 shows the total axial force and the prototype output for an insertion in the ex vivo tissue. The output is converted to force by extrapolating the calibration results. For each insertion the thickness of the different layers differs, which makes a comparison between insertions difficult. All insertions show similar profiles in that force range. The peaks show the internal puncture events because of the transitions between layers and internal structure of the inhomogeneous tissue. The FBG output shows a good correlation with total axial force with identical locations for the puncture peaks.

The converted outputs from the prototype in both experiments surpasses the total axial force measured at the hub. This means that the coefficient  $\alpha$  is overestimated. From the experiments it shows that tissue types can be identified by a gradient change of the prototype output. For this prototype the output can not be correctly converted to force when the temperature is unknown and outside the calibration range, and only the gradient change contains valuable information.

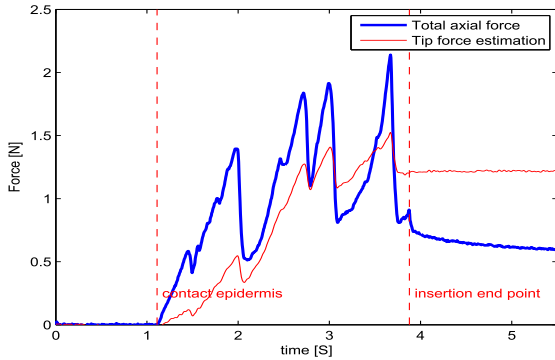
## 6 DISCUSSION

Accurate positioning of the needle tip during needle insertion is essential to ensure a maximum effect of the treatment. This work aims to aid in the research field by improving the force sensing during needle insertion, making the first attempt in the addition of a force sensor in the tip of a needle. This tip sensor measures the cutting forces and stiffness forces acting at the tip while excluding the friction force acting on the shaft. The design measures the strain caused by the tip force and the sensing element used is an FBG. Among the other advantages of FBG's is the immunity to electrical noise which makes them MRI compatible also FBG's are sterilizable, but these advantages are not considered in the sensor choice.

From the calibration results it was concluded that the needle functions and that it can measure the forces at the tip. The results show a linear force - wavelength



**Fig. 11:** Total axial force (in blue) and FBG output converted to force (in red) with extrapolated calibration coefficient. Insertion into the phantom tissue. Insertion speed 25 mm/s at 20.5 °C. The force corresponding to the FBG output is higher than the total axial force. The force corresponding to the FBG output is overestimated.



**Fig. 12:** Total axial force (in blue) and FBG output converted to force (in red) with extrapolated calibration coefficient. Insertion into ex vivo tissue sample. Insertion speed 15 mm/s at 18 °C. The force corresponding to the FBG output is higher than the total axial force. The force corresponding to the FBG output is overestimated.

relation. The accuracy does not meet the demands from the design requirements: the mean linearity error is 0.1069 N. The error is biggest in the lower region of the measurement range, this is the region where the highest accuracy is needed [7]. The calibration also shows hysteresis which is mainly caused by the drift in the interrogator when the force is held constant.

A disadvantage of the FBG sensor is the cross sensitivity to temperature, calibration showed an increasing slope coefficient for the linear relationship with increasing temperatures. This prototype can only be used in an environment with accurate known measured temperatures. From the insertion experiment it also followed that the calculated force was overestimated. The samples had a temperature outside the calibration range. A contributing reason for the force overestimation is that the temperature was measured at the edge of the container too far away from the tip of the stylet, the temperature is not uniform throughout the sample. Another effect that can cause the overestimation is that the calibration

coefficients does not behave in a linear way outside the calibrated temperature range. For this prototype a calibration is needed over the full temperature range in which it is going to be used. Further development of the presented design needs to focus on the improvement of the measurement accuracy, and the addition of means to compensate for changing temperatures. An easy solution is the addition of a strain free reference FBG in the design, common terms such as temperature, noise and drift can be removed by compensating with the output of this reference FBG.

In literature, direct measurement of the tip force was only found in the research by Kataoka et al. [9] where a needle which measures the tip forces and total axial force independently, with a seven axis load cell at the hub. The friction force is determined by subtracting the tip forces from the total axial force.

The design by Kataoka et al. [9] and the design presented in this work both measure the tip force directly. A drawback of the design by Kataoka et al. [9] is that it does not allow for needle deflection, when it is deflected the inner stylet comes in contact with the outer stylet making it impossible to measure the tip forces without these forces created by the surface contact. As stated in the requirements the design in this thesis does allow for bending. The sensor is positioned in the neutral line where there are no longitudinal strains due to bending, only axial forces. This gives possibilities to combine the design in future research with needle steering by deflection as seen in the work by Cowan et al. [5].

In the sensor design by Kataoka et al. [9] the needles can be changed, making it possible to use different sized needles with different tip types. In the design from this work this is not possible because of the stylet assembly. When the needle tip loses its sharpness the stylet has to be replaced. In clinical use these types of trocar needles are disposables and are only used once. For research in non-living tissue the design can be used multiple times but the sharpness of the needle tip decreases over time and influences the cutting force.

The functional requirements of this design will remain the same even if a needle of a different size is desired. The length of the needle does not influence the sensor at the tip of the needle. The diameter does influence the sensor design. The FBG jacket is used to increase the strain in the FBG, when the diameter (bigger Gauge size) is reduced the cross section area reduces with a quadratic scaling. The closest comparable application of force sensing FBG's was found in the work by Iordachita et al. [13]. A prototype is presented for measuring tip forces on a retinal surgery tool, and measuring forces applied on the retina. In the prototype the FBG is embedded in a 25 G (0.5 mm) shaft made from titanium. The FBG is embedded in a groove in the shaft which can easily be machined. The FBG does not lie in the centre of the needle so transverse force will affect the measurement. The area reduction is by a factor 4 and titanium has a Young's Modulus of 105 - 120 GPa which allows that

the FBG can be directly bonded to the shaft. For the design of the retinal surgery tool Iordachita et al. [13], a resolution of 0.25 mN was concluded; the error was not quantified. The resolution for the design presented here has a resolution in a similar range but the error reduces the accuracy of the device.

The goal for the insertion experiment was to validate the prototype and to research whether it can be used in the determination of tissue properties and differentiation between tissue layers. From the insertions in the experimental samples it can be seen that the output of the prototype has a good correlation with the measured total axial force. Puncture events from layer transitions and internal punctures are clearly identifiable. In the phantom tissue transitions between layers can be identified by a gradient change in the output profiles. The phantom tissue is not an optimal model because the measured force range is too low compared to experiments found in literature. The sample degraded with increasing temperature, because the temperatures were lower than the calibration range; the force - wavelength relation had to be extrapolated. The force was overestimated which is not possible, the total force is a combination of tip forces and forces on the shaft and these can't be negative.

If the results are compared to the results obtained in the work by Kataoka et al. [9] and Okamura et al. [14], similar force ranges are seen for the ex vivo tissue sample. In the research by Kataoka et al. [9] the friction force is determined by subtracting the tip forces from the total axial force. If the output for the prototype presented here is correctly converted to force this can also be done. Both the results from Kataoka et al. [9] and the results from this work show that when the insertion is stopped, the total axial force decreases to a constant value. The force at the tip also decrease to a non zero constant value and this is caused by a remaining stiffness force. There is no relative tissue movement so the cutting force can be considered zero. In the work by Kataoka et al. [9] this constant value for the tip force is around half of the total axial force. This should also be the cause if the prototype from this work is used in their experimental set-up. When the insertion is stopped there is also a remaining constant value for the friction force, caused by the viscosity causing a dragging up force acting on the shaft.

From the calibration and insertion experiments it can be concluded that improvements can and have to be made. Temperature compensation is important: the samples in which the design is used can be of non uniform temperature. Also the accuracy of the prototype needs to be improved especially in the lower region of the measurement range.

## 7 CONCLUSION

The design in this thesis is for a new force measuring trocar needle. An FBG is incorporated in the tip of the needle stylet which only measures the forces acting at

the tip. Calibration showed the the prototype functions in a environment with constant temperature, with an average measurement error of 0.1069 N. With the prototype tissue differences can be identified because of changing gradient in the output profile. The design can be used to improve needle procedures by providing force information gathered at the tip of the needle.

## ACKNOWLEDGMENTS

The author would like to thank Mario van der Wel and Geert Springeling for building the prototype presented in this work, and Harry Jansen and Patrick van Holst for their support with the calibration of the prototype.

## REFERENCES

- [1] R. Hibbeler, *Statics and mechanics of materials*, 2nd ed. Pearson/Prentice Hall, 2004.
- [2] N. Abolhassani, R. Patel, and M. Moallem, "Needle insertion into soft tissue: A survey," *Medical Engineering Physics*, vol. 29, no. 4, pp. 413–431, 2007.
- [3] P. Blumenfeld, N. Hata, S. DiMaio, K. Zou, S. Haker, G. Fichtinger, and C. M. Tempany, "Transperineal prostate biopsy under magnetic resonance image guidance: a needle placement accuracy study," *J Magn Reson Imaging*, vol. 26, no. 3, pp. 688–94, 2007.
- [4] R. Roesthuis, Y. van Veen, A. Jahya, and S. Misra, "Mechanics of needle-tissue interaction," pp. 2557–2563, 2011.
- [5] J. Cowan, K. Goldberg, G. Chirikjian, G. Fichtinger, R. Alterovitz, K. Reed, V. Kallem, W. Park, S. Misra, and A. Okamura, *Robotic Needle Steering. Design, Modeling, Planning, and Image Guidance*, ser. Surgical Robotics, 2011.
- [6] O. Gerovich, P. Marayong, and A. Okamura, "The effect of visual and haptic feedback on computer-assisted needle insertion," *Computer Aided Surgery*, vol. 9, no. 6, pp. 243–249, 2004.
- [7] D. Van Gerwen, J. van den Dobbelsteen, and J. Dankelman, "Needle- tissue interaction forces: A survey of empirical evidence," *Medical engineering physics*, vol. 34, no. 6, pp. 665–680, 2012.
- [8] S. Hao and G. Fischer, "A 3-axis optical force/torque sensor for prostate needle placement in magnetic resonance imaging environments," pp. 5–9, 2009.
- [9] H. Kataoka, T. Washio, K. Chinzei, K. Mizuhara, C. Simone, and A. Okamura, "Measurement of the tip and friction force acting on a needle during penetration," vol. 2488, pp. 216–223, 2002.
- [10] C. Simone and A. Okamura, "Modeling of needle insertion forces for robot-assisted percutaneous therapy," *2002 IEEE International Conference on Robotics and Automation, Vols I-Iv, Proceedings*, pp. 2085–2091 4353, 2002.
- [11] J. Peirs, J. Clijnen, D. Reynaerts, H. V. Brussel, P. Herijgers, B. Corteville, and S. Boone, "A micro optical force sensor for force feedback during

- minimally invasive robotic surgery," *Sensors and Actuators A: Physical*, vol. 115, pp. 447–455, 2004.
- [12] Y. Park, S. Elayaperumal, B. Daniel, R. Seok Chang, S. Mihye, J. Savall, R. Black, B. Moslehi, and M. Cutkosky, "Real-time estimation of 3-d needle shape and deflection for mri-guided interventions," *Mechatronics, IEEE/ASME Transactions on*, vol. 15, no. 6, pp. 906–915, 2010.
- [13] I. Iordachita, Z. Sun, M. Balicki, J. Kang, S. Phee, J. Handa, P. Gehlbach, and R. Taylor, "A sub-millimetric, 0.25 mm resolution fully integrated fiber-optic force-sensing tool for retinal microsurgery," *International Journal of Computer Assisted Radiology and Surgery*, vol. 4, no. 4, pp. 383–390, 2009.
- [14] A. M. Okamura, C. Simone, and M. D. O'Leary, "Force modeling for needle insertion into soft tissue," *Biomedical Engineering, IEEE Transactions on*, vol. 51, no. 10, pp. 1707–1716, 2004.



**Mart Gähler** obtained his BSc. degree in Mechanical Engineering in 2010 from Delft University of Technology. This paper is part of the Master thesis to obtain the degree of MSc. BioMedical Engineering from Delft University of Technology. Research interests include development of medical instruments, with a focus on minimally invasive techniques.



**MSc. Kirsten Henken** received the B.Sc. degree in mechanical engineering in 2006 and the M.Sc. degree in biomedical engineering in 2009 from Delft University of Technology. After that she was appointed as researcher at the department of biomechanical engineering of Delft University of Technology. Since 2010 she is pursuing the Ph.D. degree at the same department while investigating force and shape sensing with fiber Bragg gratings for steerable needles in robotized percutaneous interventions. Her re-

search interests include the integration of sensors in smart instruments for medical application and medical robotics.



**Dr. John J. van den Dobbelsteen** obtained his degree in psychophysics in 1998 from the University of Groningen. He received his Ph.D. title in 2003 from the department of Neuroscience at the Erasmus MC in Rotterdam for research into human motor control, motor learning and sensorimotor integration. In 2007 he became an assistant professor with the section Minimally Invasive Surgery and Interventional Techniques (MISIT) at Delft University of Technology.

Research interests include the development of medical instruments and measurement devices for instrument-tissue interaction in minimally invasive techniques.



**Prof. Dr. Jenny Dankelman** obtained her degree in mathematics from the University of Groningen in 1984. She obtained a Ph.D. title in 1989 from the Man-Machine Systems group at Delft University of Technology, for research into the dynamics of the coronary circulation. In 2001 she became professor of BioMechanical Engineering, and since 2007 she is head of the section Minimally Invasive Surgery and Interventional Techniques (MISIT). Research interests include medical training and simulation, patient

safety, and the development of medical instruments, with a focus on minimally invasive techniques.



# Report





# 1 Introduction

Needle-based interventions are among the most common procedures in medicine. For the procedures into solid organs in deep seated parts of the body small diameter needles are used to create a passage through multiple soft tissue layers to reach a target area. Examples are liver, prostate and breast. When the needle tip has reached the target area different procedures are possible which can be either diagnostic or therapeutic. For diagnostic purposes needles are used to take biopsies; through a hollow needle tissue or fluid samples are extracted. For therapeutic interventions drug delivery, seed placement, thermal ablation and drainage are some of the possibilities.

Accurate positioning of the needle is essential to ensure maximum effect of the treatment. Accurate positioning of these long slender needles in deep seated parts of the body is very difficult with the limited amount of feedback that is available. Inaccuracy of needle placement leads to target error; clinical studies have revealed that target error is due to imaging limitations, image misalignments, target uncertainty, human errors, target movement due to tissue deformation and needle deflection [2]. As an example of target error, post seed implantation measurements showed an average misplacement of 6.5 mm on prostate gland volume in the range of 25-55 cubic centimetres [3].

## 1.1 Background

A lot of research is performed in the field of percutaneous needle procedures with the aim to improve insertion accuracy. Research fields include the mathematical modelling and insertion robotics. In the survey by Abolhassani et al. [2] an overview is given of research in needle insertions into soft tissue. Needle modelling and tissue modelling are covered as well as the application of these models for automated needle insertion.

Targeting accuracy in percutaneous needle insertion procedures can be improved by using a robot to insert needles [25]. The work by Cowan et al. [4] describes the advances made in needle design, modelling, planning and image guidance for the steering of flexible needles. Robotic insertion systems are used in combination with track and target planning to actively steer the needle tip through different tissue layers to the desired goal.

For all these research fields the use of accurate force data is important. Accurate real time force measurement is a valuable tool for needle interventions [7]. In the survey by Van Gerwen et al. [28] experimental needle-tissue interaction force data were collected available in literature. The amount of useful data is small, and many research questions about forces in needle interventions remain open for investigation. The method for measuring forces in most researches is the same and measures the external total axial force at the hub of the needle, and models are used to reconstruct the different components in the load distribution.

The challenge is to directly measure these force components. Literature shows the developments in force sensors for needle interventions, such as multiple degree of freedom sensors at the hub where the main focus lies on MRI compatibility [8]. In the work by Kataoka et al. [15] a seven-axis load cell at the hub of the needle was designed to independently measure the tip and friction forces. The current thesis is the first step in gathering force information directly at the tip of the needle using a sensing element inside the shaft of the needle.

---

## 1.2 Goal

The goal of this current study is to directly measure the forces acting at the tip of the needle and to design a needle which can directly measure these forces with a sensor at the tip and to prove the feasibility of such a design. This design can be used to improve force information needed to increase the accuracy of needle interventions and to investigate if this force information can be used to determine tissue properties and differentiate between tissue layers.

## 1.3 Layout

This report will be structured as follows. It is divided in two parts. In the first part the concept design of the needle is described. The description of the design and prototype can be found in Chapter 2. The calibration of the prototype is described in Chapter 3. This is followed with a conclusion 3.4 about the results of the needle design. The second part contains the description of the measurements performed with the prototype in different samples, see Chapter 4. In Chapter 5 the methods and results are discussed for both parts. Chapter 6 contains the conclusions for this thesis. The last chapter of this thesis contains recommendations for further study (see Chapter 7). At the end of the report additional appendices can be found. Containing the results of an ex vivo pilot test, and the results from the deflection measurement with another prototype. The appendices also include the technical drawings for the prototype and the method for assembly.

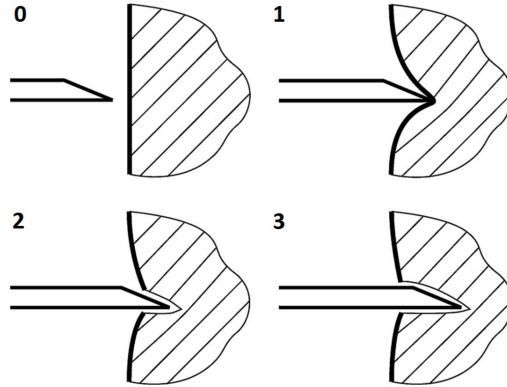
## 2 Conceptual Design

The needle design presented in this thesis is meant to be used during existing needle procedures. The design has force sensing capabilities to measure the forces at the tip of the needle, in which it differs from existing needles. The needle can be handled manually by a clinician. The design can also be used in an insertion system. Before such a design is presented the requirements and limitations are considered in Chapter 2.1. With these requirements a general concept is presented in Chapter 2.2.1. The needle design makes use of a transducer and three options are considered in Chapter 2.2.2 and 2.2.3. In the Chapter 2.3.1 the overview of the final design is given. Sections 2.3.2 - 2.3.5 describe the details of the components in the design.

### 2.1 Requirements

The goal is to design a needle which can measure forces. Before explaining the details of the design requirements the forces during needle interventions have to be looked at. The total axial force  $f_{total\ axial}(z)$  for the insertion (at the hub of the needle) is a combination of normal and shear loads distributed along the surface of the needle. The total axial force is a summation of three components [15].

$$f_{total\ axial}(z) = f_{stiffness}(z) + f_{cutting}(z) + f_{friction}(z) \quad (1)$$



**Figure 1:** Needle insertion phases. Phases: (0) No interaction, (1) Pre-puncture, (2) puncture, and (3) tip and shaft insertion [28].

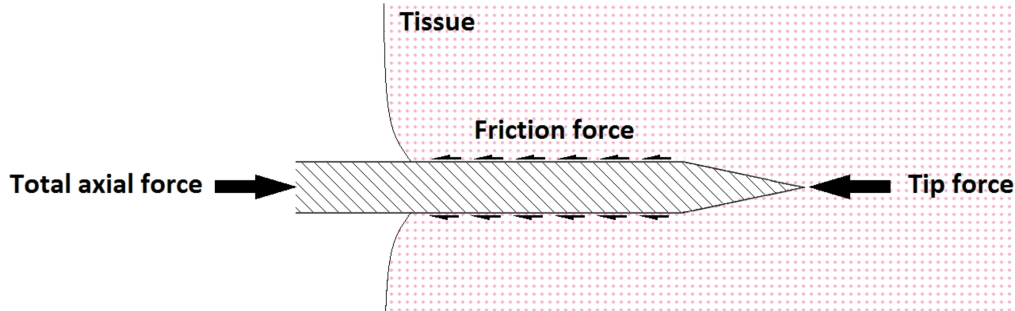
The components in this equation can best be explained by looking at the different phases of needle insertion. These phases are divided by the location of the tissue surface with respect to the needle (see Figure 1). When a needle is inserted, the phases can be distinguished for each tissue boundary the needle encounters.

- Phase zero there is no contact between needle and tissue.
- Phase one is the pre-puncture phase. The tip of the needle is in contact with the tissue, but does not penetrate the tissue yet and the tissue boundary moves together with the tip tenting inwards. During this phase the total axial forces increase because the stiffness force increases. The stiffness force  $f_{stiffness}$  is due to the elastic properties of the soft tissue [2]. The stress in the material will build up until a threshold level is reached and the tip penetrates the boundary.

- Phase two is the puncture phase. The threshold is reached and a crack is formed in the tissue. The shape of the crack and the force needed for this crack depends on the shape of the needle tip. The crack growth can be gradual, stable cutting or unstable rupture depending on the tissue properties. In the total insertion force, puncture can be seen as a peak. This is because the stiffness force rapidly decreases due to the puncture. The indentation of the tissue will spring back, which results in a sudden increase of relative velocity between tissue and needle. The force contributions in this phase are due to the cutting ( $f_{cutting}$ ) and wedging from the needle tip to create the passage for the cannula.
- Phase three is the tip and shaft insertion phase. The needle is advanced far enough so that the surface of the shaft is in contact with the tissue see Figure 2. The tissue boundary has passed the transition from tip to shaft. From this point the friction force ( $f_{friction}$ ) increases due to the increasing contact area between shaft and tissue. The friction in axial direction is a summation of Coulomb and viscous friction.

The magnitude of these forces is of interest as well. Van Gerwen et al. [28] conducted a survey in needle tissue interaction forces, which included papers that present force measurement data obtained during needle insertion. The amount of measured data which is accurate is small. From all the papers included in the survey Table 1 gives an indication of the magnitudes encountered during insertions irrespective of the experimental conditions.

All studies report the total axial force that is measured at the hub of the needle, but no studies have been found where the cutting and stiffness are directly measured with a sensor at the tip. Some studies also report the friction force that is measured by withdrawal of the needle. The other forces (cutting and stiffness forces) are derived by subtracting the friction force from the total axial force.



**Figure 2:** The forces acting on a needle in soft tissue. Tip forces at the tip consists of cutting and stiffness force. Friction force acts on the shaft of the needle [15].

**Table 1:** Maximum axial force values reported in papers [28]

Description	Number of papers	Median [N]	Range [N]
Total axial force	63	5.0	0.00004-92.1
Puncture force	24	1.22	0.0005-19.2
Cutting force	10	0.95	0.05-1.3
Friction force	10	1.0	0.15-2.8

To measure the cutting and stiffness force directly a force sensor in the tip of the needle is needed. For such a design the following requirements were defined. These requirements for a needle with a

force sensor in the tip are divided in functional requirements and geometrical requirements. The functional requirements define the design space for the needle which is the direct measuring of the cutting and stiffness forces at the tip of the needle. The geometrical requirements determine in which needle type this function is incorporated.

#### Functional requirements

- The needle must be able to measure the axial forces directly at the tip. The forces to measure are the cutting and stiffness force (see Equation 1).
- Bending of the needle should not affect the measurement on the tip of the needle.
- The function of the needle should not change due to the addition of a sensor system inside the needle in comparison to non sensorized needles in the same category. The main goal of the needle is to perform a procedure, the added force measurement must only improve the quality and quantity of the force feedback of the needle.
- The measurement range for the needle is from 0 to 15 N. In Table 1 the measured forces in literature are given. The puncture force has a range to 19.2 N but the median is very low at only 1.22 N. The cutting force is even lower with a median of only 0.95N [28].
- The accuracy of the needle must be lower than 0.01 N, in order to measure the force with enough detail. In the work by Peirs et al. [22] the accuracy of a force sensor for a needle driver was set at 0.01 N, based on in vivo tests with different needles puncturing different tissues.
- The sampling frequency must be above 100 Hz. This frequency ensures that all the information in the force profile of insertion is recorded. Soft tissue is inhomogeneous; there are a lot of internal puncture events.

#### Geometrical requirements

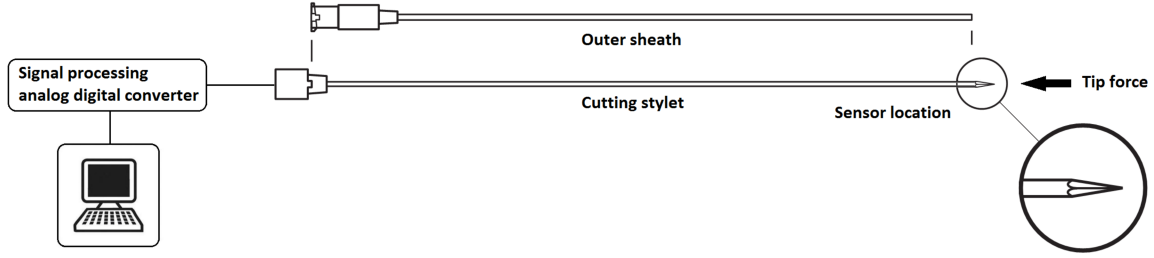
- The sensing element must fit inside an 18 G trocar needle. The size of the needle is an 18 G needle according to the Stubs wire gauge (ISO 9626)[12]. This needle size is typically used in liver, prostate and breast procedures [21].
- The type of needle is a trocar needle. Trocar needles are used in procedures for non-vascular access into solid soft tissues. Trocar needles consist of an inner stylet (trocar)  $\varnothing 1$  mm, and an outer needle (sheath)  $\varnothing 1.270$  mm. The sheath is a thin walled tube through which the intended procedure is executed. In case of diagnostic procedures this is usually the removal of tissue or fluid. The cutting stylet makes the passage for the needle and the tip forces act on the cutting stylet as discussed above. Therefore the sensing elements must be incorporated inside the stylet. Once the trocar needle is at the targeted location the stylet is removed in order to perform the procedure. The removal of the inner stylet may cause slight bending of the sheath because the needle becomes less sturdy, but the tip of the sheath stays at the targeted tissue.
- The length of the trocar needle is 20 cm. This length is the same as a commercially available 18G standard trocar needle (Cook Medical Trocar needle G02901 DTN-18-20.0-u, Cook Medical Inc., Bloomington, USA). So these can be compared, the length of the needle should be irrelevant for the manner in which the sensor system operates.
- The sensor must be placed as close to the tip as possible in order to exclude the friction forces from the force measurement.

With these requirements the design space is defined and concepts can be generated for the design of the needle.

## 2.2 Concept

### 2.2.1 General concept

The design of the needle has to meet the requirements stated in 2.1. In this section the general concept is explained. The needle is a trocar needle consisting of an outer sheath and a cutting stylet see Figure 3. The sheath is taken from a standard commercially available needle (Cook Medical Trocar needle G02901 DTN-18-20.0-u, Cook Medical Inc., Bloomington, USA), because the design of the sheath does not change.

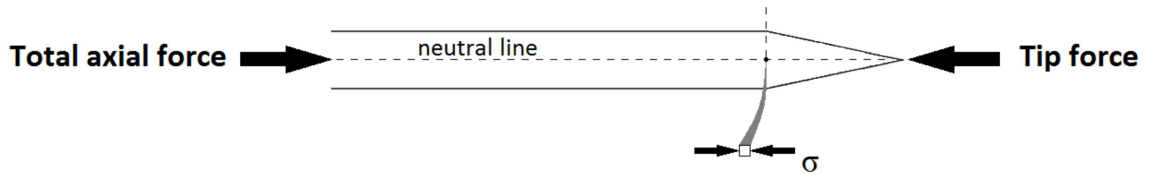


**Figure 3:** Schematic representation of the general concept. Trocar needle consisting of outer sheath and cutting stylet. The stylet contains the sensing element in the tip. The signal is converted to a digital signal so data analysis can be performed on a computer.

The cutting stylet will be equipped with a sensing element to measure the cutting and stiffness forces acting on the tip of the needle see Figure 4. From the literature it can be found that force measurement techniques which fulfill the geometrical requirements, are based on measuring strain in the material where the force acts upon[11][23]. The forces acting on the surface of the needle will give a stress distribution in the needle. The cutting and stiffness forces acting at the tip are applied axially causing a normal compressive stress. With Hooke's law the strain can be determined from the stress  $\sigma$  at a location in the needle stylet [10].

$$\sigma = E\varepsilon \quad (2)$$

In this law,  $E$  is the materials Young's modulus,  $\varepsilon$  the corresponding strain. To avoid friction forces acting on the needle the strain must be determined in the tip. In Figure 4 the vertical dotted line indicates where the friction force on the shaft is added in the stress distribution. In Figure 4 the neutral line is drawn. This indicates the neutral surface, in which the stress can only come from the normal stress components.



**Figure 4:** Force acting on the stylet causing stress in the material. See the stress  $\sigma$  at an element. In the neutral line there is no stress caused by bending of the needle [10].

The physical quantity to measure is strain, and the ideal position is determined. The following sections will give three possible sensing techniques that can fulfill these requirements.



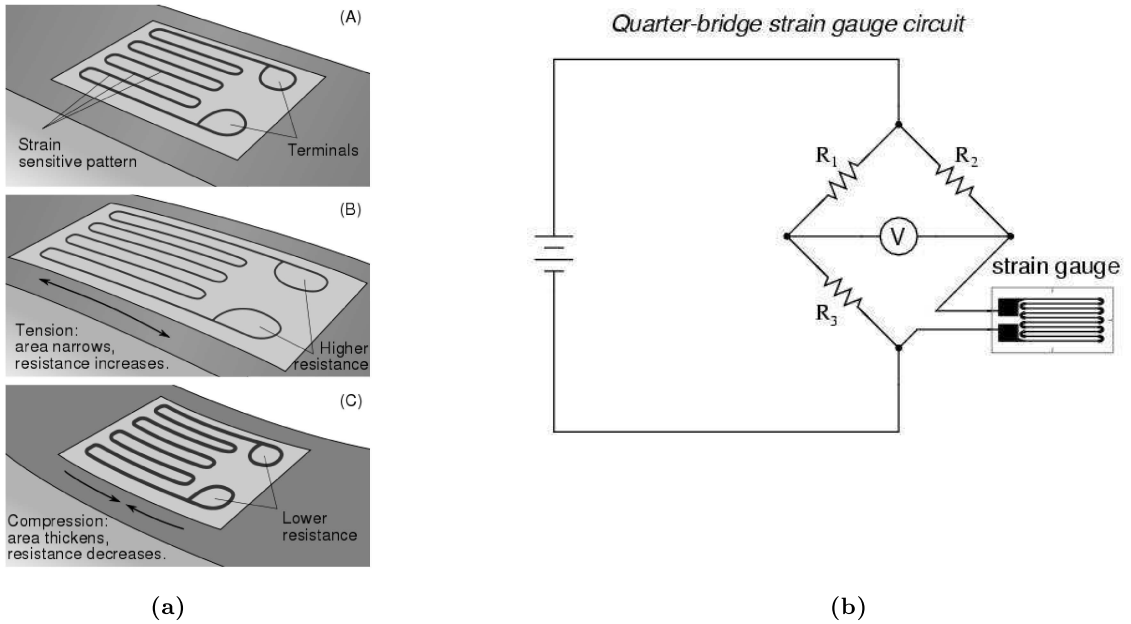
### 2.2.2 Resistive based sensors

Force sensors are often based on the measurement of strain in the material. One of the most used sensing principle for strain is the change of resistance due to deformation. Strain gauges usually consist of a metallic wire pattern or foil bonded to the structure that deforms.

As the structure deforms under loading, the resistance in the gauge will change (see Figure 5a). This change in resistance can be measured electrically. These changes are very small and are measured using a bridge circuit such as a Wheatstone bridge [26]. The strain in the gauge can be expressed as.

$$\varepsilon = \frac{\Delta L}{L} = \frac{\Delta R/R_g}{GF} \quad (3)$$

In this expression,  $\varepsilon$  is the measured strain,  $R_g$  the gauge resistance in stress free condition,  $\Delta R$  the change in resistance due to stress and  $GF$  the gauge factor. The sensitivity of the sensor gauge increases when the gauge factor increases. For metallic foils, this factor is around 2 depending on the material type.



**Figure 5:** (a) Working principle of strain gauge. The resistance in the strain sensitive pattern increases when the structure is elongated due to tension. (b) Quarter-bridge strain gauge circuit [26].

One of the smallest commercially available strain gauges is the FLK-1-17 (Tokyo Sokki Kenkyujo Co.Ltd.), which has a pattern with the dimension of 1mm by 0.7mm on a backing of 4.5mm by 1.4mm.

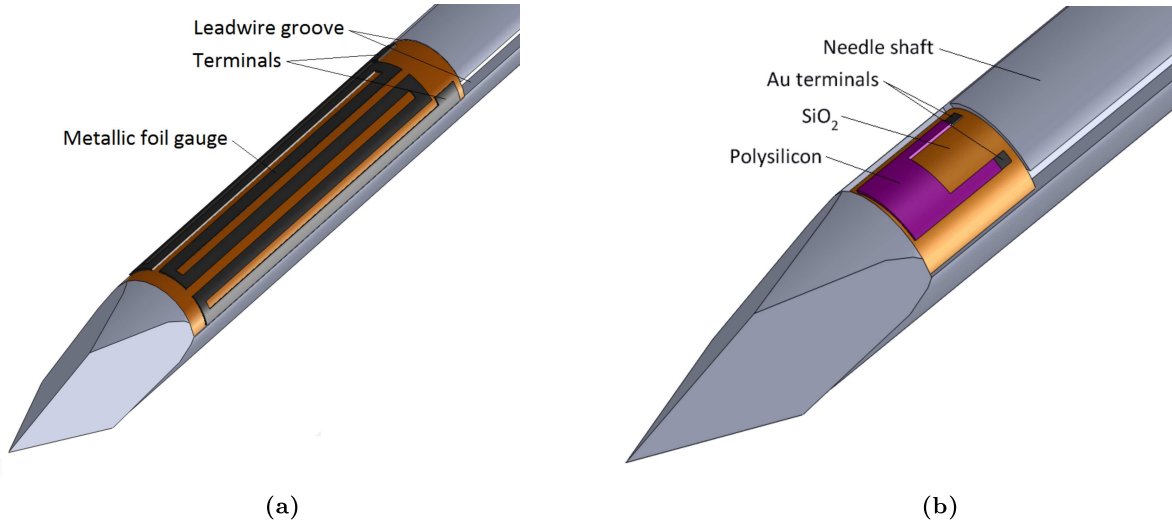
Another type of strain gauges based on the change in resistance are piezoresistive strain gauges. Piezoresistive gauges are like metallic foil strain gauges based on the changing resistivity due to applied stress. The change in resistance is mainly determined by the change in resistivity  $\rho$  instead of the change in geometry of the sensing element[13]. This stress dependent resistivity of

the material results in a much higher gauge factor in comparison to the metallic foil gauges.

$$\rho_{\sigma} = \frac{\left(\frac{\partial \rho}{\rho}\right)}{\varepsilon} \quad (4)$$

Piezoresistive sensors are fabricated in micro fabrication procedures in which piezoresistive materials are deposited onto a substrate [30]. They can be made sufficiently small to fit within the geometrical requirements for the needle stylet.

Concepts were made for the incorporation of the sensors inside the needle stylet. Figure 6 shows the tip of the needle stylet with the resistive based sensors mounted below the surface. The sensors need to be mounted below the surface to meet the geometrical requirement to create a trocar needle. In comparison to the needle stylet the metallic foil gauge is very big. As can be seen in the figure the sensors are not mounted in the neutral plane/axis of the stylet. In the case of both sensors, a lot of production steps have to be executed in order to meet the design requirements. This is because a lot of changes have to be made to the shaft of the stylet for optimal positioning of the sensor. In addition to the sensors themselves, the lead wires for the signal have to be incorporated in the stylet shaft.



**Figure 6:** Concepts of alternative sensors for tip force measurement. (a) Metallic foil strain gauge (FLK-1-17) on the surface of a cut away section. (b) Piezoresistive strain gauge on the surface of cutting stylet.

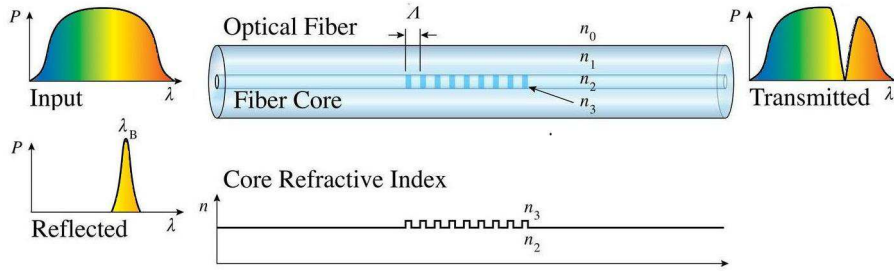
Both these concepts were not chosen to be used as the sensing technique for the prototype design which is explained in Chapter 2.2.4. The following section describes the optic strain sensing technique.

### 2.2.3 Fibre Bragg grating

A fibre Bragg grating (FBG) sensor is an optical sensor. An FBG is a structure written in the core of an optical fibre. The structure is a periodical change in refractive index of the core. When the optic fibre is illuminated with a light source, the FBG act as a stop band filter, and a narrow band of the light spectrum is reflected back into the core. The peak of the narrow band reflection is called the Bragg wavelength. This wavelength is given by.

$$\lambda_b = 2n_{eff}\Lambda \quad (5)$$

In this equation  $n_{eff}$  is the effective refractive index of the grating in the fibre core and  $\Lambda$  is the grating period.



**Figure 7:** The principle of Fibre Bragg Grating. An FBG is a periodic variation in the refractive index of the optic fire core. From a broadband input spectrum the Bragg wavelength is reflected by the grating. Other wavelengths pass through the grating.

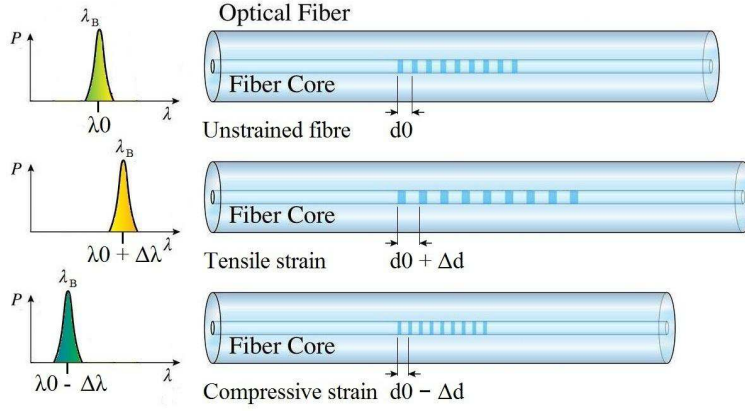
The Bragg wavelength is affected by parameters such as strain, temperature and pressure. In Figure 8 the sensing principle can be seen. When the fibre is stretched, the effective refractive index and the grating period increases. This will shift the Bragg wavelength to a higher wavelength. When the fibre is shortened, the Bragg wavelength peak will shift to a lower wavelength. The FBG has a cross sensitivity for strain and temperature. The shift in the wavelength is given by [5].

$$\Delta\lambda_b = 2\left(\Lambda\frac{\partial n_{eff}}{\partial T} + n_{eff}\frac{\partial \Lambda}{\partial T}\right)\Delta T + 2\left(\Lambda\frac{\partial n_{eff}}{\partial l} + n_{eff}\frac{\partial \Lambda}{\partial l}\right)\Delta l \quad (6)$$

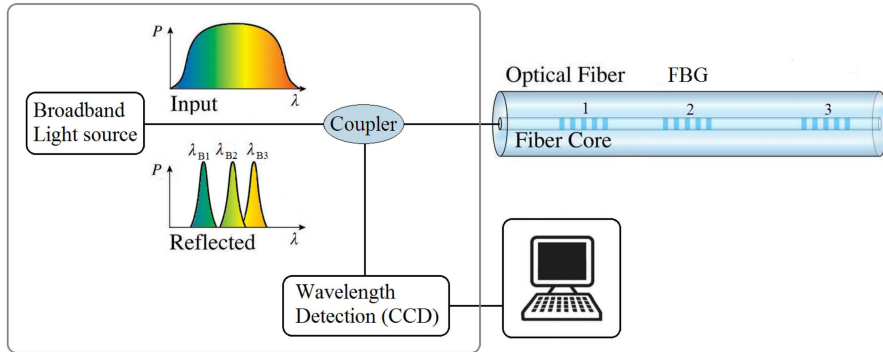
Where  $n_{eff}$  is the effective refractive index of the fibre core,  $\Lambda$  the grating period. A typical wavelength shift sensitivity to strain is  $\sim 0.64 \text{ pm}/\mu\epsilon$  and wavelength shift sensitivity for temperature  $\sim 6.8 \text{ pm}/^\circ\text{C}$  [24].

The changes in Bragg wavelength have to be interrogated. Figure 9 shows the basic setup for a sensing system. The interrogator uses a broadband spectrum input and through a coupler the reflected spectrum is separated and detected with a Charge-couple Device (CCD) linear array. Different sensing pixels on the CCD array will measure different wavelengths of light. The centre of gravity of the Bragg wavelength peak is expressed as a pixel coordinate on the CCD sensor. Multiple FBG can be interrogated and they can be spatially divided in a single optic fibre. To discriminate between different FBG sensors in the optic fibre wavelength division multiplexing can be used. Each FBG in the array has its own unique Bragg wavelength and thus its own wavelength peak in the reflected spectrum.

The fibres are very small and are immune to electrical noise, which makes it excellent in most clinical environments. There are number of ways in which they can be sterilized and have good biocompatibility characteristics.



**Figure 8:** Principle of wavelength shift. When the grating period increases due to a stimulus such as tensile strain or increasing temperature the wavelength shifts to a longer wavelength. When the period decreases for example under compression the wavelength shifts to a shorter one. [19]



**Figure 9:** Schematic diagram of the FBG sensor system. The interrogation unit (Deminsys Python) illuminates the optic fibre and a coupler separates the reflected spectrum, which is measured with a CCD. FBG sensors can be multiplexed, this example has 3 FBG's and therefore 3 corresponding peaks in the reflected spectrum. The measurement data from the interrogation is transferred to a PC [17].

### 2.2.4 Sensor choice

A sensor choice has to be made for the design of the needle, from the three sensing techniques explained in the previous sections. For all techniques holds that the functional and geometrical requirements can be met. Therefore Table 2 gives the sensor choice. The first factor to look into is the resolution in which the sensing techniques can measure range. The piezoresistive gauges have a higher gauge factor than metallic foil gauges thus are more sensitive to strain and have a better resolution. For FBG the strain is not measured in resistance but with a wavelength shift and also offers a good resolution [11][23]. An important feature is the size of the sensors. Metallic foil gauges are the biggest of the three with a large transducer element in comparison to the size of the needle. The piezoresistive can be made very small and since these are micro fabricated they can be custom fitted to the needle stylet, with sensor dimensions in micrometer scale. For metallic foil gauges and piezoresistive gauges holds that two isolated lead wires have to be connected and run through the stylet shaft. FBG's are intrinsic optic sensors, the transducer is within the optic signal carrier. With the fibre dimensions of only  $\varnothing 0.145\text{-}0.16\text{ mm}$  they offer the best possibilities to mount them in the stylet. The sensor has to be positioned at the tip of the needle in the neutral axis. The position of the transducer is dependent on the size of the transducer, but the transducer size of piezoresistive sensors and FBG are comparable. With the circular cross section of the optic fibre, the transducer can be fitted axis symmetrical in the centre of the stylet in the neutral axis. Last of the assessment factors is ease of fabrication; a prototype of the needle must be produced. The piezoresistive sensor has to be microfabricated. For a single prototype these are a lot of production step to create the sensors it self. Also the modifications to the shaft of the needle are extensive to correctly position the sensor. The total score gives that the FBG has the most advantages to be fitted in the needle, and this will be the sensor technique used inside the prototype.

**Table 2:** Selection of sensor technique

	Metallic foil strain gauge	Piezoresistive gauge	Fibre Bragg Grating
Resolution	-	++	+
Size	--	+	++
Sensor position	--	+	++
Ease of fabrication	-	--	+

---

## 2.3 Design

The following section gives a detailed description of the prototype. All the components and their functions are described. The build prototype is depicted in Figure 10.

### 2.3.1 Overview design

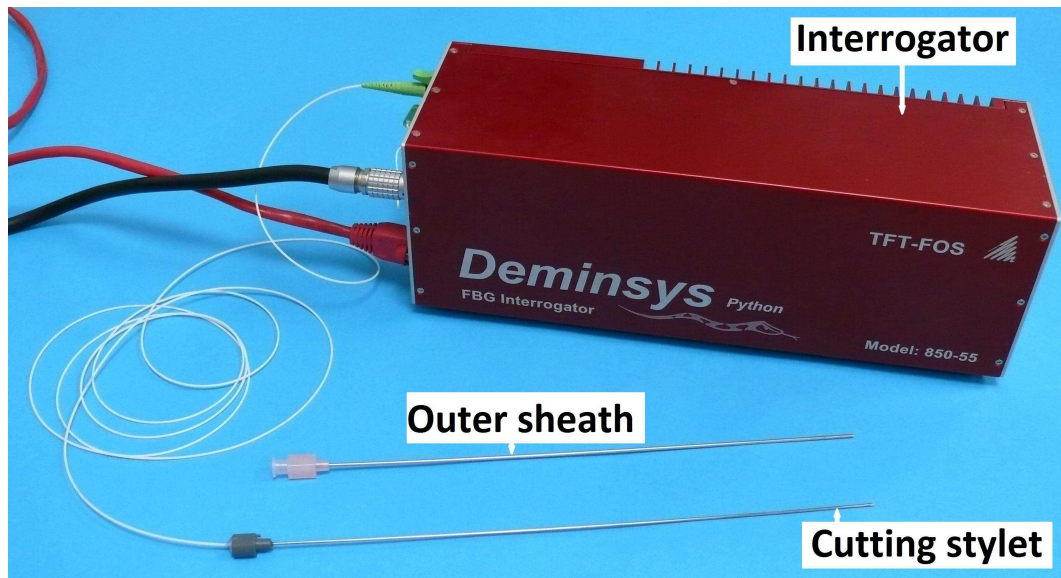
The general concept is to determine the tip force from strain measurement in the tip of the needle in the centre of the needle. From the sensing methods the optical sensing method provides the most advantages in comparison to the other sensing methods. The FBG is the smallest as a system because it is an intrinsic sensor; the signal carrier and the transducer are in a single small optical fibre. This gives the best possibilities to position the sensor in the neutral axis of the stylet shaft.

The conceptual design is a 18G trocar needle with a length of 20 cm as stated in the geometrical requirements. The type of needle is a trocar needle and the dimensions are the same as a commercially available 18G standard trocar needle (Cook Medical Trocar needle G02901 DTN-18-20.0-u, Cook Medical Inc., Bloomington, USA). The needle consists out of a cutting stylet and an outer sheath. The outer sheath is taken from a regular needle because there are no changes made to the design of the outer sheath. The outer sheath has an echo tip consisting of hundreds of microscopic dimples on the needle surface which will ensure a strong echo reflection under ultrasound. The hub of the outer sheath has a Luer taper (ISO 594) to form the connection between the cutting stylet or other medical equipment which is needed for a specific procedure.

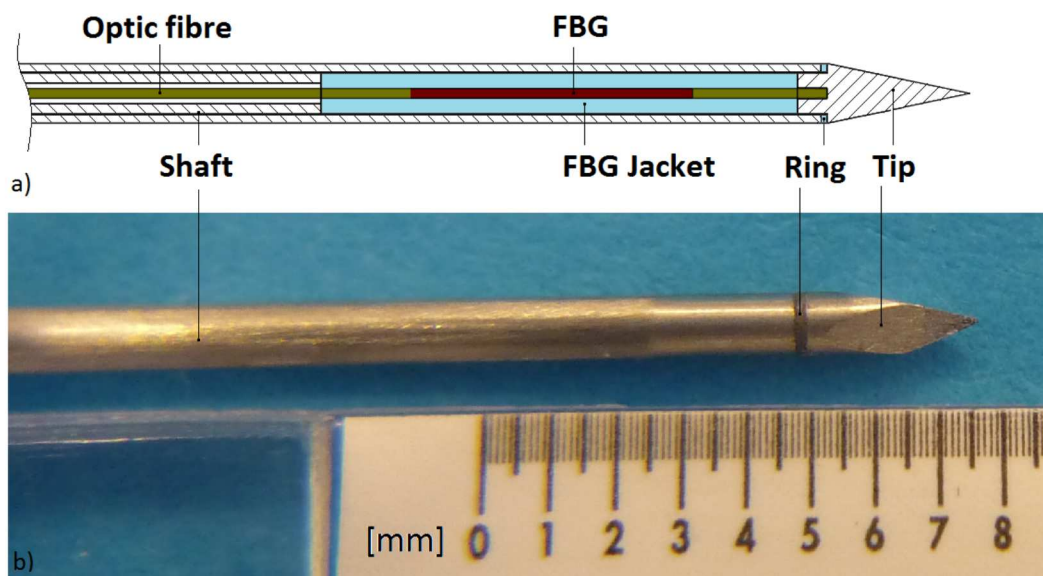
The cutting stylet contains the sensing FBG to measure the tip forces. In Figure 11 the tip of the cutting stylet can be seen with a cross section. When the needle is inserted in soft tissue the diamond shaped tip creates a passage. The forces acting on the tip create a stress inside the needle shaft. The tip has a single degree of freedom because the ring forms a compliant connection between the tip and the shaft. The needle tip compresses the FBG jacket, which is bonded to the FBG in optic fibre running through the centre of the needle. The jacket surrounding the FBG has a low stiffness so the stress in the material creates a strain big enough to satisfy the functional requirements of the measurement range and resolution. The optic fibre runs through the centre of the shaft to the hub of the needle. The optic fibre is connected to an interrogation unit which will measure the wavelength shift corresponding to the strain. It is expected that the force-wavelength behaves according to a linear relationship. The concept design consists out of seven custom parts which need to be fabricated and assembled.

The following section describes each of the parts and their function in detail. Detailed drawings of the parts can be found in the Appendix F





**Figure 10:** Prototype needle with sensing element in the cutting stylet. Outer sheath taken from Cook 18 G trocar needle (Cook Medical Trocar needle G02901 DTN-18-20.0-u, Cook Medical Inc., USA).

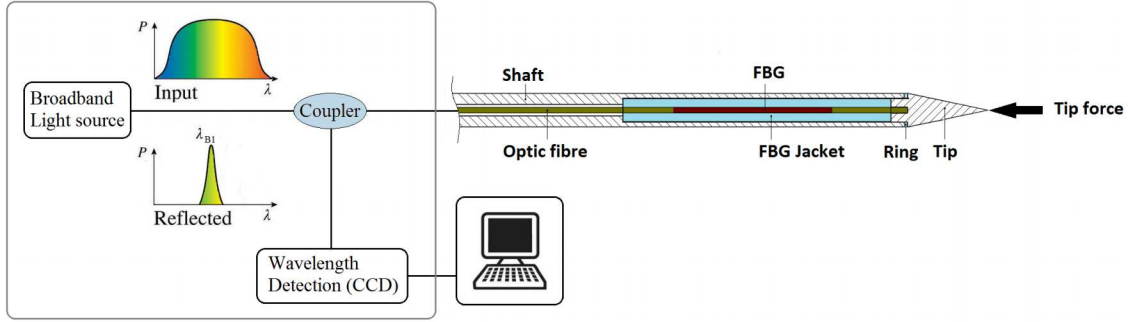


**Figure 11:** a) Cross section of the needle tip of the concept design. The tip creates the passage through the tissue and compresses the FBG jacket. The ring forms the connection between the tip and the shaft. The FBG jacket surrounds the FBG which measures the strain. b) Photograph of prototype needle tip.

### 2.3.2 Optic fibre

The optic fibre contains the Fibre Bragg grating which is the sensing element for the prototype. The optic fibre has a recoating diameter between 0.145-0.165 mm. The FBG has a length of 5 mm with a central wavelength (Bragg wavelength in strain free condition) of 856 nm  $\pm$  0.5nm. The interrogation of the FBG in the prototype needle is performed with an FBG interrogator (Deminsys Python 850-55, Technobis Mechatronics BV, Uitgeest). This interrogator has the following optical specifications.

- Wavelength of operation: 830 - 870 nm
- Maximum sampling frequency: 20 kHz
- Number of optical channels: 1 - 3
- Maximum number of gratings per channel: 8
- Wavelength repeatability:  $\leq 2$  pm
- Spectral spacing sensors: 5 nm
- Strain repeatability:  $\leq 3$   $\mu$ strain



**Figure 12:** Schematic diagram of the prototype needle. The interrogation unit (Deminsys Python) illuminates the optic fibre and a coupler separates the reflected spectrum which is measured with a CCD. The data are recorded onto a PC and analyzed in Matlab.

In Figure 12 the schematic view of the system is shown. The interrogator is connected to a PC where the data are logged onto hard drive. The data analysis will be performed in Matlab R2011b (Matlab R2011b, The Mathworks Inc., Natick, USA). The output of the interrogator is given as a pixel coordinate with a range of 0 to 255. The expected relationship over the measurement range is a linear relation between the applied tip force and the measured FBG output.

$$\Delta F[N] = \alpha * \Delta \lambda [Pixel] \quad (7)$$

In this equation the force  $F$  change is given in Newton, and the change in pixel coordinate is multiplied with a gradient  $\alpha$ . This relationship has to be verified and the gradient has to be determined through calibration of the needle. As can be seen in the overview of the design and in this section there is only one FBG in the optic fibre so compensation for temperature is not possible. For this prototype the temperature of the operating environment has to be known in order to compensate for temperature.



### 2.3.3 FBG Jacket

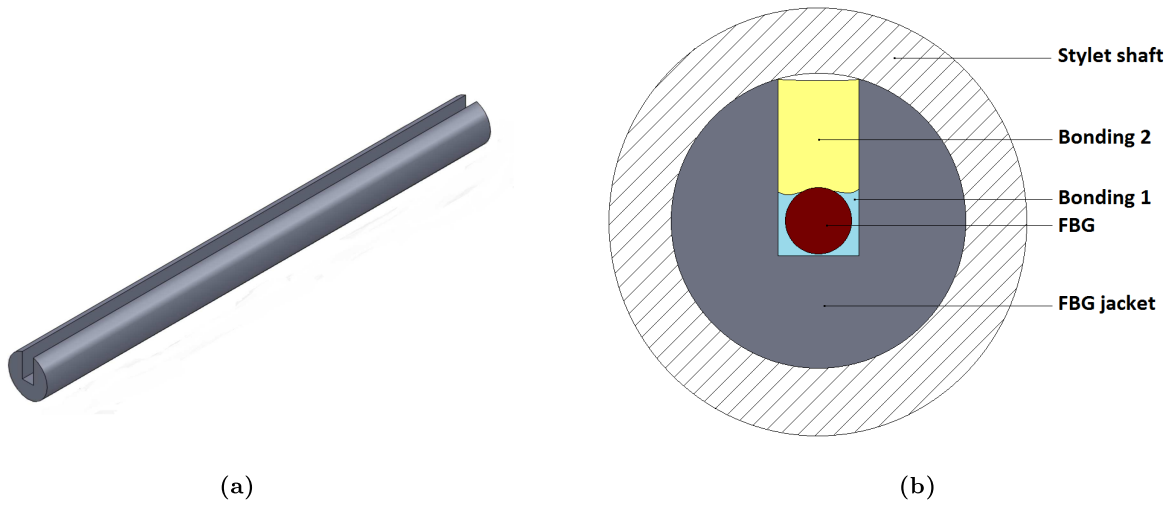
The tip force is measured as strain in the FBG. The FBG is located in the centre of the stylet. The stress  $\sigma$  in the material caused by the tip force has to be transferred to the FBG, so the FBG has to be bonded to the stylet. In the simplest case the FBG is bonded directly to the metal of the stylet. If the optic fibre is bonded directly to the metal of a needle with the geometry as stated in the design requirements, the maximum measured strain that corresponds to a maximum force of 15 N is,

$$\varepsilon = \frac{\sigma}{E} = \frac{F}{A * E} = \frac{15N}{(\pi(0.5015mm^2 - 0.08mm^2)^2 * 200GPa)} = 97.4\mu\varepsilon \quad (8)$$

In this equation  $E$  is the materials Young's modulus (for the stainless steel needle this is 200 GPa),  $A$  is the cross sectional surface area of the FBG. This strain is very low. Looking at the commercially available FBG sensors and the corresponding FBG interrogators the strain repeatability is  $\leq 3 \mu\varepsilon$ . This strain needs to be increased for the desired measurement range and resolution. To increase the strain over the measurement range from Equation 8 either the cross sectional surface area has to be decreased or the Young's modulus of the material has to be decreased or both.

As can be seen in the cross section in Figure 11 the FBG is encapsulated by a jacket. This tip compresses this jacket. The jacket is made from a different material with a lower Young's modulus. PVC is the chosen material for the jacket it has a low Young's modulus of 3.3 GPa in comparison to the metal shaft. The jacket reduces the cross-sectional surface area and therefore increases the strain. The shape of the FBG jacket is a tubular section, and to fit inside the geometry of the stylet it is  $\varnothing 0.7$  mm and has a loose fitting (f7, NEN-ISO 286-2 ). The diameter is the same as the inner tube of the shaft (see Chapter 2.3.5). The length of the jacket has to fully enclose the FBG and thus requires a minimum length of 5 mm. The FBG location is not visible from the outside of the fibre. To provide a safety margin for assembly the length of the tubular section is set to 8 mm. In Figure 11 it can be seen that the tip also compresses the ring (explained in Chapter 2.3.4), the maximum strain for the maximum force that can be measured in this configuration is estimated to be  $\geq 182.2 \mu\varepsilon$ . For this estimation the metal tip is considered rigid.

To fit the optic fibre in a tubular section over this length it is not possible for conventional methods to drill a hole with the diameter of the fibre ( $\varnothing 0.16$  mm) over the length of the section. Therefore a groove is milled over the length of the section to a depth of half the diameter of the jacket plus half the diameter of the optic fibre. The fibre is positioned in the groove with the FBG in the centre and bonded to the surface (see Figure 13b). The bonding is an acrylate adhesive with a low viscosity (Loctite 4061, Henkel KGaA, Germany). The space that remains left in the groove is filled up with a filling bonding (see Figure 13). This makes sure that the FBG is fully encapsulated within the jacket. The bonding for this must have a higher viscosity to fill the gap (Loctite 4031). Both these bondings are appropriate for the use in medical devices such as needles and catheters.

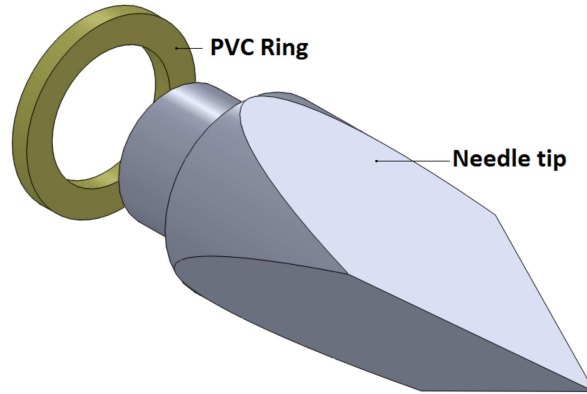


**Figure 13:** (a) FBG Jacket. The PVC jacket is bonded to the FBG. A groove is machined over the length of the tubular section for the optic fibre. (b) Cross-section of the stylet prototype. The FBG is bonded in the FBG jacket with an acrylate bonding (bonding 1). And the jacket is filled with a bonding (bonding 2) to form a circular section.

### 2.3.4 Tip & Ring

To transfer the forces to the FBG the tip has to compress the FBG jacket directly. The tip has to have flexibility of movement to do this so the connection between the tip and the shaft has to allow for this compliance. A direct connection is not sufficiently compliant. Therefore a plastic ring is introduced between the shaft and the tip (see Figure 11). The tip has a stepped diameter and is inserted partly into the shaft (see the cross-section in Figure 11). The fit between the shaft and the tip is a loose fit (f7, NEN-ISO 286-2). The stepped diameter also prevents the tip from tearing by unintentional transverse forces on the tip. The surfaces that have to be bonded to each other are the surface between the top of the FBG jacket and the back of the tip. The top and bottom of the ring are bonded to the shaft and the tip. It has to be prevented that glue forms a direct connection between the tip and the metal shaft, because this would negate the flexible movement of the tip. The bonding is an acrylate adhesive (Loctite 4061, Henkel KGaA, Germany). This is a biocompatible bonding often used in assemblies of limited contact span devices such as needles and catheters. The ring has to have a lower Young's modulus than the metal of the shaft and tip, but still has to form a sturdy connection in order to be functional as a cutting stylet for the needle. The ring is therefore chosen to have a thickness of 0.1 mm, it is made of PVC. If the prototype is used in living tissue, the ring is the part that is exposed to the tissue. PVC is a biocompatible plastic and often used in medical applications [1]. For the application in needles, the plastic has to be evaluated according to ISO 10993 as a limited contact span implant device. If the tip of the needle is considered rigid, the amount of strain for the maximum measurement range is estimated to be  $\geq 182.2 \mu\epsilon$ . A similar FBG set-up has been used successfully in medical instruments where this force range and thus the strain range was much lower [11].

The needle tip is a tri-facet diamond shape tip used for trocar needles. The tip is rotational symmetric around the axis of the needle. For symmetric needles the resultant force from the load distribution on the cutting faces goes through the centre of the needle. This prevents needle bending which is the case for non-symmetric shaped tips (such as beveled or Tuohy). If necessary the needle tip shape can be changed without changing the method by which the tip force is measured. The needle tip for the prototype is produced by customizing tip from a commercially available 18G standard trocar needle (Cook Medical Trocar needle G02901 DTN-18-20.0-u, Cook Medical Inc., Bloomington, USA).

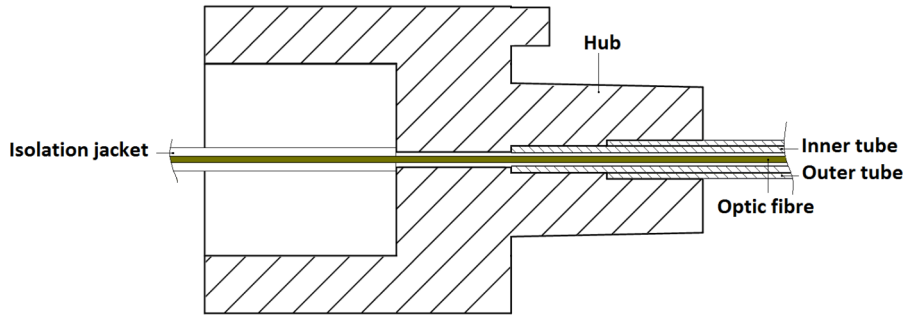


**Figure 14:** Tip of the prototype needle, tri facet diamond tip shape, and the PVC ring. The tip creates the passage through the tissue and the tip compresses the FBG. The ring forms the connection between the tip and the shaft.

---

### 2.3.5 Shaft & Hub

Unlike a regular cutting stylet, the shaft of the design is hollow. This is because the optic fibre runs through the lumen of the shafts. The shaft could be made out of a single tube with a diameter of  $\varnothing 1 \text{ mm} \times 0.35 \times 222.95 \text{ mm}$  where a stepped bore is made for the FBG jacket. However, a bore with the length of the FBG jacket and the diameter of the jacket is difficult to manufacture. Therefore two tubes are fitted within each other to form the cutting stylet shaft as can be seen in Figure 11 and 15. The tubes are stainless steel (AISI 304) capilair tubes with the outer tube dimensions of  $\varnothing 1 \text{ mm} \times 0.70 \times 222.95 \text{ mm}$  and the inner tube dimensions of  $\varnothing 0.7 \text{ mm} \times 0.35 \times 217 \text{ mm}$ .



**Figure 15:** Cross section of the needle hub and part of the shaft. Shaft is built out of two tubes within each other. The optic fibre runs through the lumen of the inner tube.

The hub of the cutting stylet holds the needle shaft. The hub is made of PVC because it is easy to fabricate and because it bonds to the shaft of the needle with the same bonding used between the optic fibre and the FBG jacket (see Chapter 2.3.3). The hub has a stepped bore to bond both the inner and the outer tube. The optic fibre runs through the centre of the hub, and it is bonded to the hub. There's a flexible isolation jacket between the hub and the connector to protect the optic fibre. Through the centre of the hub runs the optic fibre and the sheath is bonded to the hub. The hub of the cutting stylet fits onto the hub of the trocar (outer cannula) with a Luer taper (ISO 594) Normally needle hubs are color coded and the color for 18 G needles is pink, but since this is a prototype for evaluation, the coding is omitted.

### 3 Calibration

In Chapter 2 the concept design is presented for a needle that can measure forces at the tip of needle. A prototype of this design is built with an FBG as the sensing element for the tip forces. Calibration of the prototype is needed to determine the behaviour of the sensor. The output of the sensor is a wavelength peak shift expressed in a pixel coordinate. This has to correlated to the force applied at the tip. The main goal of the calibration is to determine the accuracy of the prototype, and to test whether the force measurement meets the design requirements of Chapter 2.1. The design for this first prototype is also sensitive to temperature changes. The calibration has to determine the magnitude of this effect. In section 3.1 the calibration set-up is described. The calibration protocol is explained in section 3.2. The results of the calibration and the analysis of these results can be found in 3.3. This chapter ends with a conclusion 3.4 of the calibration results.

## Material & Methods

### 3.1 Calibration Set-up

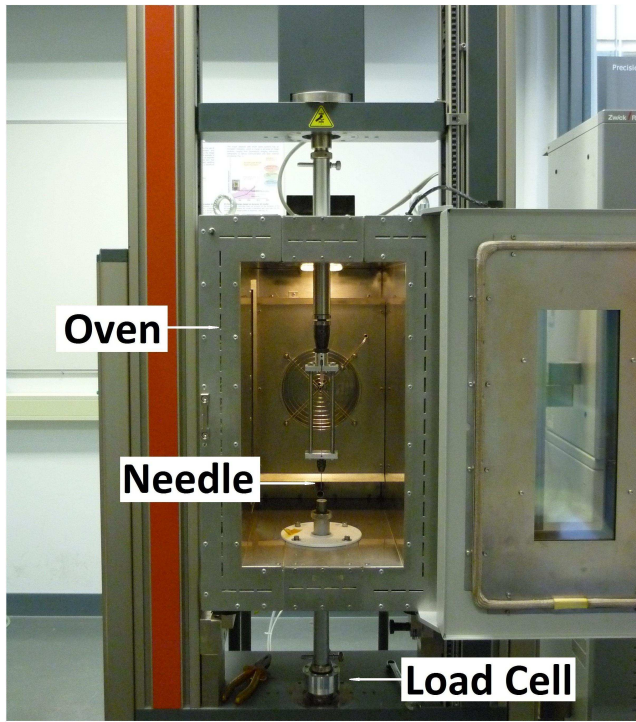
Calibration was carried out in a universal testing machine (Zwick Roell Allround-line Z005, Zwick Roell GmbH Co. KG, Ulm, Germany), which is considered the standard to which the prototype is being calibrated.

The calibration is performed inside a temperature chamber. The universal testing has a 1 degree of freedom linear translation stage. The needle is mounted to the translation stage in a vertical plane. The needle is positioned perpendicular to the load cell which is located at the bottom outside the temperature chamber. The needle is mounted in a vise, the tip of the needle is supported with a self centering three jaw chuck (see Figure 16) which prevents buckling of the needle during calibration.

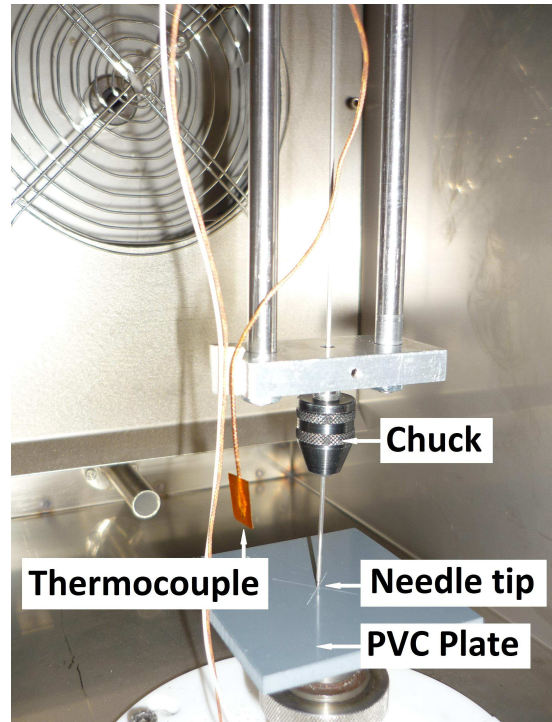
During the calibration the needle is axially translated onto a PVC plate, in order to protect the sharp stylet tip. The shape of the tip is set in the PVC. The PVC is mounted on the load cell of the universal testing machine. The load cell of the testing machine has an accuracy of  $<\pm 0.5\%$  (ISO 7500-1) and is sampled at a frequency of 10 Hz.

The temperature inside the chamber is held constant during calibration and an extra thermocouple is used to measure the temperature near the tip of the needle (see Figure 16). This extra thermocouple is used instead of the thermocouples from the temperature oven because these are located too far away from the needle tip. The universal testing machine is operated with testXpert2 (testXpert2, Zwick Roell GmbH Co. KG, Ulm, Germany) which also logs the data from the load cell and testing machine. The quantities that are recorded and digitized are position, speed, force and temperature.

The output of the FBG interrogator (wavelength shift expressed in pixel coordinate) for the prototype is down sampled to 100 Hz. For both setups the recorded data are exported and analysed in Matlab R2011b (Matlab R2011b, The Mathworks Inc., Natick, USA).



(a)



(b)

**Figure 16:** Calibration setup on the universal testing machine. (a) Setup is within a temperature chamber. The needle is placed in a vise attached to the translation stage. The needle is mounted perpendicular to the load cell. The load cell is placed at the bottom outside the oven. (b) Setup at needle tip. The needle is held by a self centering chuck to prevent needle buckling. The tip presses on a PVC plate for protection. The PVC plate is rigidly attached to the load cell. The thermocouple measures the temperature near the needle tip.



### 3.2 Calibration Protocol

For the calibration the prototype needle is subjected to repeated measurements with a predetermined load profile (ISO-376). For a single measurement a load profile is performed over a force range of 0-10 N. The load profile consists of four parts.

In the first part (see Figure 17a) a period of 60 seconds there is no movement and there is no contact between the tip and the PVC, this is used to record the zero signal of the unloaded transducer.

The second part of the load profile is the loading of the needle by moving it in downward direction onto the PVC plate with a constant velocity of  $17 \mu\text{m/s}$ . In this part the machine is position controlled. The travel continues until the load cell reaches 10 N.

At 10 N the third part starts, for the duration of 60 seconds the universal testing machine is force controlled and held at a constant force of 10 N. After this in the fourth period the needle is unloaded by moving the needle upwards with a constant velocity of  $17 \mu\text{m/s}$ . The unloading phase stops when the load cell reaches 0 N.

The needle is calibrated at a constant temperature inside the temperature chamber. The calibration cycle is executed 5 times per temperature. After 5 cycles the temperature is increased with  $2^\circ\text{C}$  increments starting at  $26^\circ\text{C}$  till  $40^\circ\text{C}$ . Temperatures below  $26^\circ\text{C}$  in this setup were not possible because the temperature chamber is not equipped with a cooling unit.

During a calibration cycle the quantities position, force, temperature and time are recorded from the universal testing machine, and the wavelength shift expressed in pixel coordinate is recorded from the FBG interrogator. After the calibration results are gathered data analysis is performed in Matlab R2011b. The raw data are filtered to remove unwanted noise components. The filtered datasets are correlated to each other and force is plotted against pixel coordinate, and for this the linear relationship is determined.

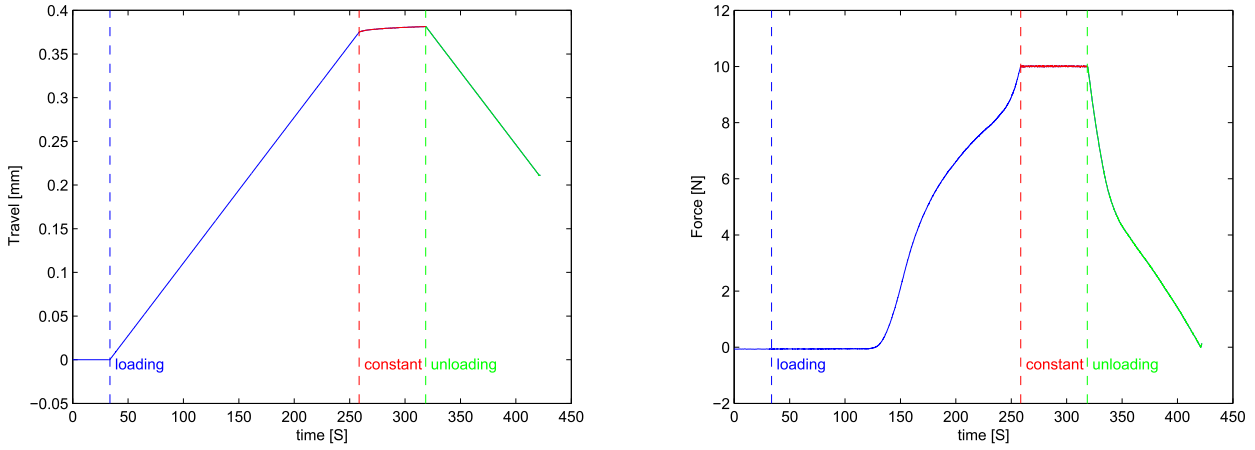
**Table 3:** Summary of calibration

Number of calibration cycles	45
Force range	0 - 10 N
Temperature range	$26 - 40^\circ\text{C}$
Temperature increments	$2^\circ\text{C}$
Speed	$17 \mu\text{m/s}$
Sample frequency universal testing machine	10 Hz
Sample frequency FBG interrogator	100 Hz
Recorded quantities universal testing machine	Force, position, temperature and time
Recorded quantities from prototype	Pixel coordinate

## Results

### 3.3 Calibration Results

During the each calibration cycle the load profile was executed. Figure 17a shows the position of the needle during a calibration cycle. During the period where the force is held constant at 10 N the position still slightly increases. This is caused by the sharp needle tip cutting into the PVC plate during each cycle. Figure 17b shows the corresponding force profile measured by the load cell is shown. The force profile shows a nonlinear increase in force with a linear increase in position.



(a) Position of the needle. Travel is  $17 \mu\text{m/s}$  during loading (blue) and unloading (green). When the force is held constant (red) the position changes due to the cutting into the PVC plate.

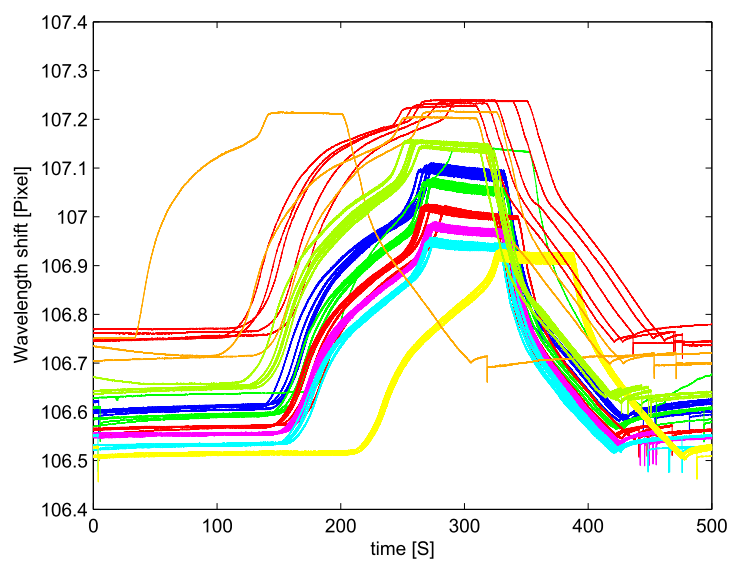
(b) Force profile. The needle is loaded (blue) then the force is constant for a period of 60 seconds (red) before unloading the needle (green). With a linear increase in position there is a nonlinear increase in force.

**Figure 17:** Example of force and position over time recorded by the universal testing machine.

The output from the FBG interrogator can be seen in Figure 18. All the cycles show a similar characteristic which resembles the force profile measured by the load cell. This gives an indication that the force-wavelength relationship is linear. The data sets are shifted in time because the calibration is manually started.

The FBG interrogator data are filtered. A low pass Butterworth filter with zero phase is used to remove high frequency noise components from the signal. The frequencies below the cut off frequency are passed uniformly, after the cut off frequency rolls off towards zero in the stopband. The higher the order of the filter the shorter the stop band. The order used in the data analysis of calibration results is a 5<sup>th</sup> order Butterworth filter with a cut off frequency of 10 Hz. After filtering the data are still erratic and a moving average filter is applied to smooth the data. The moving average filter is a type of filter which replaces each data point with the average of the neighbouring data points defined within the span of 100 sample points. The filtering applied to the output of the FBG interrogator has a root mean square error of 0.0015[Pixel].





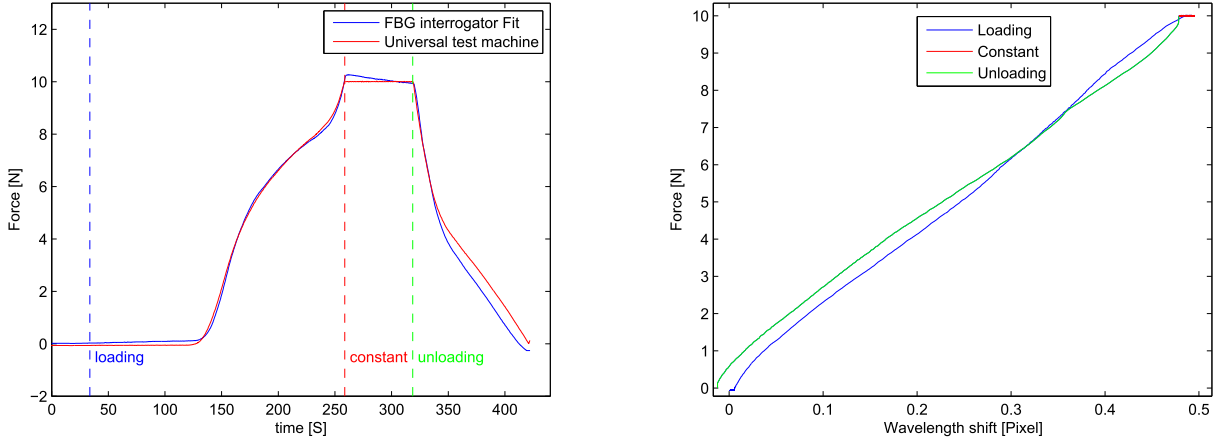
**Figure 18:** Wavelength shift expressed in pixel coordinate of all calibration data sets for all temperatures.

### 3.3.1 Data Analysis

For the calibration the data from the interrogator needs to be correlated to the data from the universal testing machine. The two systems are started manually separately so there are no easy points which can be used to correlate the sets. The relationship that needs to be determined is the force - wavelength relationship so the data from the FBG is fitted with a least squares approach to the output from the load cell. An error function is defined and this error function is minimized.

$$error(\alpha, \beta, \gamma)^2 = \sum (Z(t) - \alpha D(t + \beta) + \gamma)^2 \quad (9)$$

In this equation  $Z(t)$  is the vector containing the dataset from the universal testing machine,  $D(t)$  is the data vector from the FBG interrogator. The constant term  $\alpha$  scales the interrogator data,  $\beta$  is the shift in time and  $\gamma$  is the shift in y direction. When the prototype is used there always has to be a zero measurement in order to correct for the difference measurement of the FBG interrogator.



(a) Example of a least Squares error fit for a cycle at  $30.6^{\circ}C$ . (b) Force versus FBG interrogator output of 1 cycle at  $30.6^{\circ}C$ .

**Figure 19:** Data analysis for a single calibration cycle.

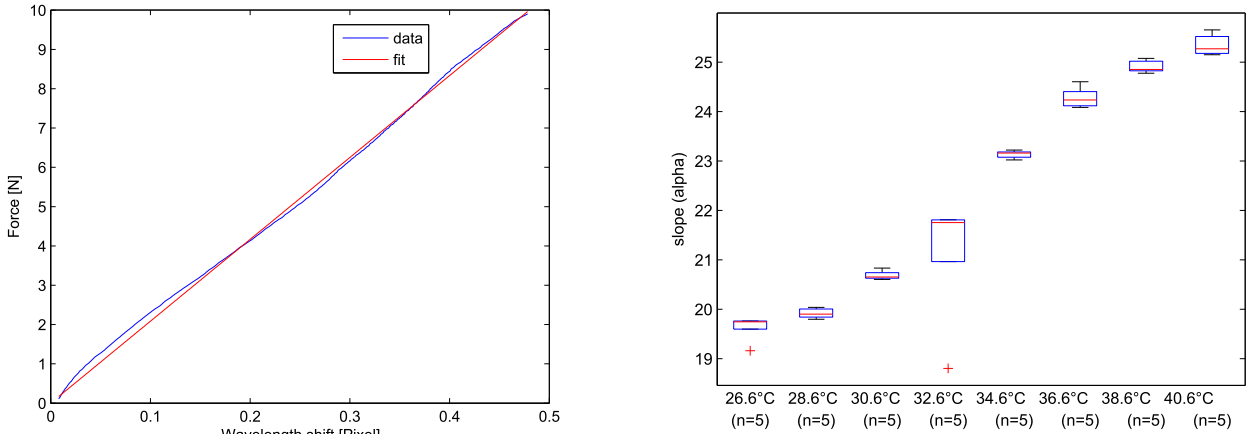
Figure 19b shows that there is some hysteresis in the prototype. At the phase where the force is held constant the output of the interrogator decreases. During the unloading it can also be seen that the fit ends below zero. The amount below zero is the same as the overshoot in the beginning of the phase where the force is held constant.

### 3.3.2 Linear Regression

Figure 19b shows, that the force-wavelength relationship appears to be linear. The linear relationship is approached with a linear regression to get a best fit straight line through zero. This can be written as follows.

$$\Delta F[N] = \alpha \Delta D[\text{Pixel}] \quad (10)$$

In this equation  $\Delta D$  is the pixel change from the FBG interrogator. This pixel change is related to the Bragg wavelength shift.  $F$  is the force in Newton and  $\alpha$  is the slope coefficient. A linear regression from 0-10 N gives the values for  $\alpha$ ; these can be seen in Figure 20b for the different temperature sets. When the temperature increases the slope coefficient increases. For all the temperature sets the standard deviations are small. Except at 32.6 °C this set contains an outlier.

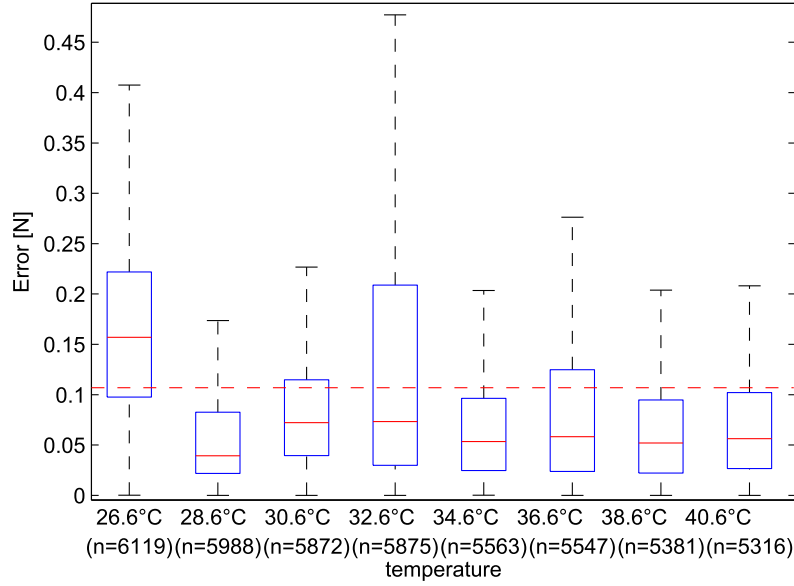


(a) Example of linear regression fit of the filtered data for 1 cycle at 30.6 °C

(b) Boxplot of slope parameter  $\alpha$  for all temperature sets see Equation 10. The red mark in the set of 26.6 °C and 32.6 °C indicates an outlier.

**Figure 20:** Linear regression

Figure 20a shows the linear regression, the difference between the data and the fit are due to non-linearity. To determine the accuracy of the sensor the linearity error needs to be quantified. The linearity error is the deviation of the output from the best straight fit line. The best straight line used to determine the linearity error makes use of the median per temperature set for the slope coefficient (see Figure 20b). Figure 21 shows the absolute linearity error for all the data points in a temperature set. In the first temperature set the error is higher in comparison to the other temperature sets. The mean of the linearity error for all the samples for all temperature sets is 0.1069 N. From the boxplots it can be seen that there are still a lot of data points which have a high error, and from 20a it can be seen that this error is the biggest in the lower region (0-4 N) of the measurement range. For all data sets the error curves around the ideal best fit in a similar method.



**Figure 21:** Boxplot of linearity error for a range of 0-10 N, for all data points per temperature set. The coefficients used for the fit are the medians of the slope coefficient in a temperature set (see Figure 20b). The red line indicates the mean of the error (0.1069 N) for all data samples from all temperature sets.

### 3.4 Conclusion calibration

From the calibration results it can be concluded that the prototype can measure force applied at the tip of the needle. The prototype is calibrated over a range of 0-10 N, and in this range the force-wavelength relationship shows a linear behaviour. For this linear behaviour a best fit straight line is fitted and to determine the accuracy of this approach the linearity error is determined (see Figure 21), the mean for this error for all the calibration cycles at different temperatures is 0.1069 N. This error between the filtered data and the fit is the highest in the lower range of the measurement (0-4 N). The slope coefficients have a small standard deviation indicating a good repeatability. In the design of the prototype it was already indicated that the FBG sensor is sensitive for temperature changes and that this prototype should operate in a temperature constant environment. The calibration confirmed this sensitivity to temperature and with a linear increasing temperature the output of the FBG interrogator increases linearly. The temperature also has an effect on the slope coefficient for the force - wavelength relationship; with increasing temperature the slope coefficient increases. This means that the temperature in which the prototype operates has to be accurately known in order to determine the slope coefficient by interpolation.

## 4 Insertion experiment

The design presented in this thesis is meant to be used in a clinical environment. The force information from the system can be used to improve needle insertion procedures. One of the uses for the force information is the identification of different tissue layers along the path of the insertion. This chapter describes the insertion experiment with the prototype needle. The aim for this experiment is to validate if the prototype needle can detect transition between different tissue layers. Insertion is performed in a phantom sample containing a membrane. The second sample is an ex vivo sample from a porcine liver. During the insertion the total axial force is compared to the output of the prototype. In section 4.1 the set-up for the insertion experiment is described. The protocol for the insertion can be found in section 4.2. In section 4.3 the samples which are used for the experiment are described. The results of the insertions and the analysis of the results are explained in section 4.4. The results will be discussed in the next chapter.

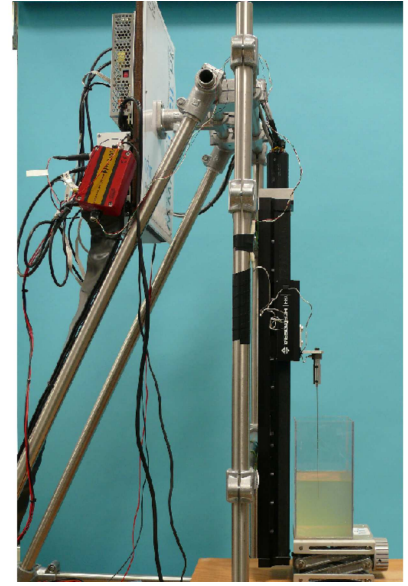
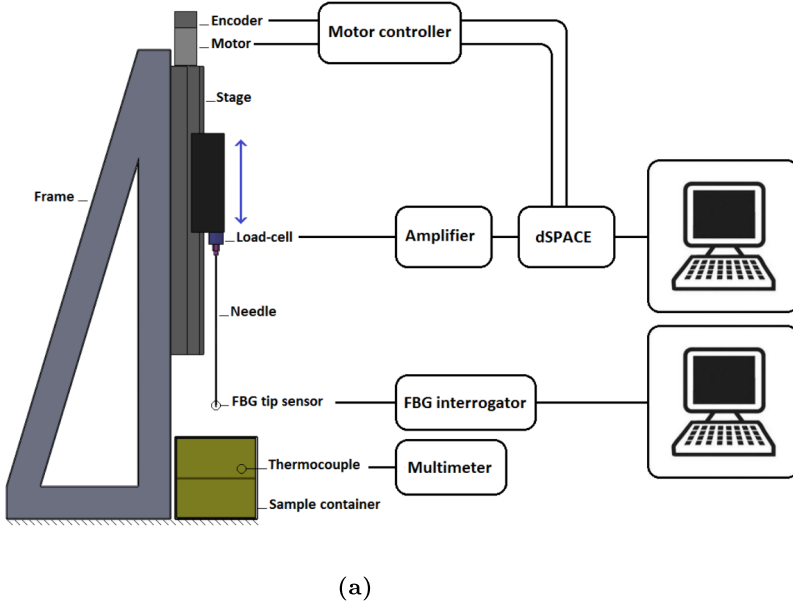
## Material & Methods

### 4.1 Experimental Set-up

The insertion experiments are executed in an experimental set-up. For this set-up a linear stage (Aerotech PRO 115 linear stage, Aerotech Inc., USA) is used to control the insertion. The linear stage is vertically positioned on a frame. A custom adapter is made to attach the hub of the prototype needle to a load cell on the stage. The load cell (RDP SLC31, RDP Electronics Ltd, Wolverhampton, United Kingdom) measures the total axial force acting on the needle. The linear stage is actuated with a motor (Maxon EC40 brushless 120W 167181, Maxon Motor AG, Sachseln, Switzerland). The position of the stage is measured with an optical incremental encoder (Scancon 2RMHF). The data capture and motor control is done with a dSPACE board (dSPACE DS1104, dSPACE GmbH, Paderborn, Germany). During the insertion the needle moves downwards into the sample in the sample container. During insertion the force from the load-cell and position are sampled at 1 kHz. The software used for control and data capture is dSPACE ControlDesk 3.4. The output of the FBG interrogator (wavelength shift expressed in pixel coordinate) for the prototype is down sampled to 100 Hz. For both setups the recorded data are exported and a data analysis is performed in Matlab R2011b. A thermocouple is inserted into the sample container to determine the temperature of the sample. This temperature is needed to determine the slope coefficient for the force - wavelength relationship from Equation 10.

### 4.2 Experimental Protocol

The insertion experiment is carried out in the set-up described in the previous section. During the experiment the prototype needle is inserted into the sample with a constant speed. For the first experiment in the phantom tissue model (see Chapter 4.3) speeds of 5, 10, 15, 20 and 25 mm/s are used. For the porcine tissue model speeds of 5, 10 and 15 mm/s are used. The starting position is set just above the tissue sample, the end point is predetermined in a way that all the layers are punctured. For the insertion in a sample the same start and end positions are used so that the insertion length is constant. For the phantom tissue model the stage travels 85 mm and for the porcine tissue model the stage travels 58 mm. After each insertion the sample container is moved to prevent the needle from being inserted in a previous passage. A minimum of 5 insertions are made for each speed. During each insertion the force, position, speed, temperature and FBG output are recorded. Both the data from the FBG interrogator and the data from the load cell are filtered to remove noise components. A low pass butterworth filter with zero phase is used to



**Figure 22:** (a) Schematic drawing of the experimental setup for the insertion experiments with prototype needle. The needle is mounted at the hub to a load cell on the slider of the linear stage. The slider moves in vertical direction. (b) Experimental set-up with the a phantom tissue in the sample container. The FBG interrogator is not in view. The thermocouple has to be inserted in the sample.

remove high frequency noise components from the signal. The filter is a 5<sup>th</sup> order Butterworth filter with a cut off frequency of 25 Hz. The force peaks of the filtered date were located by an algorithm which scanned the force data and indicated the peaks.

### 4.3 Experimental samples

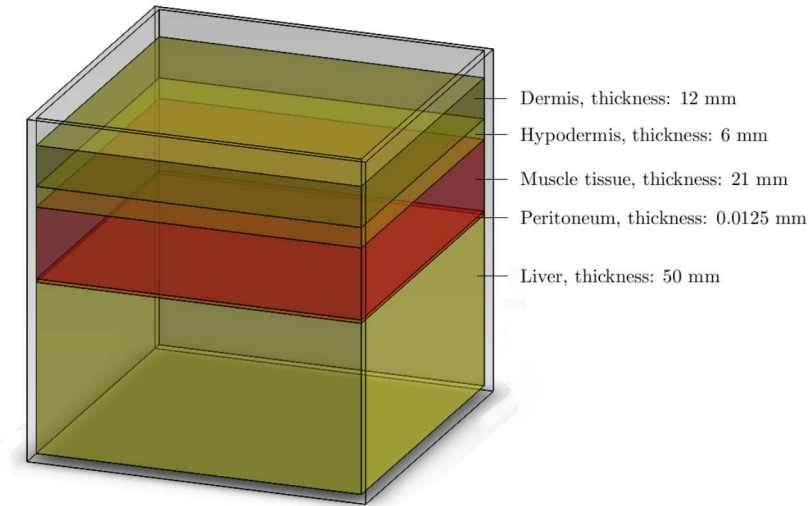
The insertion experiment is executed in a sample. Two samples are used; a phantom tissue and ex vivo tissue sample.

#### 4.3.1 Tissue phantom

The phantom tissue consists out of gelatin layers with different gelatin concentrations. The different layers are used to mimic different tissue layers that are encountered during needle insertion see Appendix A. The higher the concentration of gelatin the higher the stiffness of the gelatin. The concentration used for the sample and the measured stiffness are shown in Table 4. The stiffness is dependable on the temperature of the gelatine; if the temperature increases the stiffness decreases. The Young's modulus is measured at a temperature of 16 °C. To mimic a membrane layer such as the peritoneum or the capsule of Glisson (membrane of the surface of the liver) a layer of cellophane (0.0125 mm) is used, this has a Young's modulus in the order of 3 GPa [18].

**Table 4:** Gelatine layers and their concentration, Young's modulus measured at 16 °C

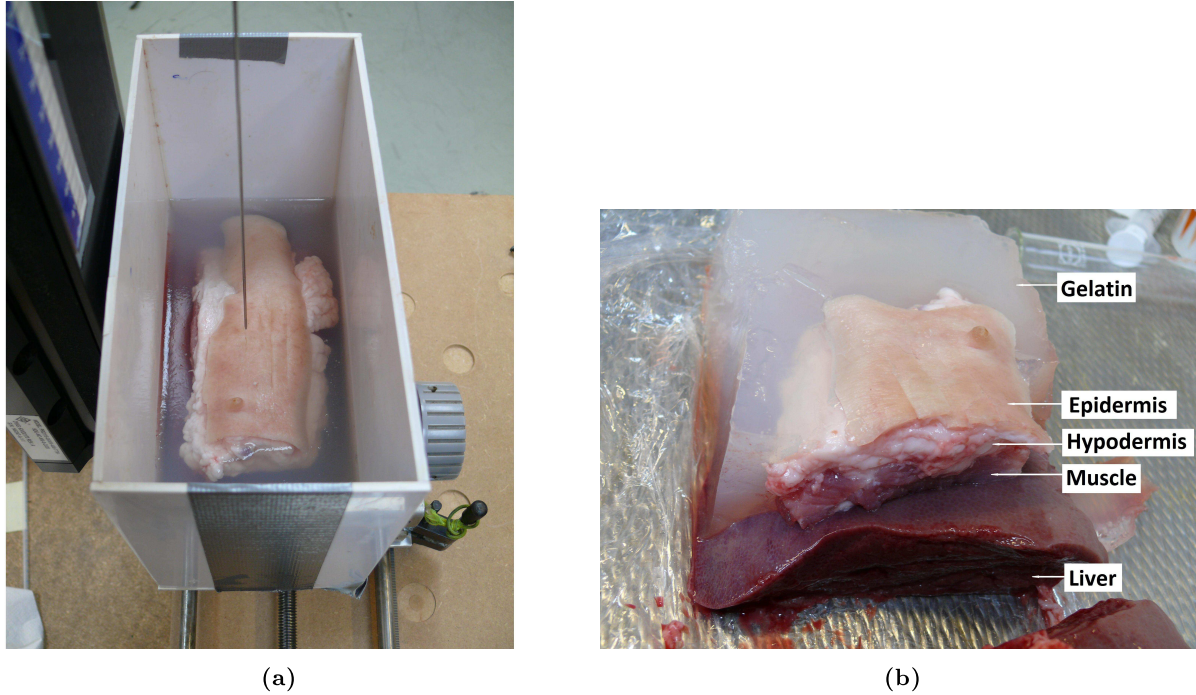
Sample type	Gelatin concentration [%]	measured Young's Modulus [kPa]
Dermis	17.8	80
Hypodermis	26.3	130
Muscle	13.0	52
Liver	6.8	15



**Figure 23:** Schematic drawing of the phantom tissue. Different layers with different gelatin concentrations are stacked to mimic soft tissue. The peritoneum is made from a layer of foil.

#### 4.3.2 Porcine tissue model

The second sample is an ex vivo tissue sample taken from porcine cadaver, created at HemoLab in Eindhoven. Tissue layers are epidermis, hypodermis and muscle on top of a liver embedded in a gelatin gel. The epidermis is a very tough layer and without a support the needle is prone to buckling. Therefore the insertion is performed after incisions have been made in the epidermis. The amount of possible insertions is limited because of the size of the sample. In the next section the results are presented for the insertion experiment.



**Figure 24:** Insertion experiment in ex vivo porcine tissue embedded in a gelatin gel. (a) Top view: sample inside experimental set-up. (b) Cross section of the ex vivo porcine tissue sample consisting out of epidermis, hypodermis, muscle and liver embedded in gelatin.

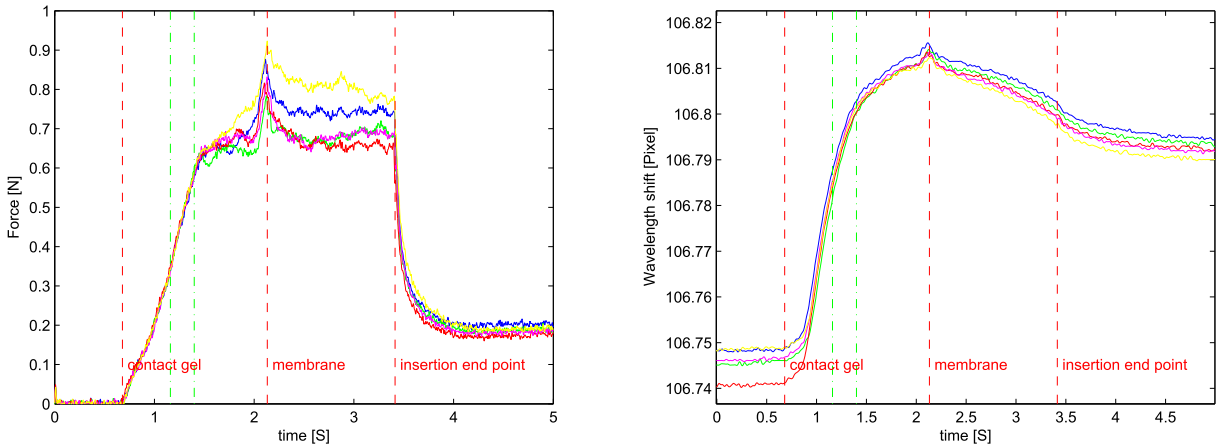


## Results

### 4.4 Insertion Results

#### 4.4.1 Tissue phantom

In the tissue phantom a total of 25 insertions were made with different constant speeds. In Figure 25 an example of 5 insertions into the gel sample can be found. It can be seen that different insertions show similar force profiles. When the insertion speed decreases the total axial force shows a similar force profile only with lower forces. In the force data from the the load cell as well as the FBG output the puncture peak for the cellophane membrane can be clearly identified. The other transitions between different gel layers are not marked by a peak but by a change in the gradient of the force profile. The first two layers have a high Young's moduli but the transition cannot clearly be recognized in the force measured by the load cell. The 'muscle' layer has a lower young's modulus and this can be seen by the lower gradient of the force profile. The change in gradient can also be seen in the output of the FBG interrogator. After the puncture of the membrane the force profile for the total axial force becomes stable in the liver. For the tip sensor the output in the liver segment of the sample decreases. Overall it can be seen that the total insertion force is very low. The temperature at which the Young's modulus is measured for the gel sample layers is  $16\text{ }^{\circ}\text{C}$ , the temperature at which the insertions are performed is at  $20.5\text{ }^{\circ}\text{C}$  in order to be closer to the temperature of the calibration range. With this temperature the Young's modulus for the gel layers will be lower and from the total axial force it can be seen that the forces are very low.



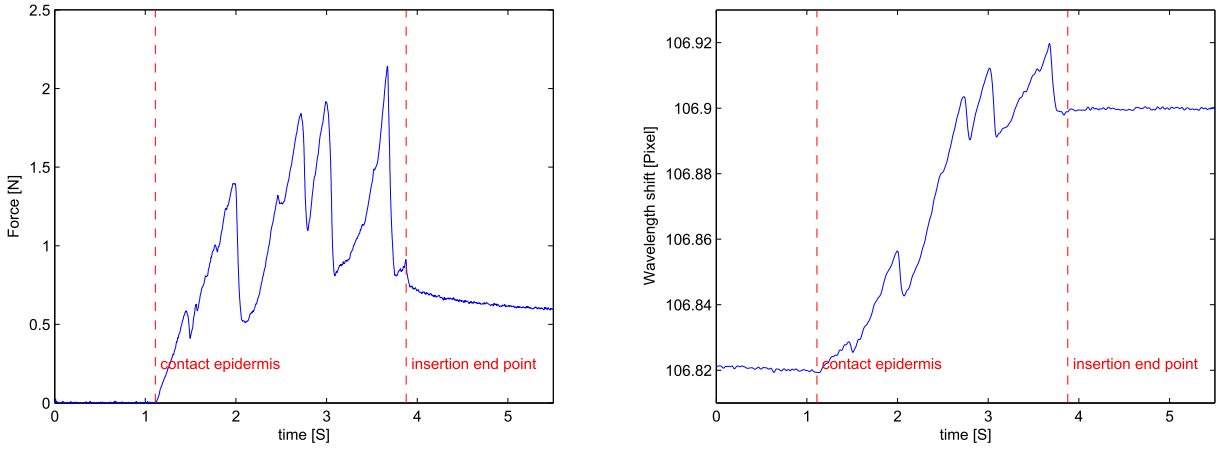
(a) Total axial force measured at the hub of the prototype needle for 5 insertions into gel sample. Insertion speed 25 mm/s sample temperature  $20.5\text{ }^{\circ}\text{C}$ . The vertical lines indicate the contact with the sample (dermis), expected layer transition based on position (green dashed dotted lines), the puncture peak when the membrane is punctured and the stop of the insertion.

(b) Wavelength in pixel coordinate of FBG in tip of the prototype needle for 5 insertions into gel sample. Insertion speed 25 mm/s sample temperature  $20.5\text{ }^{\circ}\text{C}$ . The vertical lines indicate the contact with the sample (dermis), expected layer transition based on position (green dashed dotted lines), the puncture peak when the membrane is punctured and the stop of the insertion.

**Figure 25:** Example of results in gel sample.

#### 4.4.2 Porcine tissue model

For the second sample ex vivo porcine tissue is used. In the ex vivo sample 35 insertions are made at different constant speeds. For each insertion the layer thickness differs because altering tissue thickness of the combined sample. This also makes it difficult to compare the individual insertions. The force profile shows a lot more puncture events because of the inhomogeneous tissue. In Figure 26 only a single example is shown. But for all the insertions it holds that the force profile for the total axial force shows different peaks which correspond to transitions between different tissue layers are visible. The total axial force is higher in comparison to the gelatin sample, this can also be seen in the FBG output. The FBG output shows more resembling characteristic to the total axial force, also showing the peaks for the puncture events between layer transitions.



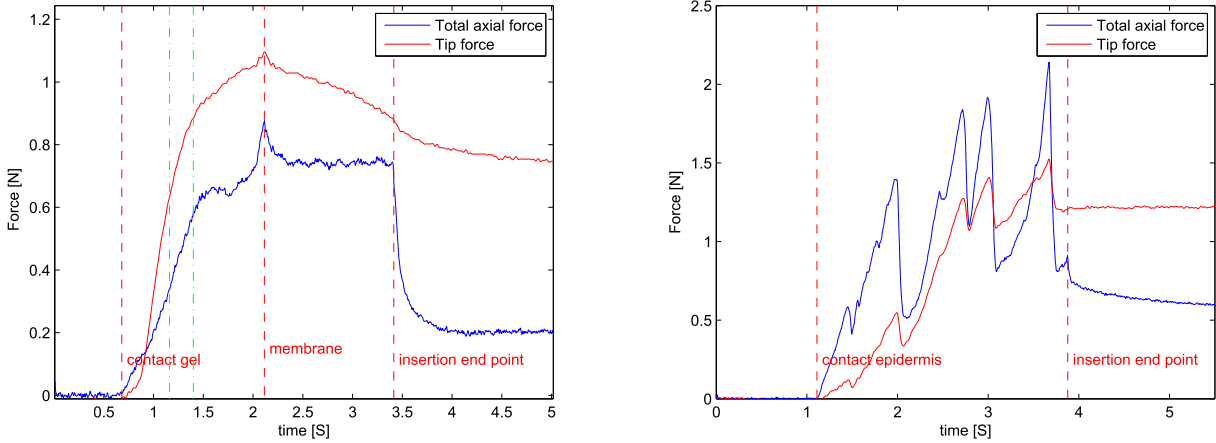
(a) Total axial force measured at the hub of the prototype needle for insertion into ex vivo porcine tissue model. Insertion speed 15 mm/s sample temperature 18 °C. The vertical lines indicate the first contact with the epidermis and the end point for the insertion.

(b) Wavelength in pixel coordinate of FBG in tip of the prototype needle for insertion into ex vivo porcine tissue model. Insertion speed 15 mm/s sample temperature 18 °C. The vertical lines indicate the first contact with the epidermis and the end point for the insertion.

**Figure 26:** Example of results in tissue sample.

## Analysis

The output for both the sensors are given in the previous sections. The output of the FBG interrogator is not converted to force with the calibration results from Chapter 3. The temperature of the sample is measured at the edge of the sample container and not close to the needle. The measured temperatures are below the calibration range. The reason not to heat up the samples to the calibrated range is because the gel deteriorates fast with increasing temperatures which can be seen by the low total axial forces measured during the insertion in the tissue phantom. The temperature during the insertion experiment was not constant as suggested in the conclusion of the calibration. If the FBG output is converted to force, the slope coefficient for Equation 10 has to be extrapolated. In Figure 27 the outputs are converted to force by a linear extrapolation. It can be seen that for the insertion experiment in the tissue phantom the force measured in the tip sensor is higher than the total axial force. This is not possible and is caused by an other effect. One of the effects is that the temperature measured in the gel sample is not uniform throughout the sample, and that the measured temperature is higher than the temperature at the needle tip. This will cause an overestimation of the slope coefficient which results in a higher force. The effect of an overestimated force can also be seen in the output of the insertion experiment into the porcine tissue model. After the insertion the remaining force is higher than the total axial force. In this stage there is no needle translation so there is no force contribution from the friction force. The force from the needle tip should be equal or lower in comparison to the total axial force. The magnitudes for the force are not correct, and valuable information should not consider the magnitude but the gradient of the FBG output.



(a) Total axial force and FBG output converted to force with extrapolated calibration coefficient. Insertion into the phantom tissue. Insertion speed is 25 mm/s, the sample temperature is 20.5 °C. The force corresponding to the FBG output is higher than the total axial force.

(b) Total axial force and FBG output converted to force with extrapolated calibration coefficient. Insertion into ex vivo tissue sample. Insertion speed is 15 mm/s, the sample temperature is 18 °C. The force corresponding to the FBG output is higher than the total axial force.

**Figure 27:** Example of results corrected with calibration slope coefficient.

---

## 4.5 Conclusion insertion

In this chapter the insertion experiments were described. The insertion experiments were performed into a phantom tissue and into an ex vivo porcine tissue model. The aim for this experiment was to indicate if tissue boundaries can be identified with the prototype design. For both insertion experiments it can be seen that the total axial force and the tip sensor have a good correlation, the change of the force gradient can be followed in both data sets. Puncture events can be clearly identified in both the total axial force and the tip sensor. These puncture events give information about the position of the needle with respect to the tissue. The gradient changes also contain information about the tissue type. In the ex vivo tissue the gradient changes rapidly and there is a wide variation of tip forces. This is due to the internal structure of the tissue which is inhomogeneous. When the calibration results are extrapolated for the temperature of the samples it can be seen that there is an overestimation of the force. This indicates that the prototype needs a temperature calibration over the full range and that the temperature of the samples has to be controlled precisely.

## 5 Discussion

Accurate positioning of the needle tip during needle insertion is essential to ensure a maximum effect of the treatment. Target error is a problem that can have a number of causes; among them are needle deformation and tissue deformation. A lot of research aims to improve the positioning accuracy. This thesis aims to aid in this research field by improving the force sensing during needle insertion, making the first attempt in the addition of a force sensor in the tip of a needle.

The total axial forces at the hub of the needle during insertion are a combination of cutting forces, stiffness forces and friction forces. From these forces the cutting forces and stiffness forces occur at the tip of the needle and the friction force occurs over the entire insertion depth acting on the shaft of the needle. In literature only studies are found where the total axial force is measured. In a few studies the friction force is measured during needle insertion. By withdrawing the friction force from the total axial force the tip forces are determined. In literature there were no examples found where the forces acting at the tip of the needle were measured directly with a sensor in the tip of a trocar needle stylet.

The goal for this thesis was to determine how to directly measure the forces acting at the tip of the needle, to design a needle which can directly measure these forces with a sensor at the tip and to prove the feasibility of such a design. The design can be used to improve force feedback information needed to increase the accuracy of needle interventions, investigate if this force information can be used to determine tissue properties and differentiate between tissue layers.

### 5.1 Design

The design created in this thesis started with a list of requirements. These were divided in functional and geometrical requirements. The needle must be able to measure the axial forces directly at the tip of the needle, measuring the tip forces in a range of 0 - 15 N, and excluding the friction force acting on the shaft. An 18 G trocar needle is selected as the basis for the geometrical requirements, which is typically used in procedures in solid soft tissues such as liver, prostate, kidney and breast [21]. The cutting stylet contains the sensor for the force measurement, and is based on a strain measurement. The ideal position for the sensor is the neutral line of the stylet, as close to the tip as possible. Three different sensor techniques were possible: resistive based strain measurement with metallic foil strain gauges or piezoresistive gauges and optic based strain measurement fibre Bragg gratings. The FBG sensor is chosen because of its small size and very good resolution. The fabrication is easier and the placement in the ideal sensor position is more accurate in comparison to the alternatives. The FBG is an intrinsic sensor in the optic fibre and runs through the centre of the needle. Among the other advantages of FBG's is the immunity to electrical noise which makes them MRI compatible also FBG's are sterilizable, but these advantages are not considered in the sensor choice.

If the FBG is directly bonded in the ideal sensor position to a metal stylet shaft, the strain over the measurement range would be very low ( $97.4\mu\epsilon$ ). The strain repeatability of the interrogator  $\leq 3\mu\text{strain}$ . To increase the strain over the measurement range the FBG is embedded in a jacket made from a weaker material: PVC. The diamond shaped cutting tip presses directly onto the FBG jacket. The tip is attached to the shaft with a PVC ring in between; this ring makes the connection between tip and shaft more compliant. The FBG is interrogated with the Deminsys system and the output is the Bragg wavelength shift given in a pixel coordinate and sampled at a maximum of 20 kHz. From this design a prototype was build.

This design is to the writer's knowledge the first application where a force sensor is applied in the tip of a trocar needle. In literature, direct measurement of the tip force was only found in the research by Kataoka et al. [15] where a needle which measures the tip forces and friction forces independently during needle insertion was developed. A seven axis load cell is designed where the tip forces are measured at the hub of the stylet with a one DOF load cell (see Figure 28a). The

---

outer sheath is attached to a six axis load cell measuring the total axial force. The friction force is determined by subtracting the tip forces from the total axial force.

The design by Kataoka et al. [15] and the design presented in this thesis both measure the tip force directly. A drawback of the design by Kataoka et al. [15] is that it does not allow for needle deflection, when it is deflected the inner stylet comes in contact with the outer stylet making it impossible to measure the tip forces without these forces created by the surface contact. As stated in the requirements the design in this thesis does allow bending. The sensor is positioned in the neutral line where there are no longitudinal strains due to bending, only axial forces. This gives possibilities to combine the design in future research with needle steering by deflection as seen in the work by Cowan et al. [4].

In the sensor design by Kataoka et al. [15] the needles can be changed, making it possible to use different sized needles with different tip types. In the design from this thesis this is not possible because of the stylet assembly. When the needle tip loses its sharpness the stylet has to be replaced. In clinical use these types of trocar needles are disposables and are only used once. For research in non-living tissue the design can be used multiple times but the sharpness of the needle tip decreases over time and influences the cutting force.

The functional requirements of this design will remain the same even if a needle of a different size is desired. The length of the needle does not influence the sensor at the tip of the needle. The diameter does influence the sensor design. The FBG jacket is used to increase the strain in the FBG, when the diameter (bigger Gauge size) is reduced the cross section area reduces with a quadratic scaling. The use of FBG sensors is successfully demonstrated in medical equipment and in needles [21][9], see Chapter 7.3. An example of force sensing was found in Iordachita et al. [11] which is comparable to the application in this work. A prototype is presented for measuring tip forces with a retinal surgery tool, measuring forces applied on the retina. In the prototype the FBG is embedded in a 25 G ( $\varnothing 0.5$  mm) shaft made from titanium. The FBG is embedded in a groove in the shaft which can be easily machined. The FBG does not lie in the centre of the needle so transverse force will affect the measurement. The area reduction is by a factor 4 and titanium has a Young's Modulus of 105 - 120 GPa which allows that the FBG can be directly bonded to the shaft.

## 5.2 Calibration

The prototype was calibrated to determine the force-wavelength relationship. The needle is axially loaded over a range from 0 - 10 N repeatedly. The needle is calibrated at different temperatures because the FBG has a cross-sensitivity to temperature. The range is taken from 26 - 40°C. When the design is used in a clinical setting this will be appropriate. The insertion experiments uncovered that a wider range is necessary because biological tissue and experimental phantom tissues are kept at low temperatures. With increasing temperatures the sample tissues degraded. For further research a wider temperature calibration range is needed.

$$\Delta F[N] = \alpha \Delta D[Pixel] \quad (11)$$

The calibration results show that the force-wavelength relationship is linear, approached with a linear best fit 10. The slope coefficient  $\alpha$  is determined and has small standard deviations at a constant temperature. With increasing temperature the coefficient increases. The best fit introduces a linearity error which is calculated with the median values for the slope coefficient, this error has a mean of 0.1069 N for all temperatures. The error is at its biggest in the lower region of the measurement range (0 - 4 N). This accuracy does not meet the demands as stated in the design requirement. The high error is a disadvantage especially because the highest error is in the low range. From the median forces in Table 1 it can be seen that in this low range the high

accuracy is required. In order to reduce the error, the data are approached using a polynomial fit. This reduces the error, but the parameters show large standard deviations and there is no clear trend seen for the parameters when the temperature changes.

The Deminsys FBG interrogator is chosen because of the possibility for high sampling frequency, but the system has some drawbacks. The interrogator makes a relative measurement meaning that for each use a zero measurement is needed, to compensate for the offset. The interrogator uses a light source which generates heat, so in order to obtain a stable output the interrogator has to be switched on at least an hour before use. During calibration it was visible that when the force is held constant, the output of the interrogator shows a drift. This output should stay constant. This effect increases the hysteresis of the prototype (see Figure 19b). It is seen that when the needle is unloaded the output ends below zero. This is because the FBG output decreases while the force is held constant. By manually shifting the unloading curve with the drift of the FBG output it is seen that the unloading step ends in zero.

In the calibration data it was seen that the force profile was nonlinear with a linear translation (see Figure 17b). In the dimensioning of the design PVC is chosen as the material for the FBG jacket and the ring. With the maximum force for which the needle is designed the stress in the material is smaller than the yield strength, so the PVC material stays within the elastic region. The non-linearity is explained by the design. In the design of the needle the FBG jacket is bonded at the bottom to the inner tube and at the top only to the tip of the needle. The sides of the FBG jacket are not bonded to the outer tube and the connection between the outer tube and the jacket is a loose fitting, this to remove the friction force component from the shaft in the measurement. When the FBG jacket is compressed the material bulges out and touches the outer tube, this makes the system more rigid and thus the force increases faster with less compression. This nonlinear behaviour does not affect the linear behaviour of the force - wavelength relationship, but it can be a reason for the large linearity error which defines the accuracy.

The slope coefficient changes with temperature because the design contains two materials with different thermal expansion coefficients. The PVC has a higher thermal expansion coefficient as the steel from the outer tube. When the temperature increases the slope coefficient for 10 increases because there is a different pre tension. If the design is constructed from a single material or from two materials with exactly the same thermal expansion coefficient it is expected that the slope coefficient for Equation 10 does not change with changing temperatures, because the relationship between temperature and FBG output is linear. With a single material the pre tension does not change. As stated the combination of two materials is chosen to increase the strain measured by the FBG because of the lower Young's modulus of the PVC. For a single material one could only use cross sectional area reduction to increase the strain.

In the design by Iordachita et al. [11] the tool uses a single material titanium and has a smaller cross sectional area. According to calibration the design goal was met and resulted in a resolution of 0.25 mN. The calibration by Iordachita et al. [11] also used a linear best fit approach but the accuracy for this design was not given. Comparing the retinal surgery instrument to the needle prototype the resolution is similar and within millinewton range but the linearity error of 0.1 N reduces the accuracy of the prototype. The prototype presented in this thesis proves that forces can be measured at the tip of the needle, and that further development of the design and prototype needs to focus on the improvement of the measurement accuracy.



---

### 5.3 Insertion experiment

The calibrated prototype was used in an insertion experiment in two samples. The goal was to validate if the prototype can be used in the identification of different tissue layers. With a linear stage the insertion is performed in a sample with constant speed. The total axial force is measured at the hub of the needle and the output of the prototype is recorded.

The first sample was a phantom tissue made of layers with different gelatine concentrations to mimic dermis, hypodermis, muscle and liver. A foil membrane is used to mimic the liver capsule. The second sample used was an ex vivo porcine tissue sample, with a layer of epidermis, hypodermis, muscle and liver embedded in a gelatine gel. At the point of entry in the epidermis incisions were made to prevent needle buckling.

From the results of the insertions it is seen that the output characteristic of the prototype resembles the force characteristic of the total axial force measured at the hub. Puncture events are clearly identifiable in the phantom sample. This can be seen by the puncture peak occurring at the foil membrane. The position of this membrane can be determined from the output of the prototype and the insertion speed of the linear stage. The transitions between other layers of the phantom tissue is not characterized with a clear puncture event but changes in the gradient of the total axial force profile can be seen. The output from the prototype also shows the gradient changes. The gradient changes are caused by the different gelatin concentrations.

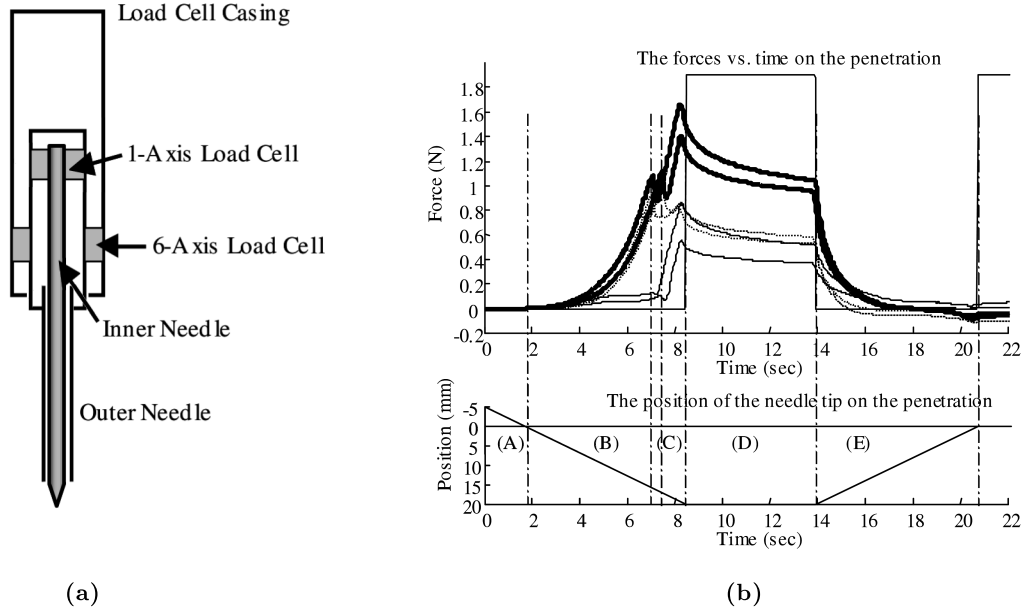
The set-up for the insertions is not performed inside a temperature controlled environment. The temperature is measured with a thermocouple. The experiments were performed at room temperature. The samples showed a decay with increasing temperature, the total axial force profile became lower in comparison to insertions made at 16 °C. The experiments were executed and the temperature of the samples was measured, these were not at room temperature. This temperature was then used to extrapolate the calibration slope coefficients. When the output from the prototype was converted to force it resulted in a larger force profile than the total axial force. The force is overestimated, which is not possible: the total axial force is a combination of tip forces and friction forces on the shaft and these cannot be negative. One of the contributing factors for this overestimation is that the sample container does not have a uniform temperature and that the position of the thermocouple is too far from the needle tip. This results in a higher temperature measurement. Therefore the results from the insertion experiments can not be converted to force.

The result of the insertion experiment can be compared with results obtained in the work by Kataoka et al. [15] and Okamura et al. [20]. If we compare the result from the insertion experiment a similar force range is seen for the ex vivo samples. The cutting forces during insertion are ideally constant and unrelated to the depth of the insertion. In the insertion experiments it can be seen that cutting forces are not constant and increase slightly with insertion depth. In the work by Okamura et al. [20] the friction force was determined with sinusoidal insertions, and the estimated friction force was subtracted from the total axial force to obtain cutting forces. These cutting forces also contain the stiffness force at the tip of the needle. They modelled the cutting forces as a constant for a given tissue, in their measurement they also found that the forces are not quite constant and increase.

With the 7 axis prototype from Kataoka et al. [15], the insertion experiment is performed into the prostate gland of a canine cadaver. The prototype measures the tip force and total axial force, and by subtracting the tip force from the total axial force the friction force is obtained. When the insertion is stopped, the total axial force decreases to a constant value. Period D in Figure 28b indicates the stopping of the insertion and can be compared with the period after the insertion is stopped, as seen in Figures 27a - 27b at the end point. The tip force goes to a constant value because of a remaining stiffness force acting on the needle tip, there is no needle and tissue movement thus the cutting force is zero. In Figure 28b it is seen that the friction force also goes to

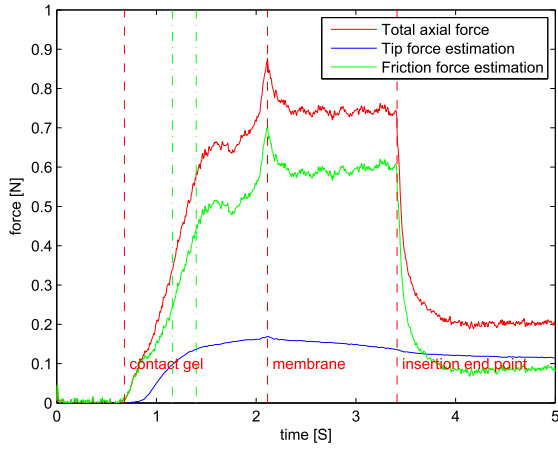


a constant value because the stiffness in the tissue creates dragging up forces acting on the shaft. These remaining forces are caused by the viscosity of the tissue. In Figure 28b the tip force goes to half of the total axial force when the insertion is stopped. During the insertion experiments the slope coefficient was overestimated. If we use the result from Kataoka et al. [15] and reduce the coefficient  $\alpha$  with a correction factor an estimation of the force profile for the tip forces can be made (see Figure 29). This tip force estimation can be subtracted from the total axial force to obtain an estimation for the friction force profile on the shaft of the needle. It can be seen that the friction force closely follows the total axial force. In the results by Kataoka et al. [15] it is seen that the friction force also closely follows the total axial force after the capsule of the prostate is punctured and the shaft comes into contact with the prostate tissue.

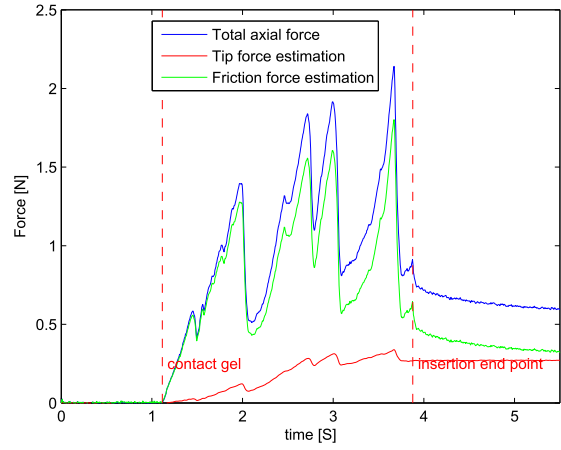


**Figure 28:** (a) Structure of the 7-axis load cell needle, for independent measurement of friction and tip forces during insertion. The stylet tip is a tri-facet diamond tip [15]. (b) The total axial force, tip force and friction force vs. time of insertion into in situ canine prostate, together with the position of the needle tip vs. time. The thick line indicates the total axial force, the dotted line indicates the tip force, and the thin line indicates the friction force. The surface of the prostate is set as 0 mm before penetration. [15]

The insertion experiments show that the output of the prototype has a good correlation with the total axial force. Puncture events can be clearly identified by the tip sensor in the prototype. Position of these puncture events can be determined with the needle insertion speed. Differences in tissue type can be seen by the gradient of the profile. The overestimation of the force indicates that temperature compensation is needed and that full range calibration is needed.



(a) Total axial force and FBG output converted to force with an estimated correction factor. Insertion into the gel sample. Insertion speed 25 mm/s at 20.5 °C. The friction force is the total axial force minus the estimated tip force from the prototype.



(b) Total axial force and FBG output converted to force with an estimated correction factor. Insertion into tissue sample. Insertion speed 15 mm/s at 18 °C. The friction force is the total axial force minus the estimated tip force from the prototype.

**Figure 29:** Example of results corrected with calibration slope coefficient and estimated correction factor.

## 6 Conclusion

The design in this thesis is a design for a new force measuring trocar needle. An FBG is incorporated in the tip of the needle stylet to measure the forces acting at the tip and to exclude the friction force acting on the needle. Calibration showed that the prototype functions in a temperature controlled environment with a measurement error of 0.1069 N which is higher than stated in the design requirements. Inserting the needle in phantom material or ex vivo tissue shows that the output of the prototype is useful in detecting different tissue types by the gradient of the output. In a temperature controlled environment this output could be converted to force. The design needs to be improved for a better accuracy and temperature compensation. The design can be used to improve needle procedures by providing force information gathered at the tip of the needle.



## 7 Future work

The prototype presented in this thesis is to the writer's knowledge the first application of a sensing element in the tip of a trocar needle stylet for tip force measurements. The discussion makes clear that the prototype shows good results. However there are points on which it can be improved. As seen in the discussion the methods on how the current prototype is used can be improved to gain more information from the measurements. For further studies a new prototype might be developed and the following aspects can greatly improve the design.

### 7.1 Temperature compensation

In Chapter 2 and 3 it was shown that the cross sensitivity to temperature reduces the functionality of the design. Further research with the prototype presented in this paper benefits from calibration over a wider temperature range. Tissue model samples such as the ones presented in Chapter 4.3 are best kept at low temperatures. For these temperatures calibration results are needed. A change in temperature during insertion changes the slope coefficient which makes it difficult to convert the FBG output to an accurate force measurement. For the current design insertion experiments must also be executed inside a temperature controlled environment in order to make an accurate force measurement.

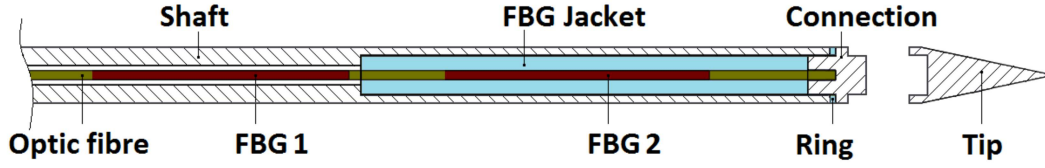
The design of the force sensing needle can be improved by adding a possibility for temperature compensation. A direct measurement of temperature at the tip as close to the force sensing sensor is desired. A simple solution is to add an extra FBG to the system in the same optic fibre. In Chapter 2.2.3 the possibility for multiplexing FBG's was discussed. Multiple FBG's can be incorporated in an optic fibre and individually interrogated. An added FBG to the sensor head must be strain free in order to measure temperature. The output of the temperature FBG can be subtracted from the FBG measuring the combination of strain and temperature. In the design presented in this thesis an FBG can be added behind the strain measuring FBG as can be seen in Figure 30.

### 7.2 Calibration improvements

The design of the needle is a force proving instrument and for such devices calibration is necessary. In the design of the prototype calibration possibilities are limited because the sharp needle tip needs to be protected. The needle tip also cut into the PVC plate in the calibration set-up. It would be easier if the needle is calibrated before the tip is assembled onto the prototype. This means that the tip has to be separated into two components. The first component compresses the FBG jacket, and is assembled before calibration. This part has a blunt tip and on this surface the calibration test can be applied. With a blunt surface more extensive tests can be applied. The second part of the tip is the cutting tip which is assembled after calibration. It is important is that the connection between these two components is rigid and does not alter the calibration results. This connection can be achieved with a stepped bore see Figure 30.

### 7.3 Incorporating deflection measurement

Target error during needle insertion is a problem which is also caused by the deflection of the needle. Needle deflection is characterized as a function of insertion depth, needle gauge, and insertion force [2][14]. This thesis presented a design which measures the tip forces but it also is desired to know the location of the tip inside a sample when it is deflected from a straight



**Figure 30:** Cross section of recommended concept design, with an added strain FBG to measure temperature. FBG 1 is not bonded to the shaft and is therefore strain free. Tip consists out of two part; the sharp cutting tip is mounted after calibration.

trajectory. In literature examples can be found of prototype needles which can measure the local curvature of the needle and reconstruct the shape of the needle with sensors incorporated in the needle [6][9][21][29]. From these local curvature measurements the position of the needle tip can be determined. At the department BioMedical Engineering of Delft University of Technology a prototype needle is developed which can reconstruct the shape of the needle from local curvature measurements. This prototype makes use of an array of multiplexed FBG's. In Appendix C a deflection experiment with this prototype to determine the flexural rigidity is described.

This prototype design and the design presented in this thesis can be combined into a single design. This combined design has the same design requirements as stated in Chapter 2.1, adding the requirement that the needle can reconstruct the shape of the needle and determine the position of the tip with respect to the hub of the needle.

The concept design has multiple sensor locations. Figure 31 shows the concept design with the sensor locations. The tip sensor is as presented in this thesis and measures the tip forces. Along the length of the needle sensor nodes are located, and in a node the local curvature of the stylet is determined. If more nodes are incorporated a better shape reconstruction can be made.



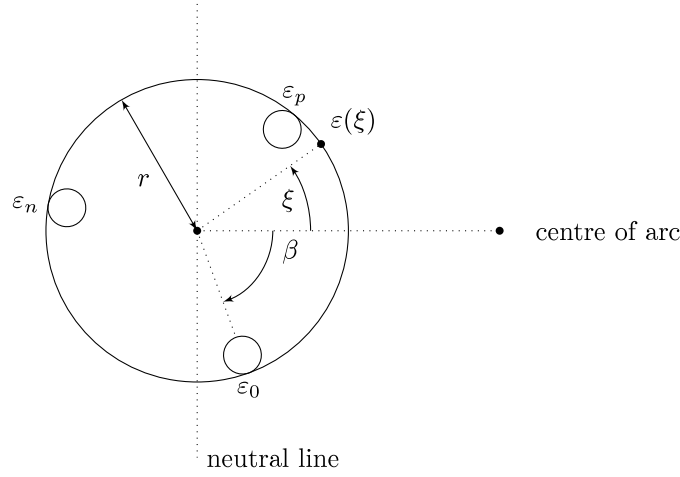
**Figure 31:** Concept of needle which can measure tip force and reconstruct the shape of the needle. Schematic sensor locations. In the nodes the local curvature is determined for the reconstruction of the shape.

To create a sensor node three identical grooves at  $120^\circ$  intervals are made on the inner stylet to embed optical fibres with FBGs along the needle length. Each optical fibre contains as many FBG's as nodes. A node is formed by three FBG's from three different fibres. To determine the local curvature from FBG's we need to relate the local curvature to strain. For a cylindrical rod under pure bending, the strain is determined by.

$$\varepsilon = \frac{r}{\rho} = r * C \quad (12)$$

Where  $\rho$  is the curvature radius,  $C$  the relative curvature and  $r$  is the distance from the neutral plane. In the concept design  $r$  is the distance from the centre to the centre of the FBG in a node.

In the cross section the strains in the FBG's can be determined, and from these strains the angle  $\beta$  can be calculated. This is the angle between the reference fibre and the curvature vector which



**Figure 32:** Schematic cross section of concept needle at a sensing node, with three FBG's sensing strain. With these strain measurements the local curvature in the node is determined.  $\beta$  is the angle between the reference fibre and the curvature vector.

is perpendicular to the neutral plane. The fibre with the smallest wavelength shift can be used as a reference fibre.

In the existing prototype for shape reconstruction the grooves run over the full length of the needle stylet. In the design presented in Chapter 2 the shaft of the stylet consists out of two tubes for an easy fabrication. When the grooves are created this outer tube is too thin and thus the shaft must be one solid part. The space for the tip force sensor must be created by a bore in the solid shaft. The grooves end just before the position of the tip force sensor. The design thus contains four optic fibres with six FBGs for shape reconstruction, one for temperature compensation and one for the strain measurement for the tip forces.

This combined concept design gives haptic information on the forces acting at the tip of the needle and the position with respect to the hub of the needle can be determined with the shape reconstruction. Such a design can ideally be used for robotic insertion systems where this sensory information can be used in real time updates of the model for track and target planning.

## BIBLIOGRAPHY

- [1] Biocompatibility of plastics. Published online. [www.zeusinc.com](http://www.zeusinc.com).
- [2] N. Abolhassani, R. Patel, and M. Moallem. Needle insertion into soft tissue: A survey. *Medical Engineering Physics*, 29(4):413–431, 2007.
- [3] P. Blumenfeld, N. Hata, S. DiMaio, K. Zou, S. Haker, G. Fichtinger, and C. M. Tempany. Transperineal prostate biopsy under magnetic resonance image guidance: a needle placement accuracy study. *J Magn Reson Imaging*, 26(3):688–94, 2007.
- [4] J. Cowan, K. Goldberg, G.S. Chirikjian, G. Fichtinger, R. Alterovitz, K.B. Reed, V. Kallem, W. Park, S. Misra, and A.M. Okamura. *Robotic Needle Steering. Design, Modeling, Planning, and Image Guidance*. Surgical Robotics. 2011.
- [5] Yanliang Du, Jianzhi Li, and Chenxi Liu. A novel fiber bragg grating temperature compensated strain sensor. pages 569–572, 2008.
- [6] M.C. Gähler. Force measurement in percutaneous needles. 2012.
- [7] O. Gerovich, P. Marayong, and A.M. Okamura. The effect of visual and haptic feedback on computer-assisted needle insertion. *Computer Aided Surgery*, 9(6):243–249, 2004.
- [8] S. Hao and G.S. Fischer. A 3-axis optical force/torque sensor for prostate needle placement in magnetic resonance imaging environments. pages 5–9, 2009.
- [9] K.R. Henken, D. Van Gerwen, J. Dankelman, and J. Van Den Dobbelsteen. Accuracy of needle position measurements using fiber bragg gratings. *Minimally Invasive Therapy Allied Technologies*, 0(0):1–7, 2012.
- [10] R.C. Hibbeler. *Statics and mechanics of materials*. Pearson/Prentice Hall, 2nd edition, 2004.
- [11] I. Iordachita, Z. Sun, M. Balicki, J. Kang, S. Phee, J. Handa, P. Gehlbach, and R. Taylor. A sub-millimetric, 0.25 mm resolution fully integrated fiber-optic force-sensing tool for retinal microsurgery. *International Journal of Computer Assisted Radiology and Surgery*, 4(4):383–390, 2009.
- [12] K.V. Iserson. The origins of the gauge system for medical equipment. *J Emerg Med*, 5(1):45–8, 1987.
- [13] W. Jianbai and K.D. Wise. A thin-film cochlear electrode array with integrated position sensing. *Microelectromechanical Systems, Journal of*, 18(2):385–395, 2009.
- [14] H. Kataoka, T. Washio, M. Audette, and K. Mizuhara. A model for relations between needle deflection, force, and thickness on needle penetration. 2208:966–974, 2001.



- 
- [15] H. Kataoka, T. Washio, K. Chinzei, K. Mizuhara, C. Simone, and A. Okamura. Measurement of the tip and friction force acting on a needle during penetration. 2488:216–223, 2002.
  - [16] J Kieft. Development and validation of a multibody guidewire model for a training simulator in interventional radiology. 2008.
  - [17] H. López and J. Miguel. *Handbook of Optical Fibre Sensing Technology*. John Wiley Sons, 2002. ISBN 978-0-471-82053-6.
  - [18] H.F. Mark and N.M. Bikales. *Encyclopedia of polymer science and technology : plastics, resins, rubbers, fibers*. Interscience Publishers, 1964.
  - [19] R. Nabiev and W. Yuen. Tunable lasers for multichannel fiber-optic sensors. *Sensor Technology and Design*, 2003.
  - [20] A. M. Okamura, C. Simone, and M. D. O’Leary. Force modeling for needle insertion into soft tissue. *Biomedical Engineering, IEEE Transactions on*, 51(10):1707–1716, 2004.
  - [21] Y.L. Park, S. Elayaperumal, B. Daniel, R. Seok Chang, S. Mihye, J. Savall, R.J. Black, B. Moslehi, and M.R. Cutkosky. Real-time estimation of 3-d needle shape and deflection for mri-guided interventions. *Mechatronics, IEEE/ASME Transactions on*, 15(6):906–915, 2010.
  - [22] J. Peirs, J. Clijnen, D. Reynaerts, H. Van Brussel, P. Herijgers, B. Corteville, and S. Boone. A micro optical force sensor for force feedback during minimally invasive robotic surgery. *Sensors and Actuators A: Physical*, 115:447–455, 2004.
  - [23] P. Puangmali, K. Althoefer, L.D. Seneviratne, D. Murphy, and P. Dasgupta. State-of-the-art in force and tactile sensing for minimally invasive surgery. *Sensors Journal, IEEE*, 8(4):371–381, 2008.
  - [24] Y.J. Rao. In-fibre bragg grating sensors. *Measurement Science and Technology*, 8(4):355, 1997.
  - [25] R.J. Roesthuis, Y.R.J. van Veen, A. Jahya, and S. Misra. Mechanics of needle-tissue interaction. pages 2557–2563, 2011.
  - [26] J.E. Seiffers, P.C. Teerhuis, and W.L. Thijs. *Mechatronica*. 2004.
  - [27] M. Swindle. *Swine in the laboratory : surgery, anesthesia, imaging, and experimental techniques*. CRC Press, 2nd edition, 2007.
  - [28] D.J. Van Gerwen, J.J. van den Dobbelsteen, and J. Dankelman. Needle- tissue interaction forces: A survey of empirical evidence. *Medical engineering physics*, 34(6):665–680, 2012.
  - [29] Y. Wenbin, A. Bonvilain, T. Alonso, A. Moreau-Gaudry, and S. Basrour. Modelling and characterization of an instrumented medical needle in sight of new microsensor design for its insertion guidance. pages 6465–6468, 2010.
  - [30] Kim Yongdae, Kim Youngdeok, Lee Chulsub, and Kwon Sejin. Thin polysilicon gauge for strain measurement of structural elements. *Sensors Journal, IEEE*, 10(8):1320–1327, 2010.

# Appendices

---

## A Pilot needle insertion in pig liver

A pilot test was performed for needle insertion into a pig liver. This test gave a general idea of the force needed to puncture the different tissue layers and the entry site for the needle puncture. The insertion in the liver was performed ex vivo in situ on a fresh cadaver. The lungs and heart of the cadaver were removed which possibly altered the natural location of the liver. The liver can be seen in Figure 33[27]. For percutaneous needle insertion, the skin, subcutaneous fascia, muscle and peritoneum have to be punctured before entering the liver 34. The first trial showed that the skin is hard to puncture and the 18G 20 cm needle would buckle if more force would be exerted. An incision into the skin is made at the needle entry site to provide access for the needle into the liver. The location of the entry site is made between the ribs under the right front leg in the coronal plane see Figure 35.

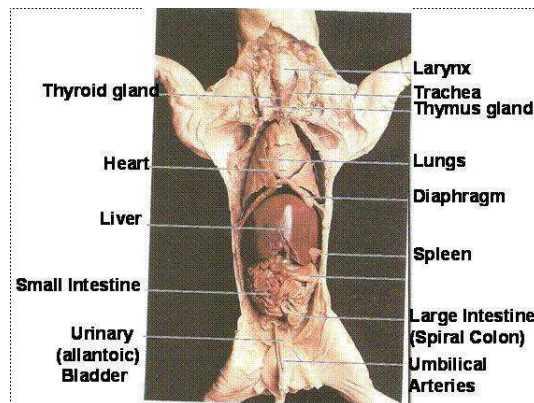


Figure 33: Anatomy of a pig, with visible liver on top

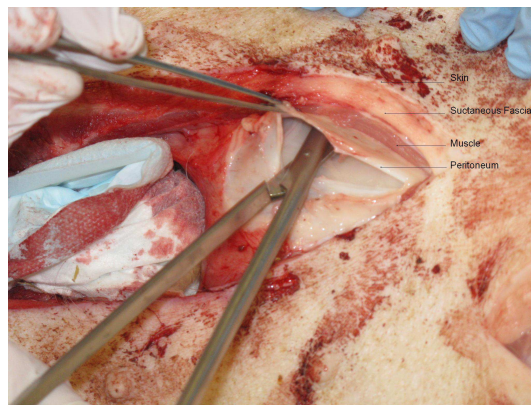


Figure 34: Tissue layers of pig, with visible skin, Fascia, muscle and fat. Picture taken at Erasmus Medical Centre (17-11-2011)

### A.1 Discussion

The test gave a clear idea on needle insertion into the liver. Manually it is clearly felt that different layers are encountered. Especially the capsule of the liver is a layer which is tougher than the other layers, which can be felt in the force feedback. The tip of the needle was already used in previous tests and not as sharp as a new tip. The sharpness might influence the needle insertion and increase the needed cutting and puncture force. Important to notice is that the needle buckles if



**Figure 35:** Percutaneous needle insertion in the liver. Location of the entry site between the ribs under the right leg in the coronal plane. Picture taken at Erasmus Medical Centre (17-11-2011)

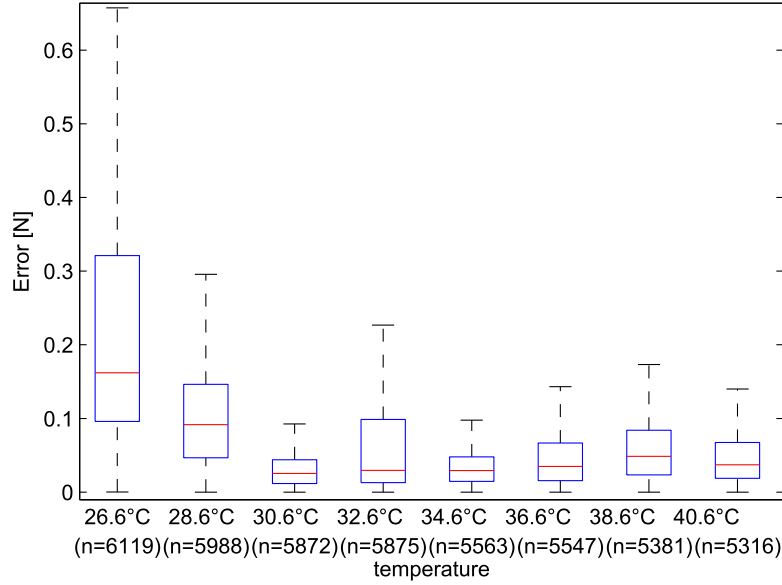
not supported when puncturing the epidermis (skin). In tests with needle insertion into biological tissue either a support has to be created or the epidermis has to be cut. In this pilot test navigation to the liver was easy because of the visibility created by the opening incision in the abdominal cavity. This gave a clear view of the liver and other organs and their locations. Direction could be established and the optimal entry site is made between ribs under the right front leg in the coronal plane. The piglets where sacrificed male piglets from around 40 kilograms. Because of the opening in abdominal en thoracic cavity and removal of heart and lungs the anatomy is changed. So the access entry can be different in other situations and has to be examined.

## B Polynomial curve fit

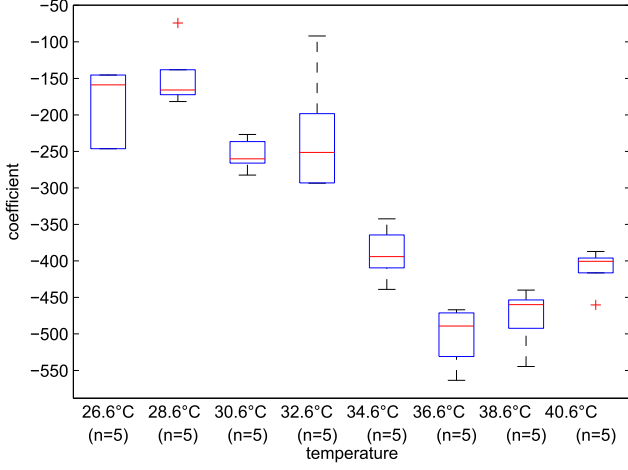
In chapter 3.3.2 a best fit straight line is used to approach the data from the calibration. From the linear regression it can be seen that the linearity error is bigger than expected. The error fluctuates around the best fit in a similar method for all the calibration cycles. To reduce this error the raw data is fitted with a polynomial curve in the form of.

$$\Delta F[N] = p_1(\Delta D[Pixel])^n + p_2(\Delta D[Pixel])^{n-1} + \dots + p_n(\Delta D[Pixel]) \quad (13)$$

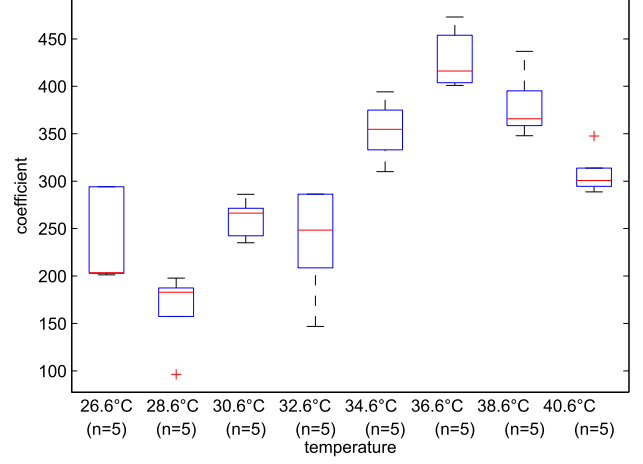
In this equation  $\Delta D$  is the pixel change from the FBG interrogator, this pixel change is related to the Bragg wavelength shift,  $F$  is the force in Newton,  $P$  are the polynomial coefficients. For this data a 4th order polynomial is used. In equation the constant term is held fixed at zero forcing the polynomial fit to intersect the origin. The polynomials coefficients are given in Figure 37. Like the slope coefficient for the linear regression the coefficients for the polynomial changes for different temperatures, but there is no clear relation between the coefficients and the increasing temperature. Also the spread of the data points is a lot larger in comparison to the spread for the linear regression coefficient. The error of the fit is the difference between the polynomial best curve and the raw data, for this polynomial the median values for the coefficients from Figure 37 are used. The errors are lower than the linearity errors found for the linear regression. Although the error is lower from the wide spread in the coefficients it can be concluded that the linear approach should be used when using the prototype.



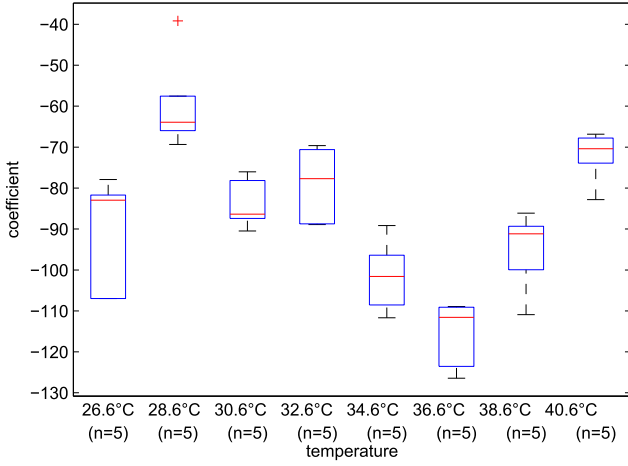
**Figure 36:** Boxplot of 4th order polynomial fit error for a range of 0-10N 13. For all data points per temperature set. The coefficients used for the fit are the medians found in Figure 37



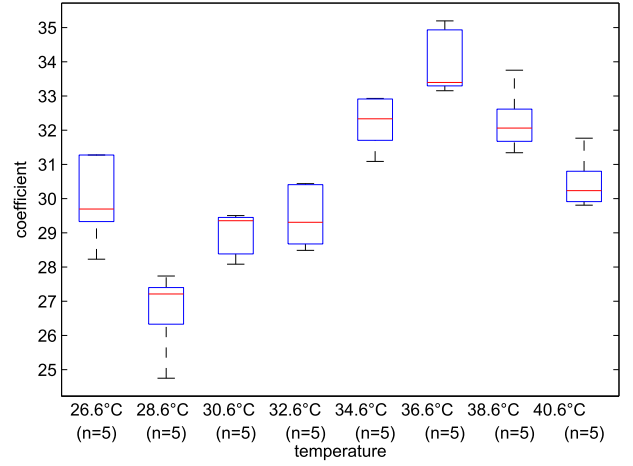
(a) Coefficient first term.



(b) Coefficient second term.



(c) Coefficient third term.



(d) Coefficient fourth term.

**Figure 37:** Boxplots of 4th order polynomial coefficients Equation 13 fit range 0-10N. For all calibrated temperatures.

---

## C Deflection experiment

### C.1 Introduction

Deflection of needles often leads to targeting errors in needle procedures. Needle design are primarily determined by diameter length and the tip type, the diameter and length of a needle effect the flexural rigidity. Increasing the diameter of a needle increases the bending stiffness of the needle. Higher stiffness causes less deflection and less deviation from the desired needle path. But an increased diameter also increases the invasiveness on the tissue with the risks for complications.

#### C.1.1 Bending stiffness

The bending stiffness, also referred to as the bending rigidity or flexural rigidity, is the resistance in flexure of a material in a certain direction. This means the force needed to bend an object to a certain configuration. The flexural rigidity is expressed as  $EI$  and has the unit  $Nm^2$ . The bending can be described by the following Euler-Bernoulli beam equation [16][10].

$$\frac{1}{R} = \frac{M}{EI} \quad (14)$$

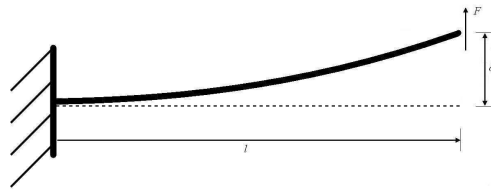
Where in this equation  $R$  is the curvature radius,  $M$  the internal moment.  $E$  is the Young's modulus and  $I$  the second moment area of inertia.

In the case of a needle with a circular geometry, the inertia is defined by

$$I = \frac{\pi r^4}{4} \quad (15)$$

#### C.1.2 Measuring bending stiffness fixed cantilever set-up

A setup to determine the bending stiffness is a fixed cantilever set-up. In a fixed cantilever setup for needles the hub of the needle is clamped as seen in 38.



**Figure 38:** Fixed cantilever set-up, needle is fixed at the hub and a force is applied at length  $l$ , the displacement is given by  $\delta$

A small displacement is applied at a location along the axis of the needle and the resulting force is measured. From the displacement and the force the bending stiffness is calculated according to.

$$\delta = \frac{FL^3}{3EI} \quad (16)$$

In which  $L$  is the length between the fixed end (the needle hub) and the point where the force is applied,  $\delta$  is the displacement of the needle at that point.  $F$  is the applied force. The load displacement data are plotted against each other.

---

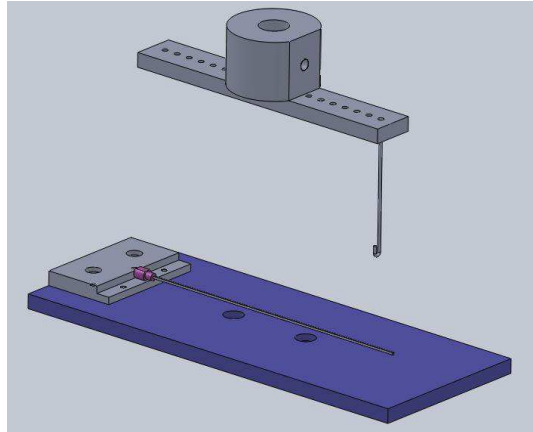
### C.1.3 Method

The experiment was carried out on a Zwick Roell z005 universal testing machine [39](#). In the set-up the needle is mounted at the hub on the base plate as seen in [40](#) and [41](#). The distance  $L$  for the applied force can be changed by placing the hook in a different hole. The holes are spaced with a 10 mm increment. The test is non destructive and remains fully elastic. The testing machine is position controlled and at each location a constant displacement  $\delta$  is applied and the corresponding force is measured at a sample frequency of 500 Hz. Each set-up is measured 5 times. And multiple locations on the needle are measured. Two 18G\*20 cm trocar needles are measured, one is fitted with 3 FBG fibres. The needle consist of an inner stylet and outer trocar needle, which are tested separately and together. During the measurement of the FBG fitted needle the optic data from the sensors are recorded. The recording of the optic data is done with Deminsys FBG interrogator with a down sample factor 200.

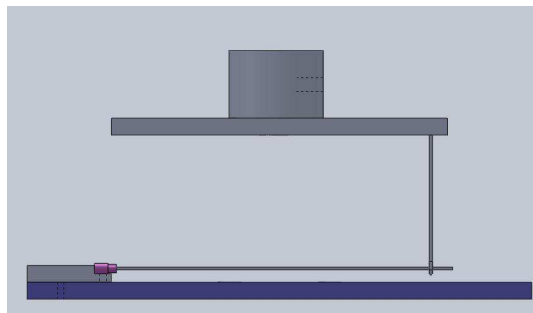


**Figure 39:** Zwick roell z005 universal testing machine

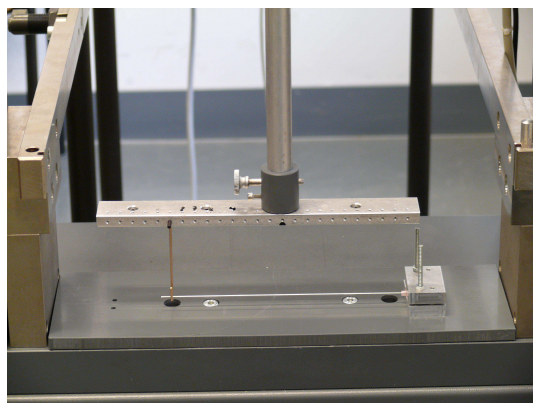




**Figure 40:** The setup for the needle deflection measurement, the point of the applied force can be changed along the axis of the needle



**Figure 41:** The setup for the needle deflection measurement, the point of the applied force can be changed along the axis of the needle



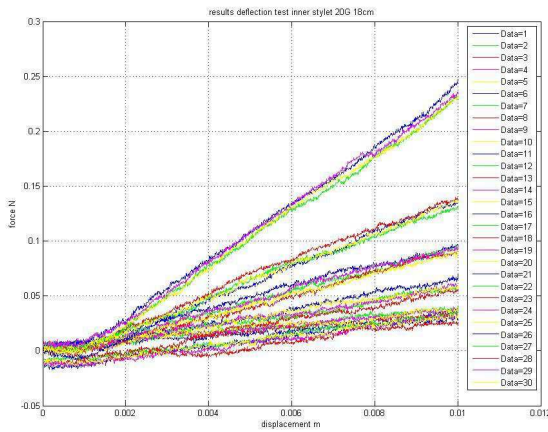
**Figure 42:** The setup for the needle deflection measurement, the point of the applied force can be changed through the different slots

## C.2 Results

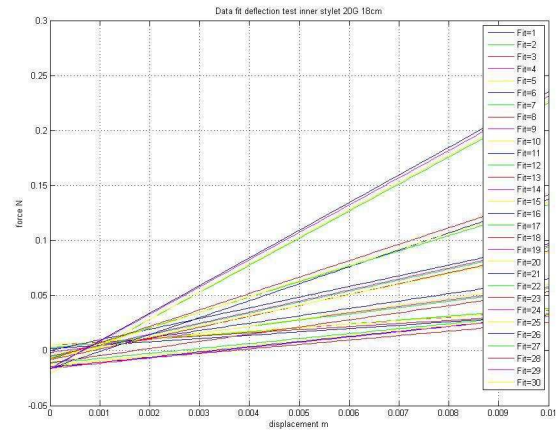
For all the dataset the forces are plotted against the position. Through each dataset a least squares linear regression is fitted. The datasets are trimmed at the beginning and the end. Reason to trim the data set is that not all entries have real values, and at start-up the force position shows nonlinear behaviour.

### C.2.1 Standard 18G trocar needle

Inner stylet The results for the inner stylet.

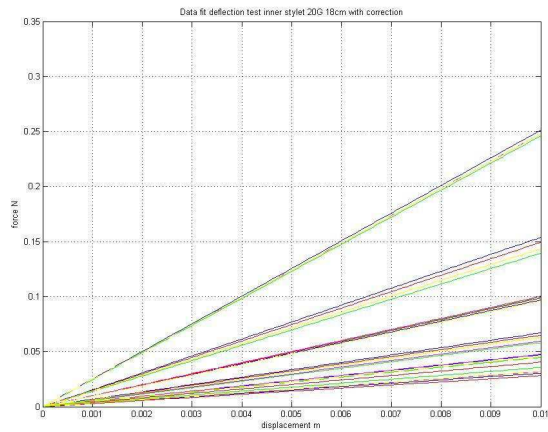


(a) Results deflection test inner stylet 20G 18cm

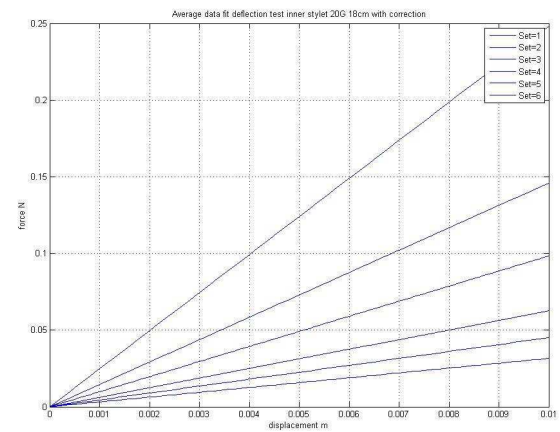


(b) Data fit deflection test inner stylet 20G 18cm

**Figure 43: Inner stylet**



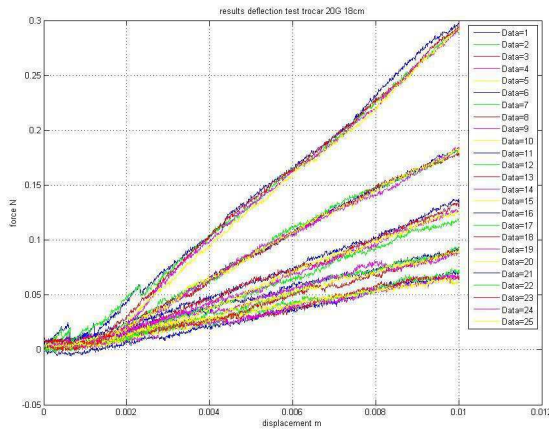
(a) Data fit deflection test inner stylet 20G 18cm with correction



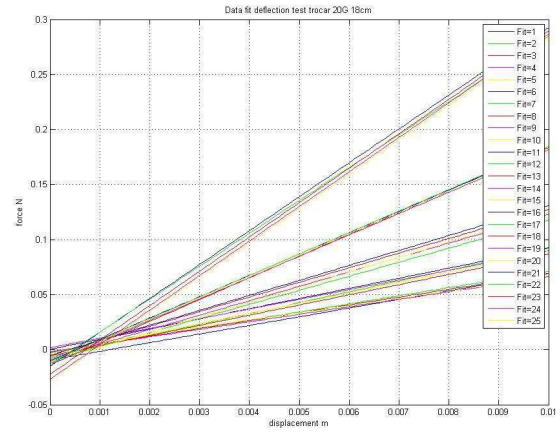
(b) Average data fit deflection test inner stylet 20G 18cm

**Figure 44: Inner stylet**

## Trocar needle without stylet

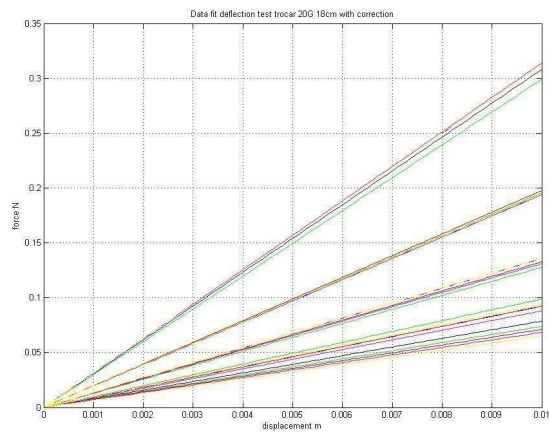


(a) Results deflection test trocar needle without stylet 20G 18cm

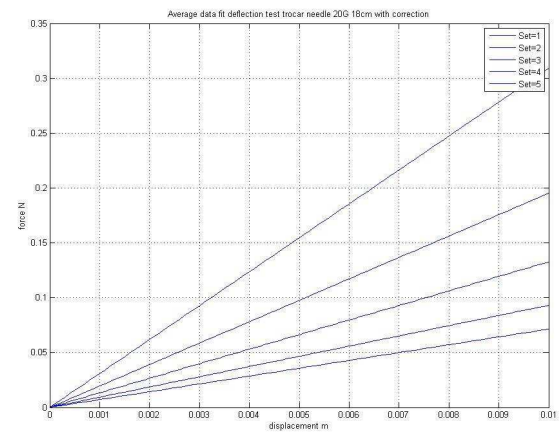


(b) Data fit deflection test trocar needle without stylet 20G 18cm

**Figure 45:** Trocar needle



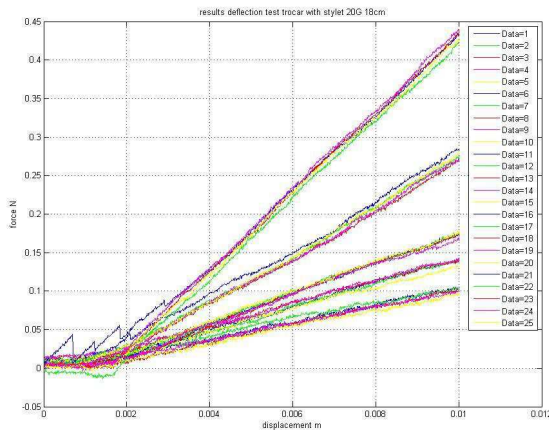
(a) Data fit deflection test trocar needle without stylet 20G 18cm with correction



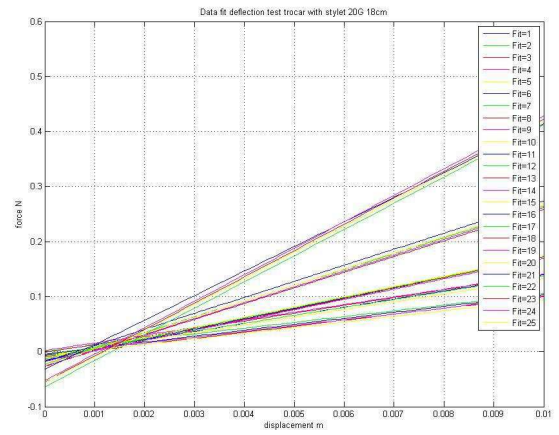
(b) Average data fit deflection test trocar needle without stylet 20G 18cm with correction

**Figure 46:** Trocar needle

## Trocar needle with stylet

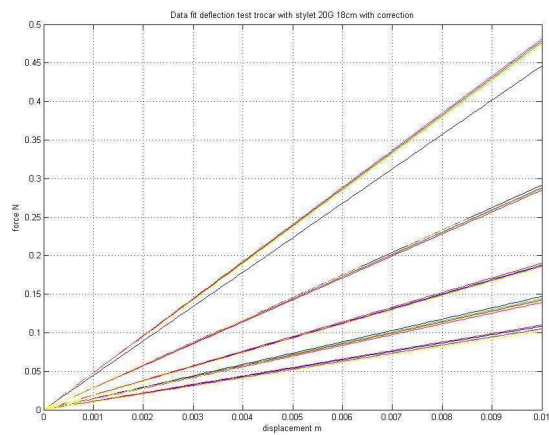


(a) Results deflection test trocar needle with stylet 20G 18cm

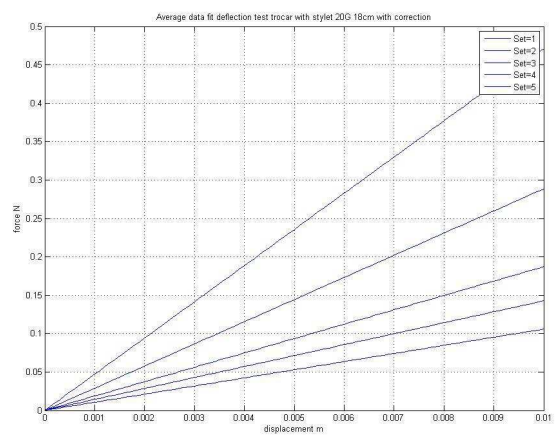


(b) Data fit deflection test trocar needle with stylet 20G 18cm

**Figure 47: Trocar needle**



(a) Data fit deflection test trocar needle with stylet 20G 18cm with correction

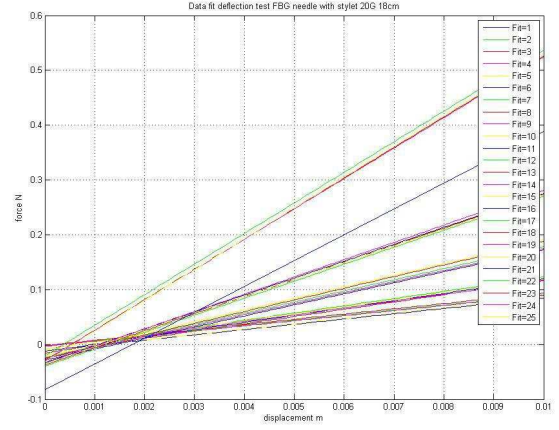
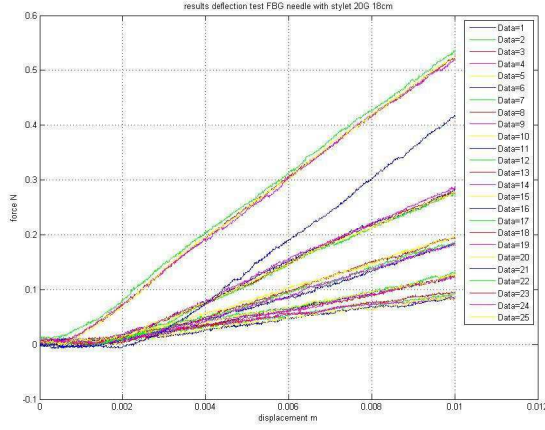


(b) Average data fit deflection test trocar needle with stylet 20G 18cm with correction

**Figure 48: Trocar needle**

### C.2.2 FBG needle

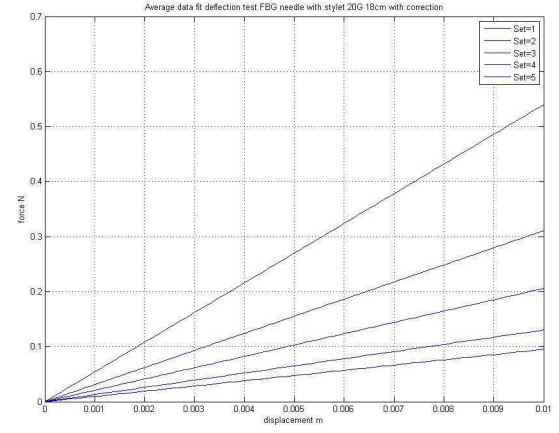
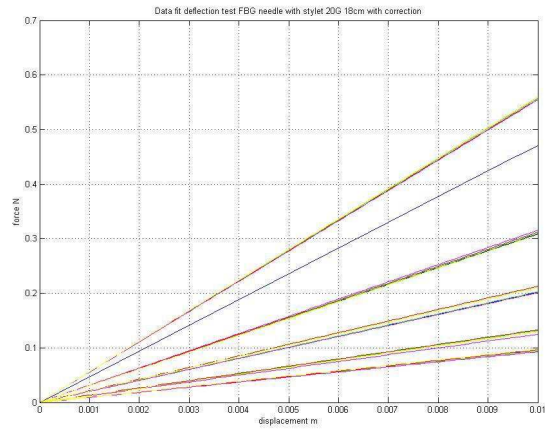
FBG needle stylet with trocar needle



(a) Results deflection test FBG needle stylet with trocar 20G 18cm

(b) Data fit deflection test FBG needle stylet with trocar 20G 18cm

**Figure 49:** Trocar needle with FBG stylet.



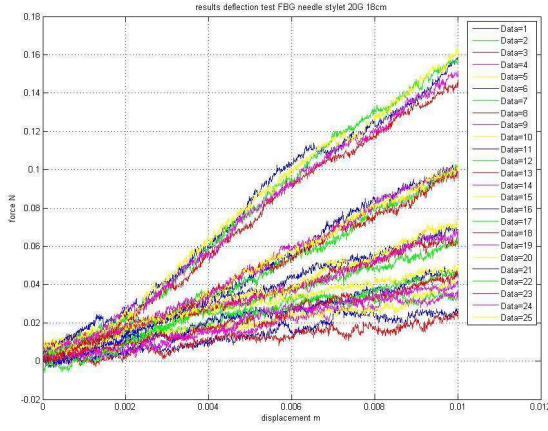
(a) Data fit deflection test FBG needle stylet with trocar 20G 18cm with correction

(b) Average data fit deflection test FBG needle stylet with trocar 20G 18cm with correction

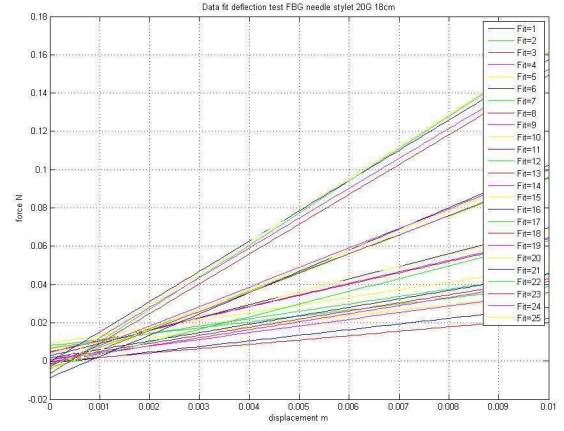
**Figure 50:** Trocar needle with FBG stylet.



### C.2.3 FBG needle stylet without trocar needle

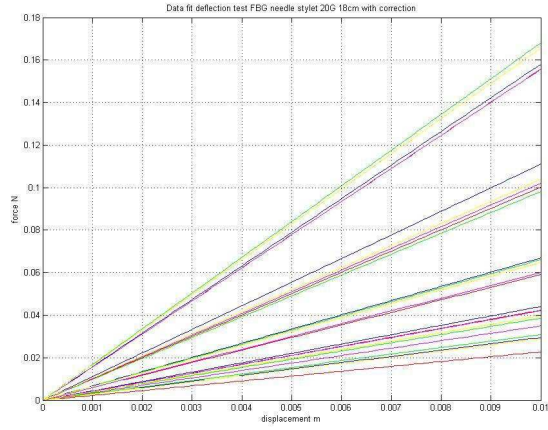


(a) Results deflection test FBG needle stylet without trocar 20G 18cm

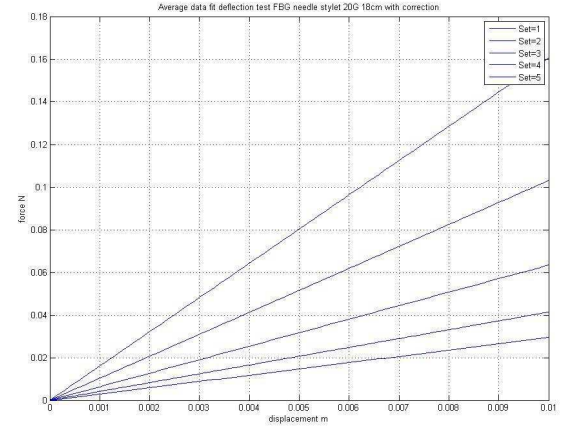


(b) Data fit deflection test FBG needle stylet without trocar 20G 18cm

Figure 51: FBG stylet.



(a) Data fit deflection test FBG needle stylet without trocar 20G 18cm with correction



(b) Average data fit deflection test FBG needle stylet without trocar 20G 18cm with correction

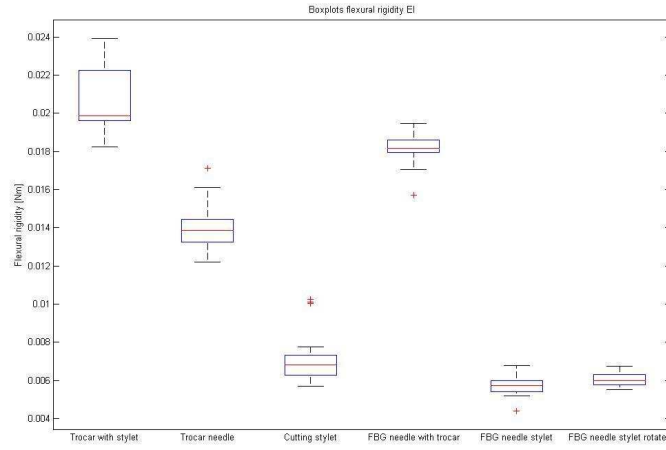
Figure 52: FBG stylet.

### C.2.4 Flexural rigidity

From the slopes of the curve we can determine the flexural rigidity using equation 16.

**Table 5:** Flexural rigidity EI for the single cantilever setup

Needle	Flexural rigidity EI [ $\text{Nm}^2$ ]	Variance
Trocar needle with stylet	0.0207993174674297	2.60622686510199e-06
Trocar needle without stylet	0.0140049326342842	1.34782245792305e-06
Cutting stylet	0.00804009296367612	1.97668237464776e-06
FBG needle stylet with trocar	0.0181951988273376	5.42972464887895e-07
FBG needle stylet	0.00568933630989326	2.14965262804076e-07
FBG needle stylet rotated 90°	0.00605813310590352	1.77117021961589e-07



**Figure 53:** Boxplots flexural rigidity [Nm]

---

### C.3 Discussion

This test measured the flexural rigidity of the prototype needle and the a regular needle. In the test the flexural rigidity of the hubs of the needle was also accounted for, by mounting the hubs of the instead of the shaft of the needle. This would also be the case in a clinical situation. From the flexural rigidity we cannot calculate the Young's modulus, because this a material property and we are measuring a combined system. Further test on these needle are needed in the design for a shape sensing needle. Sadly in the prototype an optic fibre got broken. And proceeding in this design got delayed. Therefore the my graduation project changed direction to measuring the tip forces, for which a design is made and evaluated. Eventually both these prototypes need to combined in a single system to create a design capable of measuring tip forces and the location and direction of these tip forces.

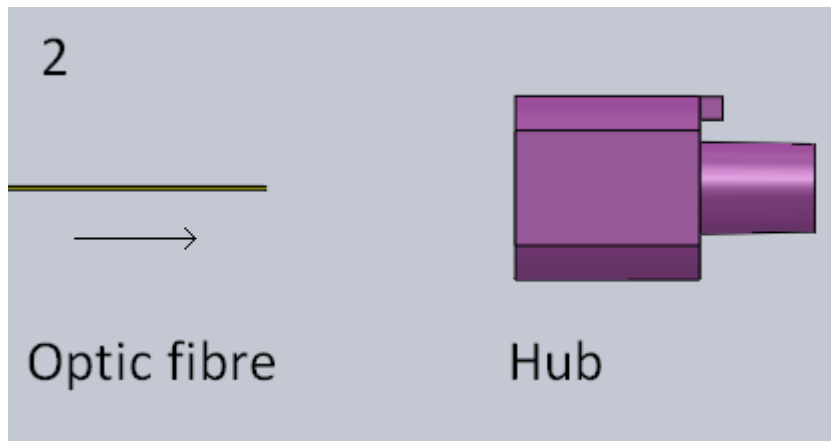


---

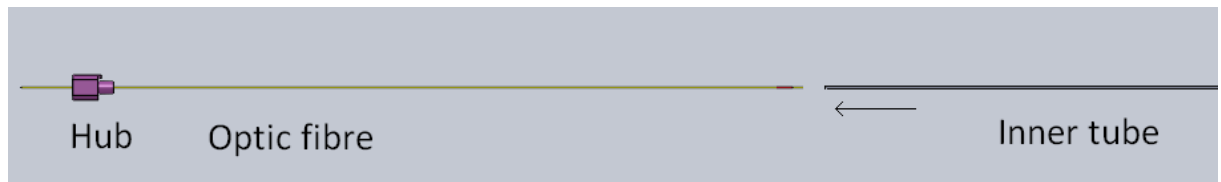
## D Assembly

## Assembly steps

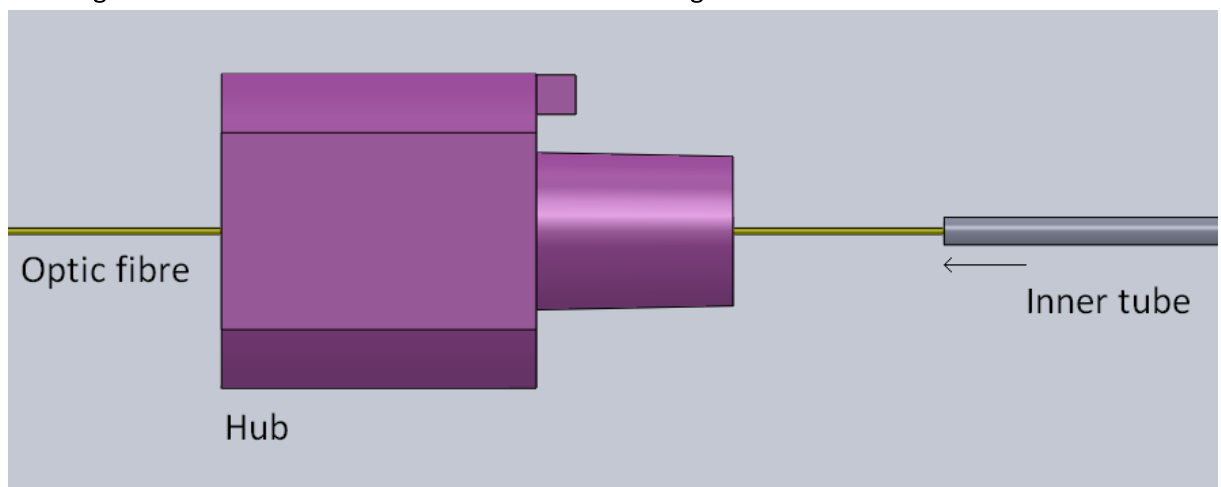
1. Strip white jacket of optic fibre to length (marked with black dot)
2. Insert optic fibre through needle hub



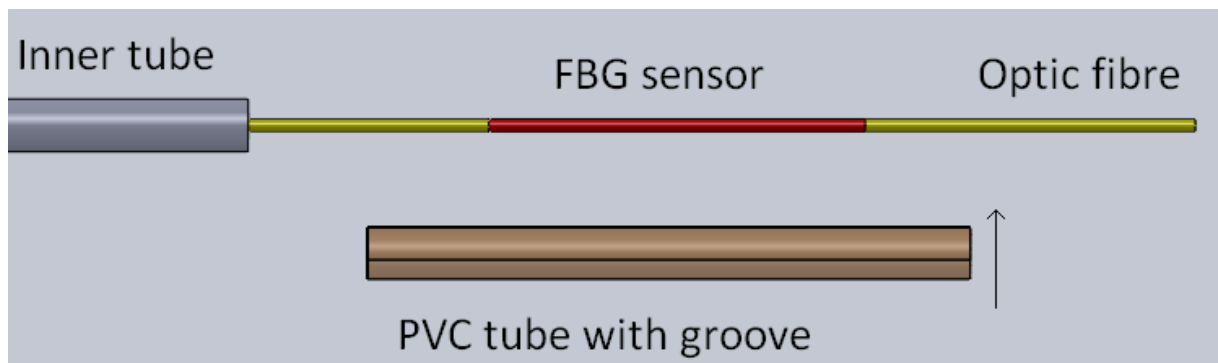
3. Insert optic fibre in the inner tube ( $\varnothing 0.7 \times 0.3\text{mm}$ ) (end with black marking first)



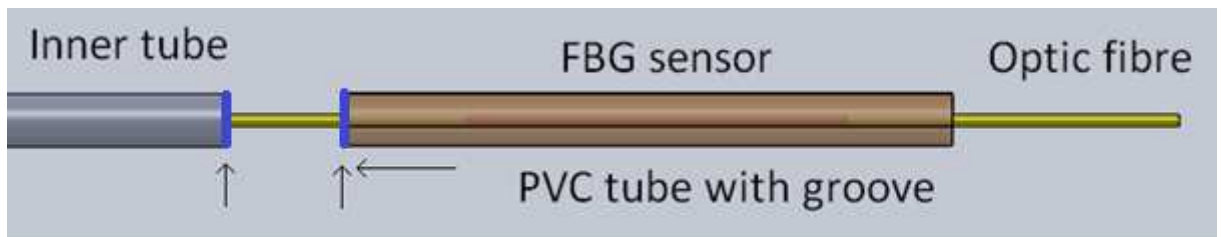
4. Fit and glue inner tube in the needle hub. Caution not to glue the fibre



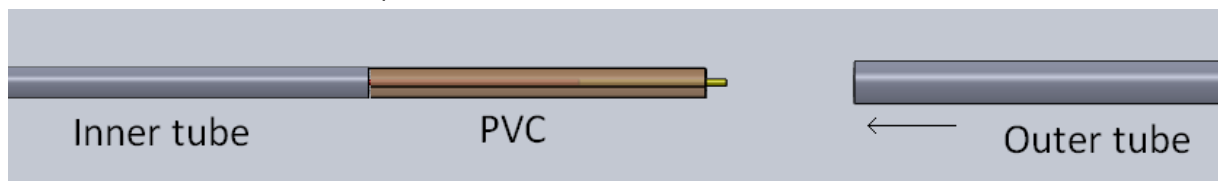
5. Glue PVC tube with groove over FBG sensor. Fill the groove with an epoxy bonding to form a smooth tubular section.



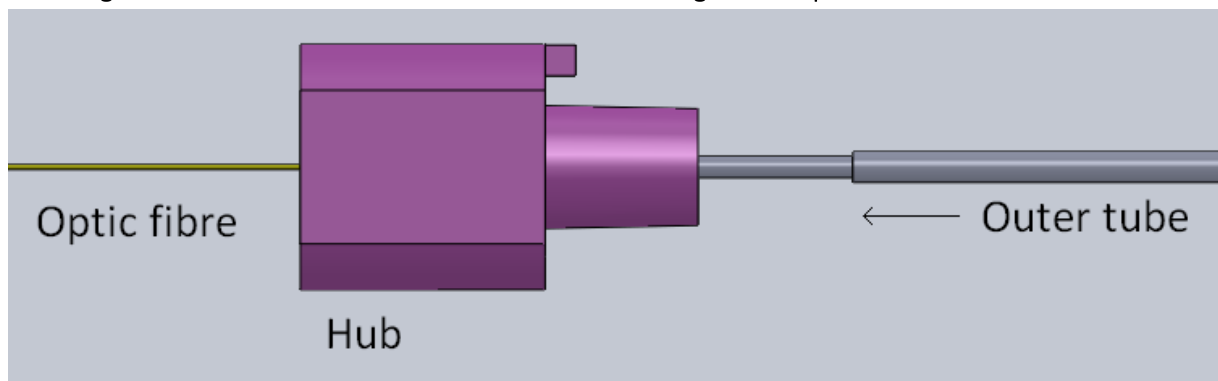
6. Glue PVC to inner tube. (Bonding surfaces marked blue)



7. Insert outer tube over assembly

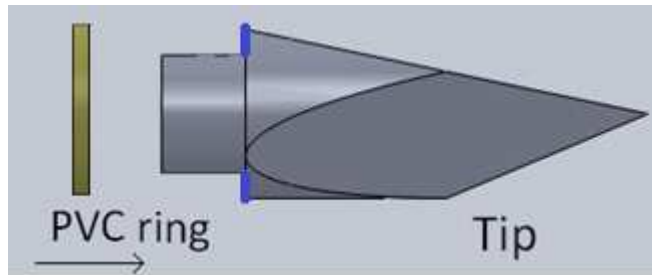


8. Fit and glue outer tube in the needle hub. Caution not to glue the optic fibre.

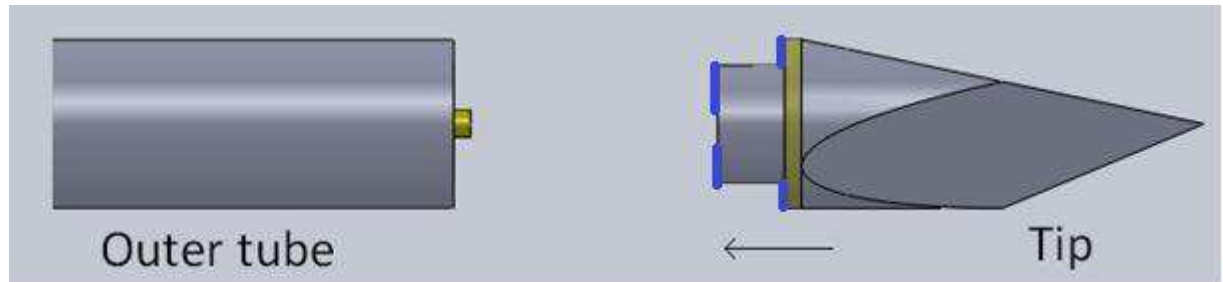


9. Cut optic fibre to length

10. Glue PVC ring to the tip of the needle



11. Glue tip to PVC end, and glue to the outer tube. (Bonding surfaces marked blue)



---

## E Calibration Protocol

The purpose of this protocol is to calibrate the prototype which is scientifically valid. By providing uniform guidelines.

- Start Deminsys interrogator. Interrogator use a light source which warms up the system. The interrogator is started at least an hour before first calibration cycle.
- Set the number of data samples the interrogator measures. This is the desired time range divided by the sample frequency. In this case that is 50000 samples at 100 Hz that is a measurement time of 500sec.
- Start test run universal testing machine without needle. To check if the designed load profile is correctly executed.

For each calibration cycle the following steps were performed.

- Check temperature inside the temperature chamber and note temperature, with the mounted thermocouple.
- Start FBG interrogator measurement
- Start the calibration cycle on the Universal testing machine

At the end of all the calibration cycles the files are exported to a .xls file type. And analysis can be performed on the data in Matlab R2011b.

## F Drawings

**Table 6:** Drawings Prototype

Part Name	Drawing Name	Quantity	Material	Remarks
Needle tip	needle_tip2	1	Metal	Taken from Cook Medical Trocar needle G02901 DTN-18-20.0-u
FBG Jacket	FBG Jacket	3	PVC Type 1	
PVC ring	pvc_ring	1	PVC Type 1	
Needle hub	needle_hub_stylet	1	Plastic	
Outer tube	tube_010_070	1	RVS	
Inner tube	tube_070_035	1	RVS	
Optic fibre	-	1	Hi 780 Polyimide recoat	
Trocar (outer sheath)	Trocar_sheath	1		Taken from Cook Medical Trocar needle G02901 DTN-18-20.0-u

A

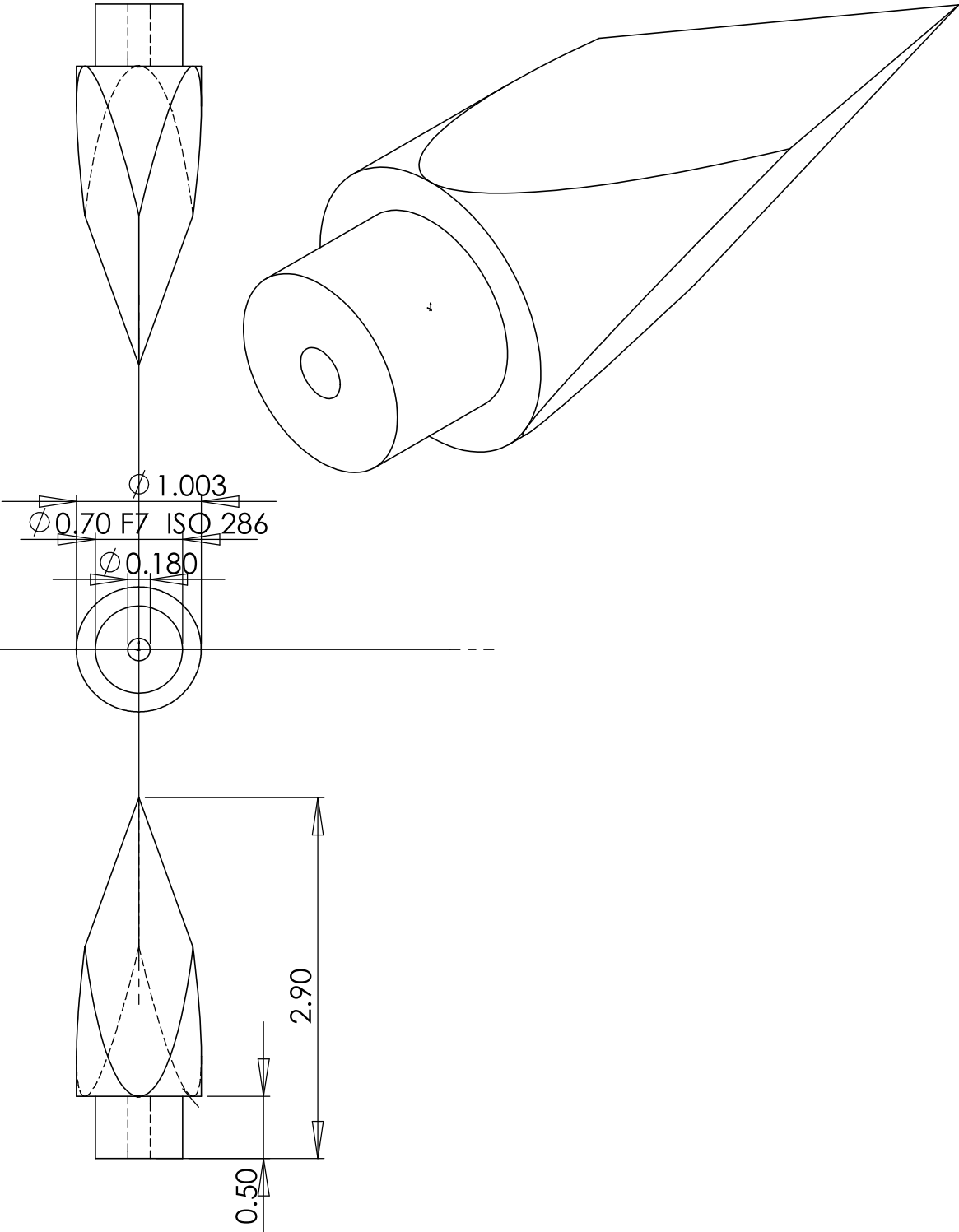
B

C

D

E

F



UNLESS OTHERWISE SPECIFIED: DIMENSIONS ARE IN MILLIMETERS SURFACE FINISH: TOLERANCES: LINEAR: ANGULAR:		FINISH:				DEBUR AND BREAK SHARP EDGES		DO NOT SCALE DRAWING		REVISION	
	NAME	SIGNATURE	DATE				TITLE:				
DRAWN											
CHK'D											
APPV'D											
MFG											
Q.A					MATERIAL: Metal tip from Cook Medical or needle G02901 DTN-18-20.0-		DWG NO.		needle_tip2		A4
				WEIGHT:		SCALE:20:1				SHEET 1 OF 1	

A

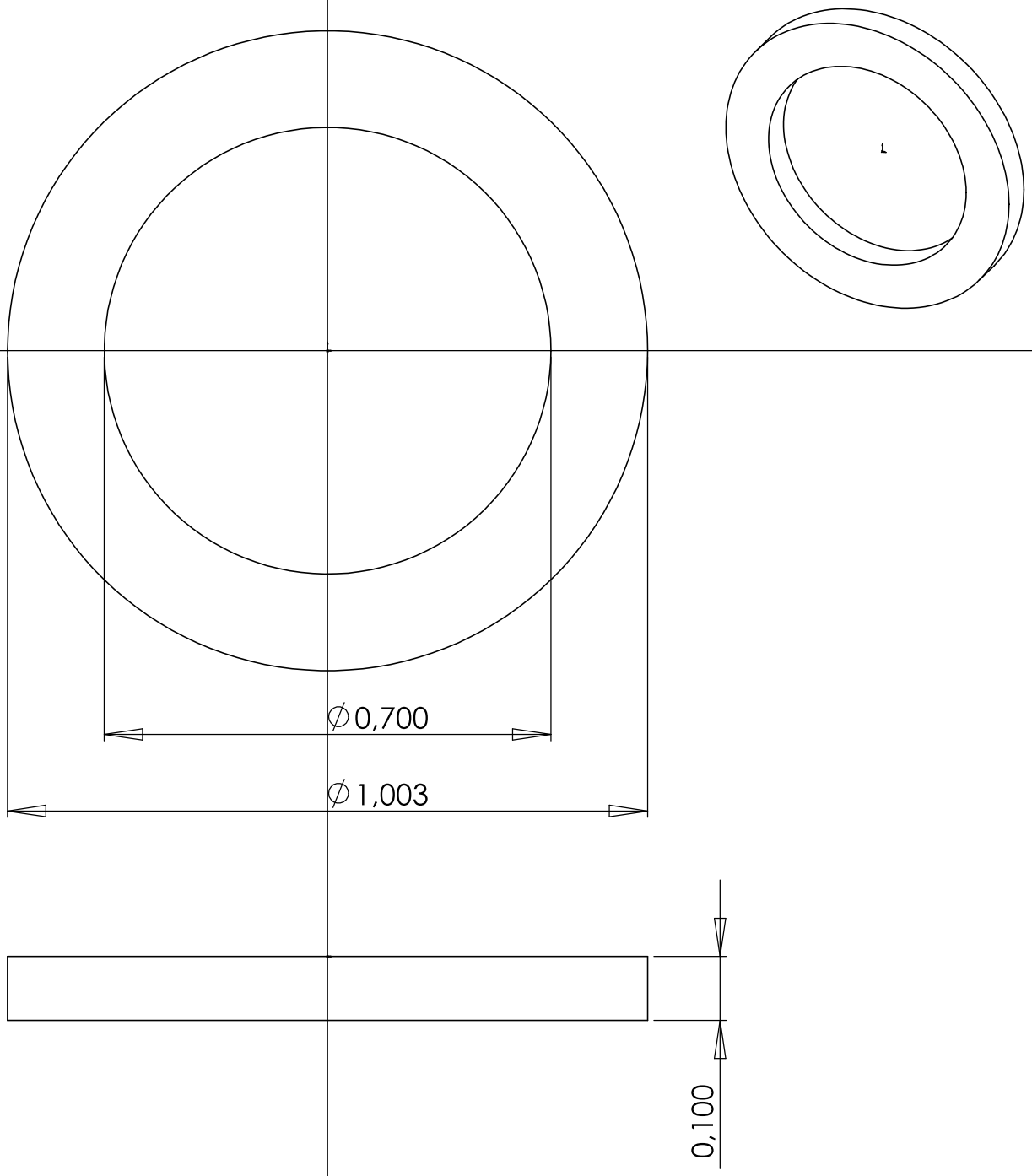
B

C

D

E

F



UNLESS OTHERWISE SPECIFIED: DIMENSIONS ARE IN MILLIMETERS SURFACE FINISH: TOLERANCES: LINEAR: ANGULAR:		FINISH:				DEBUR AND BREAK SHARP EDGES		DO NOT SCALE DRAWING		REVISION	
	NAME	SIGNATURE	DATE			TITLE:					
DRAWN											
CHK'D											
APPV'D											
MFG											
Q.A						MATERIAL:		DWG NO. <b>pvc_ring</b>			
					PVC Type 1						
				WEIGHT:		SCALE:100:1				SHEET 1 OF 1	

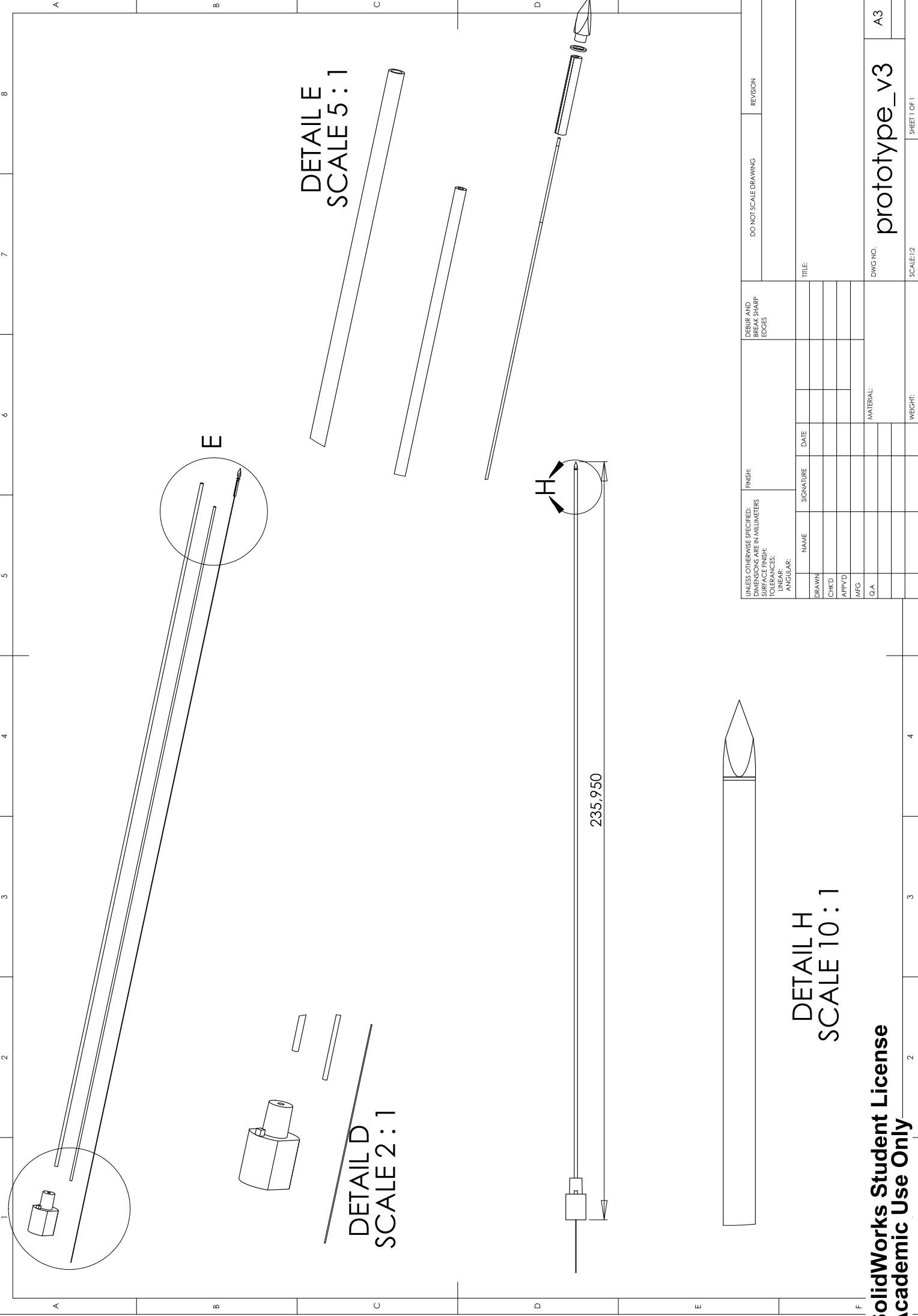







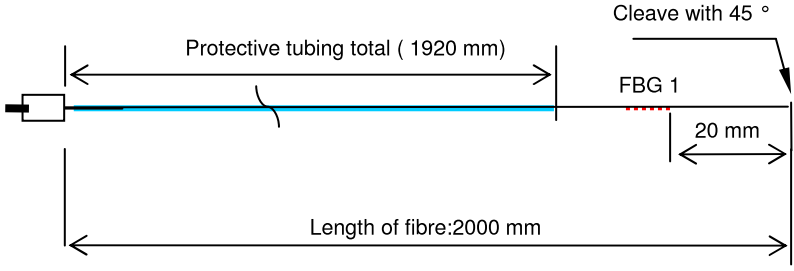


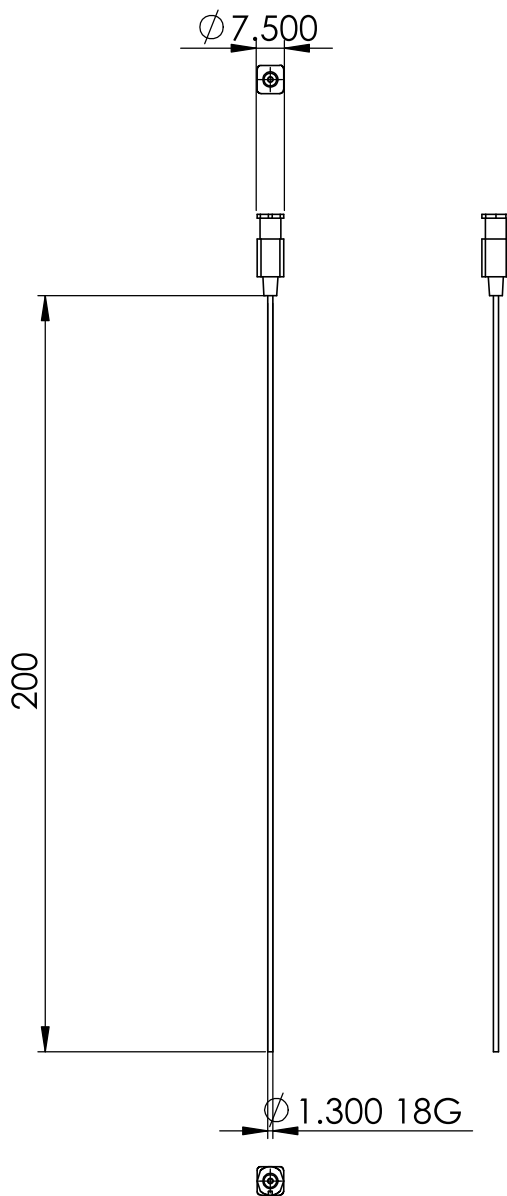




UNLESS OTHERWISE SPECIFIED: DIMENSIONS ARE IN MILLIMETERS				FINISH:		DEBUR AND BREAK SHARP EDGES		DO NOT SCALE DRAWING		REVISION	
SURFACE FINISH: TOLERANCES: LINEAR: ANGULAR:											
NAME	SIGNATURE	DATE									
DRAWN											
CHKD											
APPVD											
MFG											
Q.A											
										</	

<b>Technobis Fibre Technologies</b> 		<b>MEMO</b>	
<b>Date</b>	<b>2 mrt 2010</b>	<b>No.</b>	201009001
<b>Concerning</b>	Fiber (demo board fibre )		
<b>Author</b>	I. Deerenberg		
<b>Copy</b>			

General fiber spec:	Layout for Demo Board Fibre
<ul style="list-style-type: none"> <li>Fibre type : Hi 780 &amp; <b>Polyimide recoat</b></li> <li>Fibre length : 2 m</li> <li>E-2000-APC 0,1dB</li> <li>1 FBGs per fibre</li> <li>5 mm Sensor FBG Spec: <ul style="list-style-type: none"> <li>CW 856 nm +/- 0.5 nm</li> <li>Ref &gt;=90%</li> <li>BW@-3dB 0.23 +/-0.025nm</li> <li>SLSR &gt; 20 dB</li> </ul> </li> </ul>	



UNLESS OTHERWISE SPECIFIED: DIMENSIONS ARE IN MILLIMETERS SURFACE FINISH: TOLERANCES: LINEAR: ANGULAR:		FINISH:				DEBUR AND BREAK SHARP EDGES		DO NOT SCALE DRAWING		REVISION	
	NAME	SIGNATURE	DATE					TITLE:			
DRAWN											
CHK'D											
APPV'D											
MFG											
Q.A						MATERIAL:		DWG NO.		Trocar sheath	
SolidWorks Student License Academic Use Only						Medical Trocar needle 01 DTN-18-20.0-u		SCALE:1:2		A4	
								SHEET 1 OF 1			





